KU LEUVEN

FACULTY OF SCIENCES

Collateral sensitivity-based drug cycling in *Candida auris*:

"Breaking the Cycle" of multi-drug resistance evolution by treatment redesign

Alicia CHEN

Supervisor: Prof. Dr. Patrick Van Dijck
Laboratory of Molecular Cell Biology
Department of Biology
Faculty of Science, KU Leuven

Mentor: *Hans Carolus*
Laboratory of Molecular Cell Biology
Department of Biology
Faculty of Science, KU Leuven

Master thesis submitted in fulfillment of the requirements for the degree in Master of Science in Biochemistry and Biotechnology

Academic year 2021-2022

Acknowledgements

This past year has been nothing less than incredibly challenging, yet it has also brought me joy and contributed a great deal to my personal development. At the start, I could never have imagined that, not only, I would acquire an extensive amount of knowledge, I was also able to practice resilience, perseverance and the simple act of reaching out for help. More than ever, I've learned to avoid comparing myself to others, something that I've struggled with throughout my career as a student. Nevertheless, I wouldn't have been able to experience these valuable lessons if it weren't for Professor Van Dijck. Thank you for considering me as a master's student and giving me the opportunity to work in your lab. I'd also like to commend you on the pleasant work environment you have created as I've made wonderful memories in the lab. Next, I'd like to thank my supervisor Hans Carolus for continuously pushing me when I felt like giving up. You encouraged me to give it my all and my thesis wouldn't have attained this level if it weren't for your support and patience. Thank you for the enjoyable times in the lab and your gradual acceptance of having two gen Z females as your master's students. I hope that you'll continue to practice the lingo we've taught you and the correct times to throw a peace sign.

My thanks also go to the master's students from the MCB and BDE labs. I sincerely enjoyed getting to know each one of you and will cherish the memories we've made. You've made my whole thesis experience (as well as our shared office space) wonderful. Specifically to my fellow student Louise, thank you for going through it all with me. My year wouldn't have been as enjoyable if it weren't for our karaoke sessions, juicy stories and your great support. Additionally, I'd like to thank my fellow student Alannah for the late, yet enjoyable nights we spent together writing our theses. You were a ray of light at times I felt demotivated and I thoroughly enjoyed this year living together and spending time in the lab with you.

Lastly, I'd like to thank my boyfriend Dries for always consoling me and trying to convince me that I'm not a bad student. Your incredible support, warmth and kindness have definitely carried me through the year. Thank you for making sure that I eat my meals and get enough sleep, even though I still don't tend to succeed in the latter. You are my rock. Many thanks to my friends for all the incredibly wonderful times. I am thrilled for the upcoming chapters in our lives and tenderly hope that our friendships will last forever. To my parents, thank you for the sacrifices you've made for me to fulfill my dreams, I appreciate you tremendously. At last, to my siblings Emmely and Kevin, thank you for accepting my little sister behaviour and irresponsibility at times. I immensely treasure the bond we have and the support we always give to one another in difficult times. Finally, thank you to my aunt Lien, you have shaped me to become the person I am today.

Table of Contents

Acronyms

MOPS	4-Morpholinepropanesulfonic acid
5-FC	5-Fluorocytosine
FdUMP	5-Fluorodeoxyuridine monophosphate
5-FU	5-Fluorouracil
5-FUMP	5-Fluorouridine monophosphate
5-FUTP	5-Fluorouridine triphosphate
AMB	Amphotericin B
ANF	Anidulafungin
ABR	Antibiotic resistance
AB	Antibiotics
AP-1	AP-1-like transcription factor
AUC	Area under the curve
BDA	Broth dilution assay
CDR	Candida drug resistance
Candida species	Candida spp.
CAS	Caspofungin
CHX	Chlorhexidine
CPX	Ciclopirox
CS	Collateral sensitivity
XR	Cross resistance
DMSO	Dimethyl sulfoxide
ERG	Ergosterol biosynthesis
EDTA	Ethylenediaminetetraacetic acid
FLU	Fluconazole
FMGX	Fosmanogepix
FUR1	5-Fluorouridine resistant 1
GOF	Gain-of-function
GEL	Geldanamycin
GOI	Genes of interest
Hsp90	Heat-shock protein 90
HR	Homologous recombination

IBX	Ibrexafungerp
LOF	Loss-of-function
MGX	Manogepix
MCA	Micafungin
MCO	Micoconazole
MFC	Minimal Fungicidal concentration
MIC	Minimum Inhibitory Concentration
MDR	Multi-drug resistant
NIT	Nitroxoline
ORF	Open reading frame
PD	Pharmacodynamic
PK	Pharmacokinetic
PCI	Phenol pH 6.7-chloroform-isoamylalcohol (25:24:1)
PBS	Phosphate buffered saline
POS	Posaconazole
PMF	Proton-motive force
qPCR	Quantitative polymerase chain reaction
ROS	Reactive oxygen species
RR	Resistance ratio
RPMI	Roswell Park Memorial Institute
S. cerevisiae	Saccharomyces cerevisiae
SC	Single colony
SNP	Single nucleotide polymorphism
SDS	Sodium n-Dodecyl Sulfate
TAC1	Transcriptional activator of CDR genes 1
TAE	Tris-acetate-EDTA
TE	Tris-EDTA
UDP-glucose	Uridine Diphosphate Glucose
VVC	Vulvovaginal candidiasis
WGS	Whole genome sequencing
YPD	Yeast Peptone Dextrose

Summary

Candida auris is a recently emerging fungal pathogen, characterized by its ability to develop multi-drug resistance (MDR) and rapidly spread in healthcare settings. As the slow and challenging search for novel antifungals is not able to keep up with the emergence and spread of MDR pathogenic fungi such as *C. auris*, the design of strategies with clinically approved drugs that reduce resistance acquisition, is vital. In this project, we explore the concept of preventing or reducing resistance development via collateral sensitivity (CS) based drug cycling schemes.

CS is a trade-off mechanism, which has previously been observed in tumors and bacteria, that arises when resistance mutations are acquired. Accordingly, resistant strains for one drug exhibit an increased sensitivity towards another drug. This phenomenon was explored in fungi by evolving resistance in *C. auris* strains in high-throughput *in vitro* experimental evolution against nine antifungal drugs and two repurposed drugs (nitroxoline, chlorhexidine). We observed that survival in experimental evolution was linked to the fungicidal or fungistatic nature of the drugs and resistance development was only dose-dependent for 5-FC. Next, the susceptibility of the resistant strains was mapped to ten antifungal drugs and nine repurposed drugs. CS was most pronounced in caspofungin (CAS) resistant strains to posaconazole (POS), and amphotericin B (AMB) resistant strains to CAS, ciclopirox (CPX), nitroxoline (NIT), and geldanamycin (GEL). Additionally, cross-resistance (XR) was observed, which is the acquisition of resistance to more than one drug simultaneously. XR from micafungin (MCA), anidulafungin (ANF), 5-flucytosine (5-FC), and AMB resistant strains towards azoles was most outspoken.

The CS drug pairs were used in drug cycling evolution experiments in four different dose combinations. While in monotherapy evolution, 50-100% of the tested isolates acquired resistance based on MIC_{50} changes, no resistance development was observed in cycling therapy, which demonstrates the valuable potential of drug cycling to prevent resistance development.

To investigate the genetic determinants of resistance development and their link to evolutionary dynamics such as CS and XR, we performed targeted sequencing of genes of interest (GOI) that are known to be involved in resistance in *C. auris.* Mutations were found in TAC1b (azole resistance), HS regions of *FKS1* (echinocandin resistance), *ERG3* and *ERG11* (polyene resistance), and *FUR1* (5-FC resistance). Yet, the majority of the resistant strains did not show mutations in known (GOI) and thus, might harbour novel resistance mechanisms or indicate adaptation through tolerance. WGS could elucidate novel resistance mechanisms when performed on resistant strains in which sequencing of GOI delivered no results.

Samenvatting

De recente opmars van *Candida auris*, een schimmel die is gekend voor zijn resistentie tegen meerdere geneesmiddelen en nosocomiale overdracht, vormt een wereldwijd gevaar. De beperktheid in antischimmelmiddelen en de uitdagende zoektocht naar nieuwe geneesmiddelen kan het gevaar dat de schimmel vormt alleszins moeilijk afwenden. Daarom is er een grote behoefte aan nieuwe therapieën die de ontwikkeling van resistentie in *C. auris* kunnen vermijden of verminderen. Deze studie richt zich tot het verkennen van collaterale sensitiviteit, een veelbelovend mechanisme waarmee we antifungale therapieën kunnen optimaliseren.

Collaterale sensitiviteit (CS) toont zich wanneer de verwerving van resistentie tegen een bepaald geneesmiddel een verhoogde sensitiviteit voor een ander geneesmiddel opwekt. In kruisresistentie (XR) gebeurt het tegenovergestelde en zal resistentie tegen een bepaald geneesmiddel leiden tot resistentie tegen een ander geneesmiddel. Deze fenomenen werden al eerder onderzocht in tumoren en bacteriën, maar nog niet in pathogene schimmels. We onderzochten CS in *C. auris* door een stam die gevoelig is aan alle antifungale geneesmiddelen te evolueren tot resistentie via *in vitro* experimentele evolutie. Dit werd uitgevoerd voor negen antifungale geneesmiddelen en twee repurposed geneesmiddelen, die initieel voor andere doeleinden werden geproduceerd, maar wel een antifungale werking vertonen. We ondervonden dat bepaalde geneesmiddelen leidden tot uitsterven van sommige populaties in het experiment en resistentie-verwerving enkel in 5-fluorocytosine (5-FC) afhankelijk was van de dosis van het geneesmiddel. Vervolgens werden CS en XR in kaart gebracht en CS was het meest uitgesproken in caspofungine (CAS) resistente stammen tegen posaconazole (POS) en amphotericine B (AMB) resistente stammen tegen CAS, ciclopirox (CPX), nitroxoline (NIT) en geldanamycine (GEL). Daarnaast constateerden we uitgesproken XR in micafungine (MCA), anidulafungine (ANF), 5-FC en AMB resistente stammen tegen de azolen.

De geneesmiddelparen die CS vertonen, werden gebruikt in cyclische evolutie experimenten, waarin de wildtype *C. auris* stam sequentieel werd behandeld met de twee drugs. In vergelijking met monotherapie, waarin 50 tot 100% van de geïsoleerde stammen resistentie vertonen op basis van een verhoogde MIC_{50} ten opzichte van de wildtype MIC_{50}, ondervonden we geen resistentie-verwerving in de cyclische therapieën. Dit toont het veelbelovende potentieel van cyclische therapieën in de strijd tegen resistentie-verwerving in *C. auris* en mogelijks andere schimmels.

We onderzochten ook de genetische determinanten van resistentie-verwerving in de resistente stammen om hun evolutionaire dynamiek, zoals CS en XR tegen andere drugs, te verklaren. Dit werd gedaan aan de hand van het sequeneren van genen die al eerder werden gelinkt aan

resistentie tegen bepaalde antischimmelmiddelen in *C. auris*. We vonden mutaties in *TAC1b* (azolen resistentie), hot spot regio's in *FKS1* (echinocandinen resistentie), *ERG3* en *ERG11* (polyenen resistentie) en *FUR1* (5-FC resistentie). Nochtans heeft de meerderheid van de resistente stammen geen mutaties in de gesequeneerde genen, wat betekent dat deze stammen ofwel via andere resistentie mutaties of mechanismen resistentie hebben opgewekt of tolerantie vertonen in plaats van resistentie. Via gerichte sequenering van andere genen gekend in de literatuur of via genoomwijde sequenering, kunnen nieuwe mutaties of resistentie mechanismen ontdekt worden.

1. Introduction

1.1 *Candida auris*, surfacing from swamps to hospitals

Candida species are one of the most prominent causes of fungal infections, responsible for both superficial (skin, mucosa) and systemic (bloodstream) infections in mostly immunocompromised patients [1, 2]. *Candida albicans*, an opportunistic commensal [3], is the most predominantly occurring *Candida spp.* causing candidiasis, a term commonly used to describe infections caused by *Candida*. Subsequently, cases involving *Candida glabrata* have surged due to its intrinsic and acquired resistance against azoles, which are the most widely used antifungals [1, 4].

Recently, *Candida auris*, known for its ability to cause invasive candidiasis, has emerged progressively. The pathogen is halo- and thermotolerant (37°C - 42°C), commonly multi-drug resistant (MDR) and does not develop (pseudo)hyphae [5]. It was initially isolated in Japan, 2009 from an ear sample, hence it being dubbed as *C. auris*, which is derived from the Latin word for ear, auris [6]. Upon inspection of earlier obtained *Candida* isolates, bloodstream isolates had already been recovered from patients in South Korea in 1996 [7], revealing that infection is not only confined to the ears but *C. auris* can also cause deadly, invasive, and nosocomial bloodstream infections [8]. At the phylogenetic level, it closely resembles *C. haemulonii, C. pseudohaemulonii* and *C. duobushaemulonii* [6], as depicted in Figure 1. These belong to the Saccharomycetales order in the Clavispora clade of the Metschnikowiaceae family, notoriously known for its predisposition for multi-drug resistance [9]. Phenotypically, they are hard to distinguish from each other, thus the necessity for more accurate identification methods is urgent as *C. auris* proposes a tremendous hazard and immediate measures to control this pathogen are crucial [10].

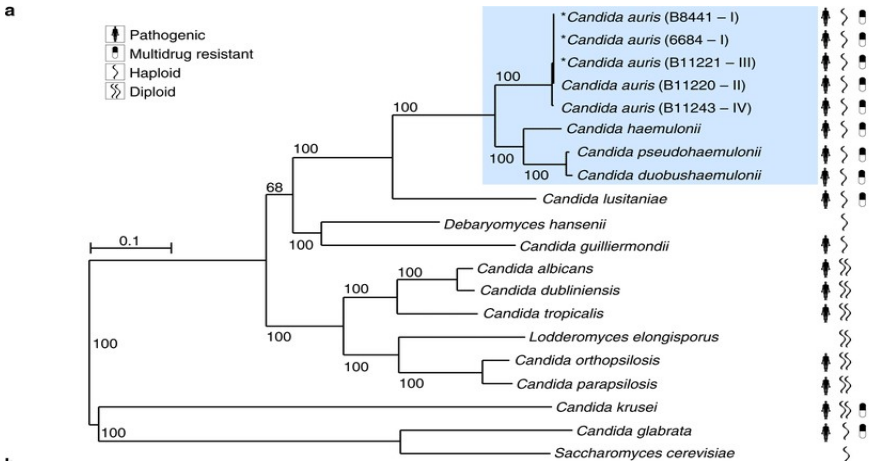

Figure 1: Phylogenetic tree of *Candida spp.* Phylogeny was based on the Maximum Likelihood between 1570 core genes of 1000 replicates from 20 genome assemblies. The database included sequences from *C. auris, C. haemulonii and C. pseudohaemulonii.* Average number of changes per site is specified by the branch lengths (Muñoz et al, 2018).

C. auris mostly infects immunocompromised people or patients that carry catheters. Common risk factors include immunosuppression, diabetes, surgeries, prolonged hospitalization, and recent exposure to antifungals or antibiotics [3]. Generally, patients experience fever and prolonging chills, yet various complications can arise based on the site of infection. Wound infections, for example, are associated with inflammation, redness, discharge of pus, tenderness of the wound, and fever. Ear infections, on the other hand, are characterized by reduced hearing, ear drainage, pain in the ear canal, and even permanent hearing loss when left untreated [11]. Furthermore, as described by Nett (2019), human neutrophils fail to phagocytose *C. auris*, and in the presence of *C. albicans*, neutrophils have a stronger tendency to kill the latter. A plausible explanation is missing, but the genetic diversity of *C. auris* might play a role in its evasion of these neutrophils [12].

Several hypotheses regarding the emergence of *C. auris* have been proposed, such as the extensive use of antifungal drugs and human-induced environmental changes, the latter of which was suggested by Casadevall et al. (2019), as depicted in Figure 2. They described *C. auris* as a plant saprophyte, commonly found in wetlands, that has developed high salinity- and thermal tolerance due to global warming. These high ambient temperatures allowed for the selection of thermotolerant *C. auris* strains, which would go on to breach the mammalian thermal barrier. The adapted strains subsequently may have colonized birds, present in these wetlands, which carried the pathogenic fungus to rural areas [13].

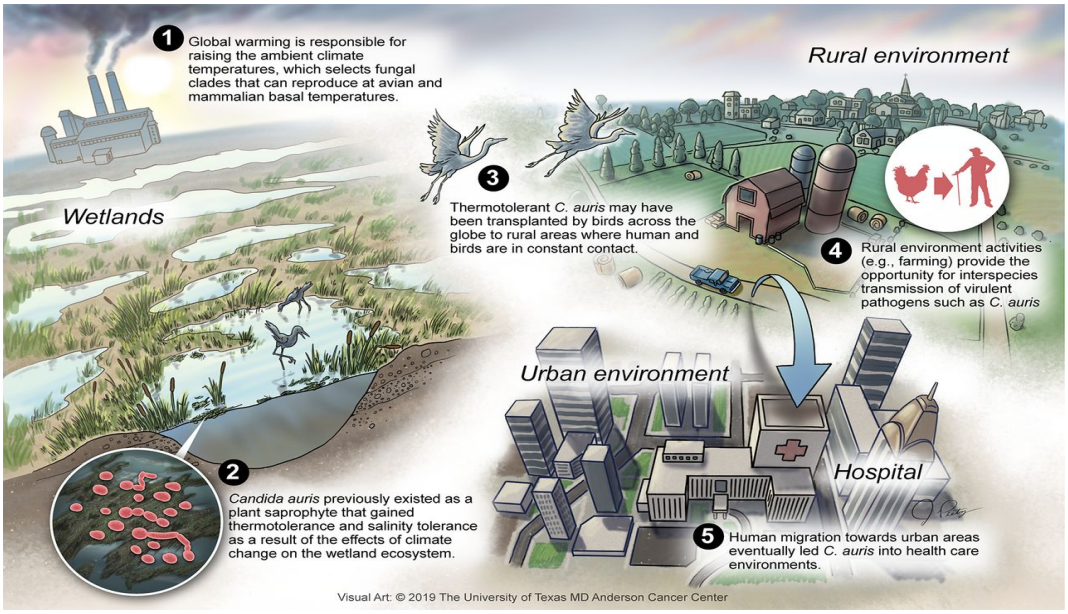

Figure 2: Casadevall's hypothesis on the emergence of *C. auris*. It was believed that *C. auris* derived from wetlands and climate change, which supposedly catalyzed the transition of *C. auris* to a human pathogen (Casadevall et al., 2019).

1.1.1 Clade differentiation and Geographical Distribution

Whole Genome Sequencing (WGS) studies were performed for *C. auris* isolates, which were classified into four geographically distinct clades, as depicted in Figure 3: South Asia (I), East Asia (II), South Africa (III), and South America (IV) [14, 15]. Whereas, clades I, II, and IV can cause healthcare outbreaks and invasive infections [16, 17], the East Asian clade seems to only infect the ears [18].

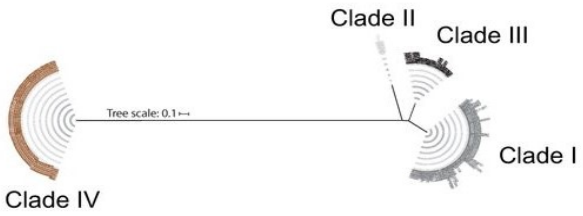

Figure 3: Clades of *C. auris*. Phylogenetic tree was created based on Maximum Likelihood of WGS of 304 *C. auris* genomes and *C. auris* is clustered into four major clades (clade I, II, III, IV) (Chow et al., 2020).

Studies on the gene sequences have shown that each clade is highly characterized by thousands of single-nucleotide polymorphisms (SNPs). However, within each clade, there's a low level of genetic diversity between the isolates, which insinuates that all four clades have possible emerged concomitantly and independently from each other [14], as depicted in Figure 4 . Recently, the first

case of *C. auris* in Iran was reported. It was revealed to be a genetically distinct isolate, which was proposed by Chow et al. (2019) to represent the fifth clade [19].

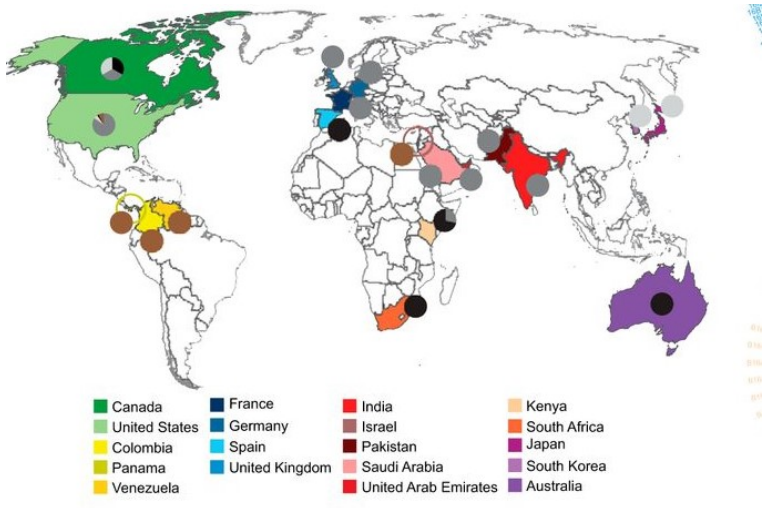

Figure 4: Geographical distribution of *C. auris* clades. The following colors display the different *C. auris* clades: clade I (dark grey), clade II (light grey), clade III (black), clade IV (brown) (Chow et al., 2020).

The five geographic clades of *C. auris* can be distinguished by their distinct genetic makeup. *C. auris* has emerged most prevalently on the Asian continent, as at least three clades are present (clade I, II and V) [19]. After its initial discovery in Japan, the fungal pathogen rapidly spread to other regions, causing major hospital outbreaks in Pakistan, India, and China [20]. Furthermore, *C. auris* had only emerged in 2 African countries thus far in 2018 [20]. The first reported isolate was revealed to belong to clade IV, yet the South African clade (clade III) is mostly present on this continent [21]. Previous studies suggested that clade III isolates often exhibit fluconazole resistance, while resistance against amphotericin B is rare. Meanwhile, in clade IV isolates, the highest percentage of resistance against echinocandins was recorded, while this rarely occurs in clade I and III [17].

C. auris has also made its entrance in Europe, North- and South America, and Australia [20]. In Europe, the ECDC recorded 620 cases between 2013-2017 in six countries: Germany, Norway, Spain, France, Belgium, and UK [22]. The first EU cases of *C. auris* candidemia were reported in Spain (2016), when four patients were hospitalized in the ICU. The strain proved to be affiliated with clade III [23]. In South-America, clade IV isolates were found in 2013 in a hospital in Venezuela [24]. Further advances in sequencing have elucidated many *C. auris* cases in other South American countries [20]. In the Northern counterpart, the four major clades seem to have established since 2017, suggesting that almost all *C. auris* isolates have been introduced in the USA

[16]. Noteworthy, the first cases of multi-drug resistant *C. auris* were reported in Canada in 2017 [25] and Central America in 2018 [26]. Meanwhile, in Australia, no cases were reported up until 2018. However, *C. auris* possibly could have remained undetected [20]. Yet, Heath et al. (2019) had recorded a case in Australia regarding a 65-year-old male who had undergone ICU treatments in Kenya. The isolates were revealed to be related to clade III [27].

1.2 New superbug on the block

Three major concerns are associated with the recently emerging superbug *C. auris*: misidentification, nosocomial transmission, and multi-drug resistance.

1.2.1 Misidentification

C. auris is commonly misidentified, allowing the pathogen to go undetected and spread. A contributing factor is the use of inefficient biochemical and phenotypical assays, such as VITEK-2 and API 20C. These systems have mistakenly identified *C. auris* as the closely related species *C. haemulonii, C. duobushaemulonii, C. pseudohaemulonii, and C. lusitaniae* [3]. Additionally, identification of *Candida* at species-level is not common, yet this should be a standard procedure as *C. auris* has species-specific characteristics. Furthermore, *C. auris* commonly exhibits MDR. [28], thus treating possible *C. auris* infections thoughtlessly with the wrong antifungal drugs can aggravate the problem [8].

Through reliable molecular sequencing techniques, such as qPCR/PCR and rDNA sequencing, the genetic loci of the D1/D2 region of the 26S rDNA and the internal transcribed spacer (ITS) could be targeted in an effort to differentiate *C. auris* from other closely related *Candida spp.* [29]. In addition, MALDI-TOF MS is widely used as an identification method, yet it's time-consuming as it relies on a database of reference spectra to compare the samples. However, some pre-existing databases lack spectra of *C. auris* isolates [30, 31].

1.2.2 Nosocomial transmission

In healthcare settings, *C. auris* is transmittable between patients via direct and indirect contact and may cause hospital outbreaks. It colonizes patients mostly on the skin and persists in healthcare environments for weeks after its initial colonization [32]. Similar to other *Candida spp.* such as *C. glabrata* and *C. albicans*, *C. auris* is an opportunistic pathogen [3]. However, *C. auris* acts completely differently in a hospital setting, compared to other *Candida spp.*, as it behaves more like

transmissible multi-drug resistant bacteria, such as carbapenemase-producing *Enterobacteriaceae* and *Staphylococcus aureus (MRSA)*. Therefore, precautions are required and similar measures to control infection have to be taken for *C. auris*, such as the use of chlorine-based disinfection and UV-C sterilization [33]. Additionally, chlorhexidine-based solutions seem to be effective for sterilization of equipment and disinfection of the skin. Common hygiene practices such as washing and disinfecting hands, isolation of infected patients, room disinfection, and contact precautions are also necessary to minimize the transmission of *C. auris* [33].

1.2.3 Multi-drug resistance

C. auris has developed resistance to all three major antifungal drugs, something that rarely occurs in other *Candida spp.* Evaluating the epidemiology of resistant *C. auris* proves to be challenging, as different studies present varying data regarding resistance emergence. In 2017, Lockhart et al. reported from a study including 54 isolates that 93% was fluconazole-resistant, 7% was resistant to echinocandins, and 35% showed reduced susceptibility to amphotericin B. Of these isolates 41% exhibited resistance to two different drug classes, of which 4% was even resistant to all three [14]. In addition, Chowdhary et al. (2018) collected 350 *C. auris* isolates over 8 years and found that 90% of the strains were resistant to fluconazole, 2% to echinocandins, and 8% to amphotericin B. Additionally, they uncovered that 25% of the isolates exhibited MDR to at least 2 classes of drugs, of which the most predominant combination was an azole and 5-fluorocytosine, followed by isolates that exhibited concurrent resistance to an azole and amphotericin B [34]. Generally speaking, resistance toward fluconazole in *C. auris* seems to be a recurring phenomenon.

1.3 Antifungal drugs

As the risk of invasive fungal infections and drug resistance is increasing, the search for new antifungal drugs has never been more important as of today. Fungi are eukaryotic by nature, which makes it more difficult to find compounds that specifically target fungi without affecting the host [35]. Each antifungal drug class will target specific cellular processes in the fungal pathogen, resulting in either killing the pathogen (fungicidal) or inhibiting its growth (fungistatic). Cellular processes that are interesting to target include the biosynthesis of RNA, the formation of the cell wall, and the function of the cell membrane [36]

1.3.1 Azoles

Azoles comprise the class of five-membered heterocyclic drugs, which contain two or three nitrogen atoms in the azole ring. A further distinction can be made for azoles with two nitrogens, which are classified as imidazoles, or three nitrogens, being triazoles [36].

Azoles specifically target 14α-lanosterol demethylase, the cytochrome P450 enzyme in fungi also known as Erg11, which is illustrated in Figure 5. This is an essential enzyme in the ergosterol biosynthesis pathway [36]. Ergosterol is vital for fungi, as it is the main component of fungal cell membranes and forms lipid rafts with lipids that allow signaling, mating, induction of stress responses, and nutrient transport [37, 38]. Besides, the presence of ergosterol in its membrane structures might have contributed to its evolutionary advantage, as ergosterol provides better protection against lipid peroxidation than cholesterol [39]. On the other hand, human cells remain unharmed by azoles due to the absence of ergosterol in human membrane structures. By binding 14α-lanosterol demethylase, azoles can efficiently inhibit the demethylation of lanosterol, causing a decrease in ergosterol levels inside the pathogenic yeast [40, 41]. Additionally, Erg3 and Erg6 mediate the production of a toxic, fungistatic sterol, namely 14α-methylergosta 8-24 (28) dienol, and therefore stimulate an alternate pathway through which azoles could target fungal pathogens. [40, 42]. Subsequently, azoles will also inhibit Δ^{22}-desaturation in the last few steps of the ergosterol biosynthesis pathway [41].

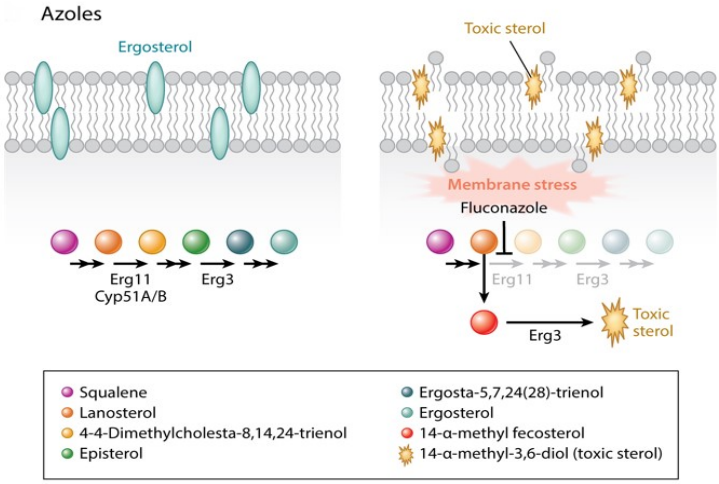

Figure 5: Azoles and their mode of action. Azoles target 14α-lanosterol demethylase, which is encoded by *ERG11* in *C. auris*. This inhibits the production of ergosterol. Furthermore, *ERG3* is activated and causes accumulation of a toxic sterol, which induces membrane stress (Shapiro and Robbins, 2011).

Additionally, azoles, and specifically miconazole, induce the generation of Reactive Oxygen

Species (ROS) [43]. Accordingly, François et al. (2006) showed that the miconazole-induced production of ROS in *C. albicans* is substantial for its antifungal activity [42]. Besides the inhibition of 14α-lanosterol demethylase, miconazole is also able to inhibit catalase and peroxidase, both of which break down hydrogen peroxide and peroxide radicals. As these enzymes are unable to perform their function, ROS levels in the cell will increase. Therefore, miconazole might display fungicidal effects [43].

1.3.2 Echinocandins

Echinocandins represent the class of cyclic hexalipopeptides [43]. These drugs are the recommended first-line treatment for invasive *Candida* infections [44, 45].

Echinocandins target the β-(1,3)-D-glucan synthesis in yeast, resulting in the inability to produce β-(1,3)-D-glucan in the cell wall, which leads to osmotic instability and eventually cell death [46]. This phenomenon, depicted in Figure 6, is achieved through the inhibition of β-(1,3)-D-glucan synthase. The enzyme constitutes a protein complex with Fks1, Fks2, and Fks3, respectively encoded by *FKS1, FKS2, FKS3*, and Rho1, which is the regulatory subunit [47]. It utilizes Uridine Diphosphate Glucose (UDP-glucose) to form β-(1,3)-D-glucan, which is an essential component of the fungal cell wall [36]. Therefore, targeting this molecule is ideal, as mammalian cells lack a fungal cell wall. Furthermore, lipopeptides are biosurfactants and therefore, absorption of these will change the properties of the fungal cell surface, such as hydrophobicity. The latter is related to adhesion- and other pathogenic processes [48].

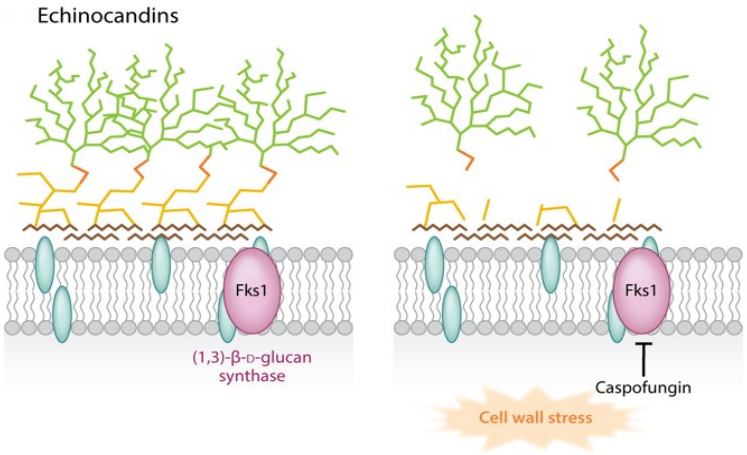

Figure 6: Mode of action of echinocandins. Echinocandins target β-(1,3)-D-glucan synthase, which is encoded by *FKS1* in *C. auris*, as non-competitive inhibitors. This causes a reduced cell wall integrity and increased cell wall stress, as β-(1,3)-D-glucan is an important component of the cell wall (Shapiro and Robbins, 2011).

The three most predominant echinocandins are micafungin, anidulafungin, and caspofungin. These antimycotics are derived from fungi, such as *Coleophoma empedri, Glarea lozoyenisi* and *Aspergillus nidulans* respectively [48]. However, the antifungal activity of this drug class differs significantly between *C. auris* and the other *Candida spp.* In *C. auris*, echinocandins behave fungistatically in concentrations at which they are fungicidal to other *Candida spp.* [46, 49, 50]. A study performed by Kovács et al. (2021). showed that *C. auris* could form aggregates in the presence of low concentrations of echinocandins that are not easily disrupted physically [49]. Additionally, higher echinocandin concentrations could stimulate the synthesis of chitin. The higher chitin content in the cell wall provides extra stabilization and reduces the impact of echinocandins [51].

1.3.3 Polyenes

Polyenes were one of the first antimycotics to hit the market and have been used ever since due to their efficiency. The most predominant drugs of this class are amphotericin B, nystatin, and natamycin, of which amphotericin B has the highest antimycotic activity. These amphiphilic polyketides were isolated from *Streptomyces spp.*, but are now chemically synthesized. They display broad-spectrum activities against well-known human fungal pathogens, in particular *Aspergillus, Candida, and Cryptococcus spp.* Furthermore, polyenes generally have a hydrophobic polyene tail and a hydrophilic region, containing a mycosamine group and polyol chain [52].

Rather than targeting an enzyme, polyenes bind to ergosterol to disrupt the cell membrane [52]. The most widely studied mechanism is the formation of ion-leaking pores due to the binding with ergosterol, destroying the proton gradient and inducing osmotic lysis, as depicted in Figure 7a [43, 53]. However, Gray et al. (2012) provided conclusive evidence that pore formation is not necessary for its fungicidal effect and the sole binding to ergosterol is enough to induce cell death [53].

Besides, other models regarding its antifungal activity have been suggested [54], such as the sterol sponge model, which is based on surface adsorption [52]. This was proven by Anderson et al. (2014), who performed NMR studies to determine the interaction between amphotericin B and ergosterol. Noticeably, they observed the formation of parallel aggregates of amphotericin B at the membrane level, which served as ”sterol sponges” by absorbing ergosterol from the membrane, as illustrated in Figure 7b [52, 55]. This would block membrane proteins that bind to ergosterol to guide several cellular processes that are ergosterol dependent. Considering the formation of amphotericin B aggregates, they also suggested that the toxicity of amphotericin B towards humans derives from the extraction of cholesterol by these aggregates [55]. However, the findings of

Anderson et al. (2014) should be reviewed as the ratio of ergosterol and phospholipids in the membrane differs significantly between *in vitro* experiments and the *in vivo* situation. Additionally, the amphotericin B aggregates would be saturated with cholesterol, as the concentration of the latter is higher in mammals and the highly rigid and hydrophilic fungal cell wall would block the passage of ergosterol, preventing the formation of aggregates [54].

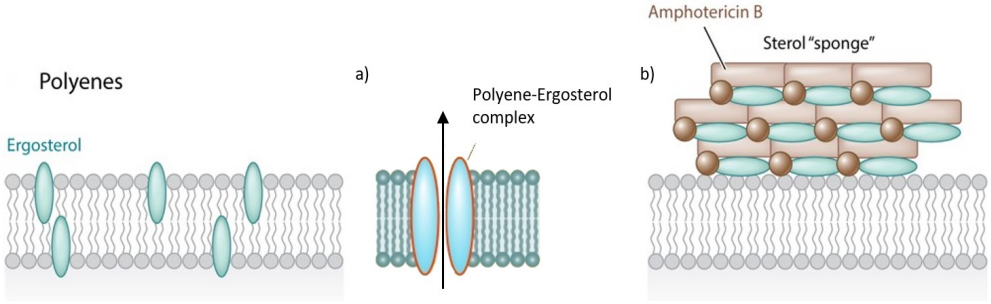

Figure 7: Polyenes and their mode of action. Polyenes perform their antifungal activity by a) binding to ergosterol, creating drug-lipid complexes that act as ion-leaking pores that can destroy the proton gradient and induce osmotic lysis. Additionally, studies suggested that polyenes can b) form sterol sponges by sequestering ergosterol, which will disrupt the cell membrane and result in cell death (Shapiro and Robbins, 2011; Robbins, 2017).

Amphotericin B is considered as the golden standard but exhibits low solubility in water, making drug absorption rather difficult. Therefore, it is regularly mixed with sodium deoxycholate, which forms lyophilizable complexes (AmBD). By adding glucose solution, the complexes could be resuscitated and form a micellular suspension, which could effortlessly be infused intravenously [43, 52, 56]. Another problem with amphotericin B is the induction of nephrotoxicity in host cells at high doses [54, 57]. Although amphotericin B is more likely to bind fungal ergosterol than mammalian cholesterol, cell membrane disruption still occurs in mammalian cells. By modifying the AmBD complexes into Lipid Formulations of amphotericin B (LFABs) through lipid-based delivery systems, not only the absorption is improved, but also the toxicity is reduced without altering its activity [57].

1.3.4 Pyrimidine analogues

5-Fluorocytosine is a fluorinated derivative of cytosine, synthesized in 1957 for its potential anti-tumor effects [58]. However, it was shown to exhibit efficacy against *Candida* and *Cryptococcus* invasive infections in mice [59], and therefore was used in an attempt to treat fungal infections in humans [60]. Nevertheless, due to the risk of developing resistance to this drug in monotherapy, the sole use of 5-fluorocytosine has been avoided. Studies have shown that 5-fluorocytosine in

combination drug therapies with either amphotericin B (to treat systemic mycoses), azoles, or even both show increased antifungal activity [61, 62].

The antifungal activity of 5-fluorocytosine can be characterized by two individual pathways, illustrated in Figure 8. Firstly, the drug is imported by cytosine permease into the fungal cell wall to be deaminated to 5-fluorouracil (5-FU) by cytosine deaminase [63]. Inside the fungal cells, 5-FU will exhibit its antifungal activity through two mechanisms [62]. The first mechanism involves the conversion of 5-FU to 5-fluorouridine triphosphate (5-FUTP), through 5-fluorouridine monophosphate (FUMP) and 5-fluorouridine diphosphate (FUDP), which is then incorporated into the RNA rather than uridylic acid. This disturbs the aminoacylation of tRNA and therefore, blocks protein synthesis [64]. The second mechanism involves the conversion of 5-FU to 5-fluorodeoxyuridine monophosphate (FdUMP) [64], which is an inhibitor of thymidylate synthetase, an essential enzyme for DNA biosynthesis as it produces thymidine [63].

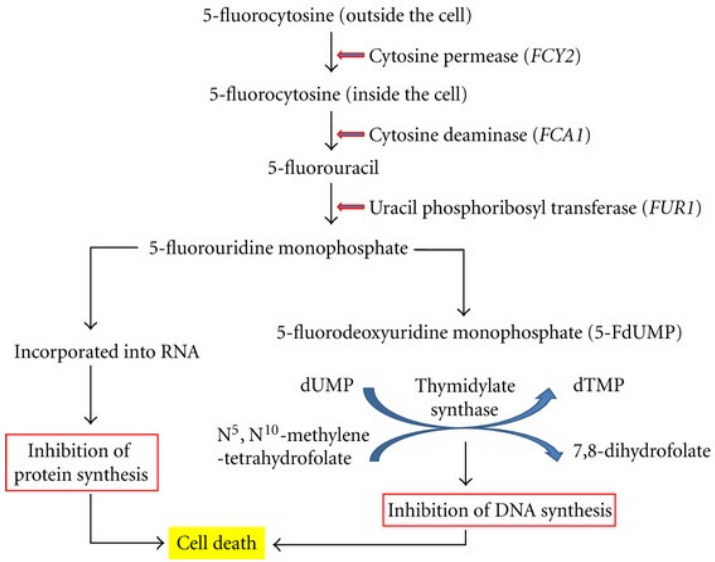

Figure 8: Schematic diagram of the mechanism of action of 5-fluorocytosine. Administration of 5-fluorocytosine will eventually lead to cell death through two different pathways, causing either inhibition of protein synthesis or DNA synthesis. Mutations in the genes that transcribe essential enzymes in the pathway (italic capital letters) will evoke 5-fluorocytosine resistance (Kabir and Ahmad, 2013).

1.3.5 Novel drugs in the pipeline

Ibrexafungerp (IBX, formerly SCY-078) is the newest first-in-class antifungal of the triterpenoids drug class [65]. Produced by SCYNEXIS, it displays promising efficacy against *Aspergillus* and *Candida* [66], including MDR *C. auris* [67, 68], both *in vitro* and *in vivo* [66]. Similar to

echinocandins, IBX inhibits β-(1,3)-D-glucan synthesis by impeding β-(1,3)-D-glucan synthase, a characteristic enzyme of lower eukaryotes. Therefore, IBX acts fungal-specific and might exhibit lower toxicity in mammals [69]. Other characteristics that distinguish IBX are its safety profile, oral intake, convenient tissue penetration, and improved activity at lower pH levels. The latter makes IBX suitable for the treatment of vulvovaginal candidiasis (VVC), which is mainly caused by *C. albicans* at acidic pH levels (4.5) in the vaginal area [66, 70]. Momentarily, IBX is in the third phase of its clinical trials [71] but has already hit the market for VVC [72]. Its antifungal activity against *C. auris* has been studied *in vivo* in mice. A reduced kidney fungal burden and stable antifungal activity were observed, with MICs ranging between 0.25 - 2μg/mL. These findings imply that IBX would be a promising drug to treat *C. auris* once it hits the market [73].

Another novel antimycotic that is currently in Phase 2 clinical trials is Appili's **ATI-2307** [74]. The arylamidine exhibits broad spectrum antimycotic activity against MDR *Candida*, *Cryptococcus*, and *Aspergillus*, both *in vivo* and *in vitro*. It presents an MIC range against *Candida spp.* between 0.00025 to 0.0078 μg/mL, revealing its potential in the treatment of *C. auris* [74, 75]. ATI-2307 selectively inhibits complexes III and IV of the mitochondrial respiratory chain. This unique mode of action allows for resilience towards developing already existing resistance mechanisms [76, 77]. Once it hits the market, it could potentially be an efficient injectable drug to treat cryptococcosis, candidiasis, and aspergillosis [75, 76].

Fosmanogepix (FMGX) is another first-in-class, broad-spectrum antifungal, currently in its second phase of clinical trials [78]. It's an N-phosphonooxymethyl prodrug, under the ownership of Pfizer, which can be used for treating *Aspergillus, Candida*, and other rare molds. It has an unique mode of action, as it is administered as a prodrug, which is then rapidly metabolized to the active drug compound manogepix (MGX) by host phosphatases [79]. MGX inhibits the fungal enzyme Gwt1 in the glycosylphosphatidylinositol (GPI)-anchor biosynthesis. Gwt1 is an essential inositol acyltransferase, responsible for anchoring mannoproteins to the cell wall and membrane of fungi. Through GPI-anchored mannoproteins, fungi can adhere to both mucosal and epithelial surfaces inside the host [80]. Due to this newfound mechanism, FMGX exhibits a high efficacy towards drug-resistant strains, such as echinocandin-resistant *Candida* [81]. Additionally, PIGW, the mammalian ortholog of Gwt1, is insensitive to MGX, as FMGX only targets fungal inositol acetylation, further revealing its appeal in treatment schemes as it is mostly safe for humans [82]. FMGX can be administered orally, as well as intravenously, providing another benefit for patients [78].

1.3.6 Repurposed drugs

Drug repurposing is a promising strategy to uncover new applications of existing drugs that have already been approved. Through this process, various drugs have been found that exhibit antifungal activity against *C. auris* [83]. De Oliveira et al. (2019) found 27 active compounds from the Prestwick Chemical library, coming from various therapeutic classes. Of those, ten were used in broth microdilution assays (BDA), described by EUCAST, to determine growth inhibiting activity against *C. auris*. Seven compounds exhibited antifungal activity *in vitro*, namely ciclopirox ethanolamine, ebselen, suloctidil, tamoxifen citrate, thiethylperazine dimalate, trifluoperazine dihydrochloride, and pyrvinium pamoate, of which ebselen was the most active compound [84]. Additionally, they screened the Pathogen Box® chemical library of the Medicines for Malaria Venture for active compounds against *C. auris*. From CLSI-based BDA, iodoquinol and miltefosine emerged as the two most inhibitory compounds [85]. Another study performed by Wall et al. (2018) delivered similar results. Using CLSI-based methodologies and *C. auris 0390* strain, which is intrinsically resistant to fluconazole and amphotericin B, and exhibits reduced sensitivity to echinocandins, 27 compounds were found to impede growth by 70%. Antifungal activities of some of these were previously already determined, and similar to de Oliveira et al. (2019), ebselen emerged as the drug with the most inhibitory activity, as it eliminated growth [86]. Additionally, alexidine dihydrochloride was found to exhibit activity against *C. auris* as well [83].

1.4 Antifungal (multi-)drug resistance

Repeated use or long-term therapy with antifungal drugs inevitably stimulates the development of resistance mechanisms. This refers to the ability of fungal cells to exhibit growth at higher drug concentrations than the Minimal Inhibitory Concentration (MIC). Nevertheless, antifungal resistance poses a serious threat to humanity due to the limited availability of drugs. Therefore, expanding our knowledge of these resistance mechanisms is of high importance. A summary of the resistance mechanisms to the three major antifungal classes is depicted in Figure 9 on page 17.

1.4.1 Molecular mechanisms of Azole resistance

Azole resistance occurs at insufficient intracellular drug concentrations [87]. Lockhart et al. (2019) suggested that the most prominent azole resistance mechanisms in *C. auris* are (1) overexpression of drug efflux pump genes (2) target alteration, and (3) overexpression of *ERG11* [88].

Decrease in intracellular drug concentration

Two independent drug efflux systems were identified: the ATP-binding cassette (ABC) superfamily and the major facilitator superfamily (MFS) [89]. The ABC transporter complex functions through ATP hydrolysis, which releases energy for transport across the membrane. ABC proteins are encoded by *CDR* (candida drug resistance) genes [87, 89]. Accordingly, *CDR1* and *CDR2* encode ABC transporters in *C. albicans* and homologs of these were found in *C. auris*. The expression of these genes is enhanced by Tac1 (transcriptional activator of CDR genes) through the binding of DRE (drug response element) in the promotor region of *CDR1* and *CDR2* [90]. Correspondingly, an ortholog of *TAC1* was found to confer azole resistance in *C. auris*, namely *TAC1b* [91]. Several gain-of-function (GOF) mutations have been annotated in *TAC1b* that cause constitutive expression of *CDR1* and *CDR2* and thus an increased drug efflux: F214L, S611P [92], and A640V, R495G, F214S [91]. MFS transporters, on the other hand, use the proton gradient generated across the membrane to power transport [41, 89]. In *C. albicans*, overexpression of *MDR1* (multidrug resistance 1) appears to confer azole resistance [41, 87, 89]. Rybak et al. (2019) determined induced expression of *MDR1* in fluconazole-resistant *C. auris* strains, yet deletion of the gene had only little effect on azole sensitivity [93]. However, in combination with *CDR1* GOF mutations, azole resistance increased by 64 to 128-fold [93, 94].

Target alteration and *ERG11* overexpression

Azoles target 14α-lanosterol demethylase, which is encoded by *ERG11*. Therefore, mutations in *ERG11* can alter its protein structure, resulting in a reduced affinity to azoles and thus resistance [87]. In *C. auris*, amino acid substitutions in Erg11 such as F126L, Y132F, and K143R, were found to confer azole resistance [14, 34, 95, 96]. Additionally, upregulation of *ERG11* was also found to cause increased azole resistance. This was studied by Flowers et al. (2012), who observed a 2-fold overexpression of *ERG11* in fluconazole-resistant *C. auris* isolates. They revealed that overexpression of *UPC2*, which encodes a Zn-cluster transcriptional regulator, was the cause of the increased *ERG11* mRNA levels [97].

Other azole resistance mechanisms

Aneuploidy of the left arm of chromosome 5 can result in the formation of an isochromosome, in which *TAC1b* and other genes associated with azole resistance, such as *NCP1* and *ERG9*, are duplicated. This is induced by azole exposure and consequently, the copy number of these genes increases, causing an increase in azole resistance [14, 98, 99].

1.4.2 Molecular Mechanisms of Echinocandin Resistance

Although resistance against echinocandins in *Candida spp.* occurs less often, *C. auris* strains that exhibit a reduced sensitivity to echinocandins have emerged [14, 100, 101]. Echinocandin resistance is mostly conferred by mutations in *FKS1* and/or *FKS2*, which encode for the catalytic subunit of the β-(1,3)-D-glucan synthase [47].

Genomic alterations in *FKS* genes

Mutations in *FKS1* are the main source of echinocandin resistance in *C. auris*, as they cause conformational changes in β-(1,3)-D-glucan synthase. This results in a reduced affinity between the target and the drug. A significant phenomenon in *C. albicans* is the reduced fitness due to the impeded glucan biosynthesis. Amino acid substitutions occur most often in three conserved, species-specific ”hot spot” (HS) regions of the *FKS1* gene, named HS1, HS2, and HS3 [45, 102, 103]. For *C. auris*, HS1 includes amino acids 635-648, H2 1351-1354, and HS3 contains aa 686-696 [99]. Lockhart et al. (2019) discovered two mutations in *C. auris*, S639P and S639F [88], which were later confirmed in mouse models and provided further evidence for echinocandin resistance in *C. auris* [104]. In other *Candida spp.*, different substitutions were found, such as F625S and S629P in *C. glabrata* [105], and F641S, S645P, and S645Y in *C. albicans* [106], which were all linked to echinocandin resistance.

Alteration of chitin synthesis

Walker et al. (2008) observed an increased chitin content in the cell wall of *C. albicans* at low levels of echinocandins. This was induced by chitin synthases Chs2 and Chs8 and simultaneously impeded the impact of echinocandins on the cells, ultimately reducing sensitivity to these drugs [107]. Consequently, this was also observed in *C. auris*, but coordinated by Chs1 instead [108]. Furthermore, an increase in chitin was associated with *FKS1* mutations as well [107, 108], as higher chitin contents, resulting in a thicker cell wall, were observed in homozygous fks1 *C. albicans* mutants. Additionally, they exhibited attenuated virulence, which was inversely related to the chitin content. These findings provide evidence that the echinocandin-resistant fks1 mutants are evolutionary at a disadvantage in the absence of echinocandins [109]. Additionally, chitin levels are regulated by PKC, Ca^{+2} calcineurin and HOG pathways [110] in both *C. albicans* and *C. auris* [111]. Remarkably, chitin synthesis inhibitors act synergistically with echinocandins to reduce the Eagle effect, which is mostly present in caspofungin. This refers to the growth of echinocandin susceptible strains at MIC exceeding drug concentrations [112].

1.4.3 Molecular Mechanisms of Polyene Resistance

Acquired resistance to amphotericin B, either by prophylaxis or extensive therapeutic use, occurs very rarely in *Candida* [52, 113]. In *C. auris*, resistance occurs in 30% of the clinical isolates [14]. Possible hypotheses for this infrequent occurrence could be that (1) amphotericin B targets the important membrane component ergosterol rather than an essential enzyme [52], and (2) resistance is often associated with a reduced fitness cost [113]. Accordingly, resistance can be conferred by changes in the sterol composition of the cell membrane due to mutations in ergosterol biosynthesis genes [114, 115]. Consequently, less ergosterol is available for binding of amphotericin B, which confers resistance to this drug [87, 116]. Another mechanism depends on the production of reactive oxygen species (ROS), which induces oxidative stress [52, 117, 118, 119].

Mutations in ergosterol biosynthesis genes

Mutations in ergosterol biosynthesis genes (ERG) have been found to confer amphotericin B resistance [99, 120]. Many reports have concluded that loss-of-function (LOF) mutations in *ERG* genes, such as *ERG1, ERG2, ERG3, ERG4, ERG6*, and *ERG11* can cause a reduction of ergosterol in the membrane or an exchange for other sterols, e.g. lanosterol, in the cell membrane [47, 113, 115]. Furthermore, mutations in a homolog of *FLO8* have been discovered in amphotericin B resistant C. auris strains. As Flo8 can induce *ERG11* expression, this could provide evidence for a potential link between *FLO8* and amphotericin B resistance.

Reduction of oxidative stress

Polyenes can induce oxidative stress due to the production of ROS, which leads to cell death. This could be caused by (1) binding of amphotericin B to the membrane [117], (2) auto-oxidation of amphotericin B which results in free radicals [118], or (3) stress caused by the drug itself [119]. However, reduction of ROS could alleviate oxidative stress, preventing cell death. This was studied by Blum (2007), who observed high levels of catalase in intrinsically amphotericin B resistant *A. terreus*. Catalases can alleviate oxidative stress by decomposing hydrogen peroxide in the cells, preventing cell death [52, 121, 122]. This detoxification mechanism has not been studied yet in *C. auris*. However, this was observed in *C. albicans*, in which signaling pathways were activated that stimulate adaptive mechanisms that will detoxify oxidative stress and repair the damage [123]. The process is mediated by Cap1 (AP-1-like transcription factor), which will induce the expression of catalase *CAT1* for detoxification of hydrogen peroxide [123, 124], and *TRX1, and TRR1* for recovery of redox homeostasis [123, 125].

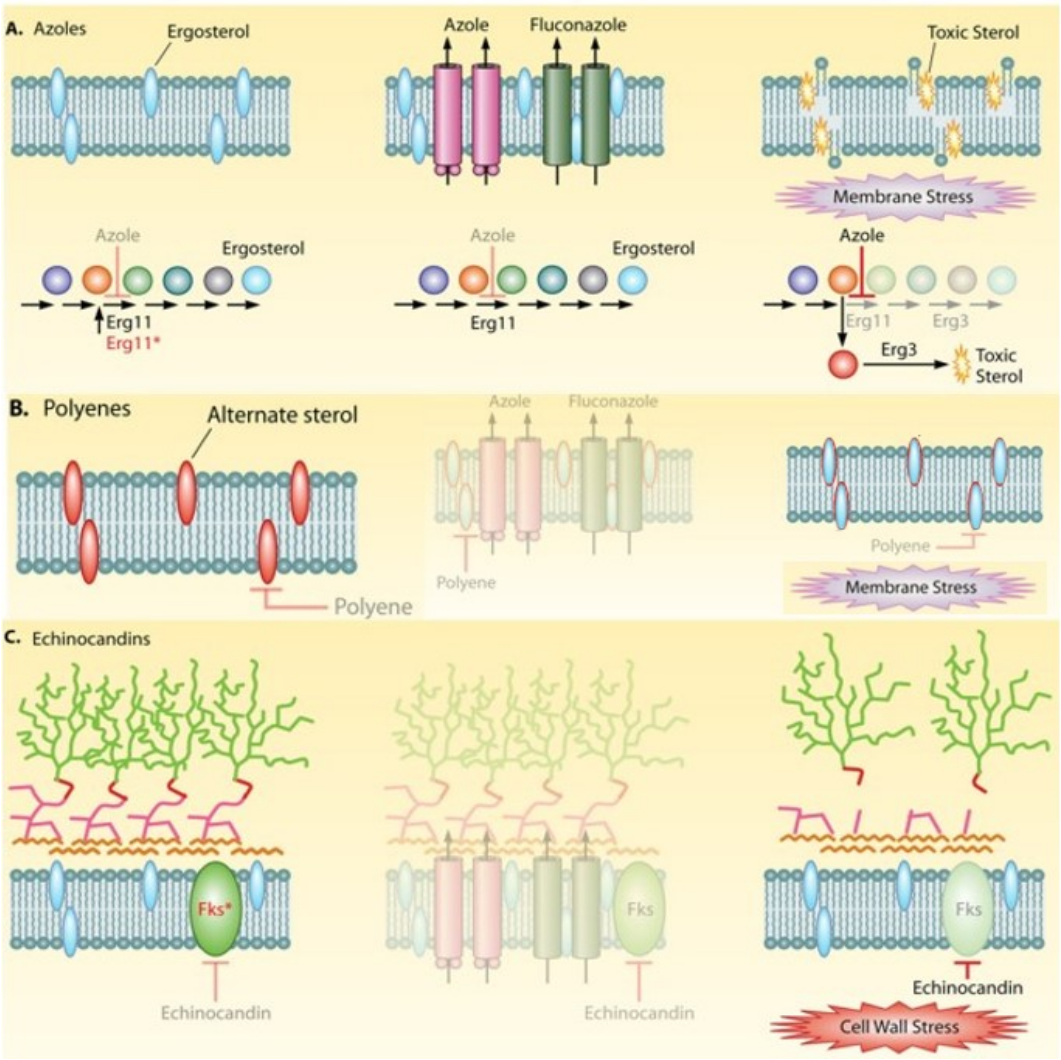

Figure 9: Summary of the main resistance mechanisms against azoles, echinocandins and polyenes. Detailed descriptions of the resistance mechanisms were given in the text above. Translucent images and texts illustrate mechanisms that are irrelevant for the mentioned drug class (adapted from Shapiro and Robbins, 2011 and Cowen et al., 2015).

1.5 Collateral sensitivity: a trade-off mechanism

Collateral sensitivity (CS) refers to a trade-off mechanism in which resistance mutations will confer resistance towards one drug and consequently, increase susceptibility to another drug [126]. As a result, mono-resistant cells for drug A could be eradicated more efficiently when using drug B. Therefore, through CS, resistance emergence in cells may be avoided when using two drugs that exhibit reciprocal or one-directional CS [126, 127, 128]. Thus, studies regarding CS mechanisms in *C. auris* are of great importance as the threat of the superbug is looming continuously.

1.5.1 Collateral sensitivity in bacteria

The first occurrence of CS in *E. coli* dates back to 1952, as Szybalski and Bryson described hypersensitivity to other antibiotics in chloromycetin-resistant *E-coli* [129, 130, 131]. Later, evidence was provided for the use of CS in multi-drug strategies to avoid antibiotic resistance (ABR) development [128, 132]. Lazar et al. (2013) discovered a CS mechanism in aminoglycoside-resistant *E. coli* strains caused by mutations in *trkH*. *trkH* encodes an ion transporter that reduces the proton-motive force (PMF) and thus the uptake of drugs across the inner membrane. Additionally, these *trkH* mutations would impede the expulsion of other antibiotics by PMF-dependent efflux pumps, such as AcrAB efflux pumps, resulting in an increased sensitivity to those antibiotics by 2- to 4-fold. Therefore, CS in these aminoglycoside-resistant strains, which carry *trkH* mutations, was believed to be associated with the AcrAB efflux system [132].

Another observed CS mechanism involved the *TET* genes, which encode proteins that transport tetracycline out of the cell. By expressing these genes extrachromosomally in gram-negative bacteria, efflux mechanisms were stimulated and therefore, tetracycline resistance could be conferred [133]. Additionally, these bacteria exhibited increased susceptibility to aminoglycoside antibiotics due to the stimulated uptake of these drugs [133, 134]. Merlin et al. (1989) observed no changes in the membrane potential that could have caused the enhanced uptake and therefore, suggested that it could either be due to (1) the increased availability of carriers in the membrane or (2) reducing the lowest membrane potential that is necessary for the uptake [134].

From there onwards, many experts have hypothesized possible ways resistance mechanisms could confer CS to other drugs: either by (1) an increased uptake/reduced efflux of the drug, (2) enhanced chemical activity of antibiotics by specialized proteins, (3) alternated regulatory pathways and cellular processes that increase the toxicity of the drug, or (4) enhanced binding of antibiotics to targets [130]. Nevertheless, clinical studies of CS have not been performed yet. At first hand, CS seems very promising as it allows growth inhibition even at low drug concentrations and more effective killing of resistant strains. However, CS has been evaluated under laboratory conditions, and consequently, possible clinical effects could be deduced [130]. These studies suggested that the increase in drug sensitivity was small [128, 132], CS was often not evolutionary conserved [135, 136], the effectiveness of CS could be reduced due to the emergence of escape mutants [137], and concentrations at which drugs were applied in laboratory conditions were too toxic in the clinic [130, 136].

1.5.2 Collateral sensitivity in tumor cells

Chemotherapy is currently the most effective treatment for tumors, yet the occurrence of drug resistance contributes to 90% of treatment failures [131]. In tumor cells, the acquired MDR can occur in many ways. By identifying CS agents, MDR can either be prevented through adjuvant delivery during chemotherapy or re-sensitization by selectively killing the resistant tumor cells in the heterogenous population [131].

MDR in tumors is prominently caused by overexpression of ABC transporters that function as drug efflux pumps in the plasma membrane, decreasing the therapeutic concentration of anti-cancer drugs intracellularly [127, 138]. The most studied transporter is P-glycoprotein (P-gp, ABC1, MDR1), which has a low chemotherapy response [139]. Many anti-cancer drugs used in the clinic are substrates of this transporter, such as paclitaxel, doxorubicin, and verapamil [127, 138, 140]. In some tumors, overexpression of P-gp is associated with CS, as some resistant tumor cell lines exhibit hypersensitivity to drugs that are not lethal to normal tumor cells. Several studies have demonstrated an increased sensitivity to verapamil in P-gp-expressing cells compared to P-gp negative cells [141, 142]. In this mechanism, verapamil will stimulate ATPase activity of P-gp1 by increasing ATP hydrolysis intracellularly through futile cycling. The resistant cells lack the ability to replenish the ATP supply, and therefore, experience oxidative stress due to the increase in ROS production, ultimately resulting in apoptosis [131, 138, 143]. Furthermore, cells that overexpress P-gp were thought to be susceptible to compounds that disturb cellular metabolic pathways, such as glycolysis [131]. This hypothesis was supported by two findings: (1) 2-deoxy-D-glucose (2DG), an antimetabolite of glycolysis, could mimic glucose deprivation in P-gp expressing cells, selectively killing these tumor cells by inducing oxidative stress [144], and (2) inhibitors of the mitochondrial electron transport chain, including antimycin A and rotenone, could enhance the 2DG-induced oxidative stress [145]. Furthermore, for some CS compounds, it was proven that they could alter the biophysical properties of the membrane in P-gp-expressing cells, further contributing to CS. Pentazocine and verapamil were able to reduce membrane fluidity in tumor cells. However, P-gp does not directly contribute to the changes in membrane fluidity but can make the cells more susceptible to these membrane perturbations [131, 146].

1.5.3 Collateral sensitivity treatment re-design: drug cycling

CS can be exploited to prevent the development of MDR. One way to make use of this phenomenon is drug cycling, which is the scheduled rotation of drugs that exhibit CS towards each other [128, 147, 148], whether this is reciprocal or one-directional [128, 147, 148, 149]. Ideally, these drugs

have different modes of action so that cells are optimally targeted [147]. The main takeaway of this treatment strategy is the decrease in resistance emergence as drug exposure is limited and resistant strains might be eradicated by the drug to which CS is exhibited. During the cycling scheme, one of the drugs is removed from the treatment temporarily, impeding resistance development towards that cycled agent. As resistance might be characterized by fitness costs in absence of the drug, the resistant strains might be outcompeted by the non-resistant strains [128, 147].

CS-based drug cycling can result in two possible outcomes, both assuming reciprocal CS, as depicted in Figure 10. In scenario a, drug A (here, CAS) is administered and induces resistance. This scenario assumes that the selection pressure of the drug is not high enough to either eradicate or evolve all wt strains. Therefore, a wt subpopulation continuously survives throughout the cycle, even when drug B (AMB) is administered. However, high selection pressure is preferred, so that only drug A resistant strains survive the drug treatment, allowing eradication of the whole resistant population as they display CS towards drug B. In scenario b, a high selection pressure of drug A is assumed, resulting in the survival of only drug A resistant strains. By cycling to drug B, drug A resistant strains will most likely die, as they exhibit CS towards drug B. Now, only drug B resistant strains will survive drug B treatment. Afterwards, the initial drug A is applied again until the emergence of resistant clones has slowly decreased and the complete population is eventually eradicated.

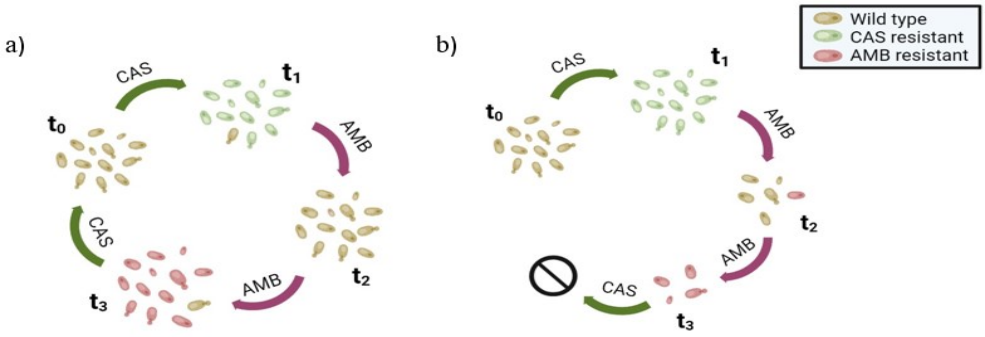

Figure 10: Hypothetical drug cycling schemes involving two drugs that exhibit CS reciprocally. Drug cycling could a) select for a wt population when the selection pressure of the drugs is low. Strains with MIC_{wt} survive throughout the cycle, while resistant strains are eradicated due to the presence of CS. In b) a high selection pressure is assumed and strains either become resistant or die. Consequently, resistant strains are eradicated throughout the cycle as the drugs exhibit CS.

Imamovic and Sommer (2013) suggested that CS-based drug cycling schemes might be effective to circumvent drug resistance development in bacteria. They evolved *E. coli* strains to become resistant to 23 antibiotics (AB) that are frequently used in the clinic. A network of collateral

sensitivity (CS) and cross-resistance (XR) was mapped of the resistant strains against different AB and two-drug combinations which exhibited reciprocal CS were chosen to design cycling schemes. Aminoglycosides and β-lactams, namely gentamicin (GEN) and cefuroxime (CXM) respectively, were selected to perform the cycling scheme. They labeled and evolved wt *E. coli* towards GEN during an exposure period of 8 days to obtain GEN-resistant strains that exhibited a 32x MIC*wt*. The CFP-labeled GEN-resistant strains were mixed with YFP-labeled wt cells and exposed to CXM. As a result, all the CFP-labeled, GEN-resistant cells were killed, leaving the wt cells unharmed. At the same time, wt cells were also evolved for CXM and treated with GEN, which also resulted in the total killing of CXM-resistant strains and allowed the wild-type cells to survive. This observation provided support for the theory that CS-based treatment would not only avoid resistance emergence but also increase the chances of complete eradication of resistant strains [128].

They also provided a rationale for the use of drug cycling in a clinical setting, in which complete eradication of the pathogen is favorable. Most often, drug concentrations higher than the MIC_{wt} are used to kill pathogens. In their study, they have determined the efficacy of 16x MIC_{wt} concentrations of GEN or CXM against both wt *E. coli* strains and resistant strains of either drug. In both scenarios, the resistant strains were more susceptible to the other drug than the wt, as they were eradicated quicker during treatment. This outcome suggested that CS in the paradigm of drug cycling could be used in the clinic, as it provides more effective eradication of resistant pathogens [128].

CS-based drug cycling in tumors

Drug cycling is also applicable in tumors. However, an important distinction between bacteria and fungi is that tumors are subjected to highly dynamic clonal evolution [150]. This model, combined with chromosomal instability which was first observed by Negrini et al. (1998), explains the heterogeneity in tumors [150, 151]. Tumors consist of subclones, all derived from the same clone but garnered different mutations throughout tumor progression. Heterogeneity subjects the subclones to selective pressure, as some have an evolutionary advantage over others [150, 151, 152, 153]. Furthermore, during tumor progression, clonal evolution might present temporal vulnerabilities [153]. This hypothesis is supported by previous findings in bacteria, which implied that acquisition of resistance mutations may induce reduced fitness due to cost compensation [154], In this case, when exposed to drug A, subclones might develop resistance to this drug, while simultaneously acquiring CS to other drugs. This would allow for a treatment strategy with higher efficacy but only during a time-limited window during the tumor progression period. This

phenomenon was termed ”temporal collateral sensitivity” by Zhao et al. (2016) [153].

Zhao et al. (2016) explored the concept of temporal CS in tumor populations by developing a mathematical model to examine the effects of fitness on clonal evolution. This model verified the theory and encouraged further screening of cell lines, which were made resistant to BCR-ABL1 inhibitors (dasatinib, bosutinib) in a preclinical Ph+ ALL (acute lymphoblastic leukemia) model [153]. This model is characterized by its rapid relapse after treatment and selection for BCR-ABL1 mutations [155]. A single missense mutation was found in *ABL1*, namely V299L, which was accompanied by CS against four drugs: crizotinib, cabozantinib, foretinib, and vandetanib. Through RNA-seq and other analyses (e.g. phenotypic, docking) it was found that the increased sensitivity was caused by on-target Abl1 inhibition, conferred by the V299L mutation. Eventually, *in vivo* experiments were carried out by injecting either wt *BCR-ABL1* or the mutant V299L into syngenic mice. V299L mutant mice exhibited lower tumor burden, reduced spleen size and fitness, and a higher survival rate upon treatment with either foretinib or vandetanib. Lastly, sequential drug administration was performed. The initial selection with *BCR-ABL1* inhibitors, followed by non-ABL1 targeting compounds resulted in the preferential evolution towards V299L mutants with either a reduced or retained CS towards vandetanib. On the contrary, selection with non-ABL1 targeting compounds first, followed by treatment with dasatinib led to the occurrence of other dominating resistant subpopulations which outgrew the V299L mutants [153]. Although true cycling schemes weren’t performed here, the sequential administration of the drugs does imply that the order in which the drugs were applied, can affect the cells.

2. Research Objectives

Drug cycling, which involves the sequential administration of drugs, might be a promising treatment strategy to suppress drug resistance development when these drugs exhibit collateral sensitivity reciprocally or one-directionally, as shown in tumors and bacteria. Therefore, the main aim of this project entails the design and validation of drug cycling schemes based on CS, to reduce resistance development in *C. auris*.

The first objective includes the determination of survival, resistance emergence, and dose-dependent resistance trends of antifungal drugs. The percentage of resistant strains, relative to the percentage of survival, will be evaluated, as well as the level of resistance and the rate of its development. This data can be obtained by performing high-throughput *in vitro* experimental evolution in four different concentrations and screening the experimentally evolved strains afterwards.

Subsequently, CS and XR will be mapped, which is the second objective. For this, susceptibility assays will be conducted between drug-resistant strains, using both antifungal- and repurposed drugs. Different parameters of evolutionary responses such as MIC_{50} and AUC_{BDA} will be investigated. By calculating the area under the curve (AUC), the growth of the cells and efficacy of the drug at each concentration are taken into account when determining either CS or XR.

The third objective involves testing CS drug pairs in cycling therapy with wild type *C. auris* strains. Drug pairs will be selected based on one-directional and/or reciprocal CS, in which resistant strains against one drug will exhibit increased sensitivity towards another drug, one-directionally or reciprocally.

Additionally, the genomic signature of resistance and CS in *C. auris* will be investigated by performing targeted sequencing of genes of interest (GOI). These GOI will be selected based on prior knowledge of resistance mutations in *C. auris* and other *Candida spp.* Mutations in the experimentally evolved strains in monotherapy will be looked for and their functional effects on the protein will be predicted. This would further enhance our knowledge on how resistance against some drugs can be developed in *C. auris*.

3. Materials and methods

3.1 Strains and growth conditions

The pan-susceptible *C. auris* reference strain B8841 (clade I) was used to conduct all experimental work. Cultures of *C. auris* were grown at 37°C on Yeast Peptone Dextrose (YPD) agar (2%), containing 2% glucose, 1% yeast extract and 2% peptone. Overnight cell cultures were prepared in RPMI-MOPS (2% glucose) and incubated at 37°C in a shaking incubator. MOPS buffered (pH 7) RPMI 1640 medium was used to conduct broth dilution assays (BDA) and evolution experiments. Single colony strains were stored at -80°C in RMPI-MOPS medium, with 25% glycerol.

3.2 Antifungal and repurposed drugs

Drugs that were used were depicted in Table 1, their modes of action in Table A1 (Addendum).

Table 1: Selected antifungal and repurposed drugs with their abbreviation, indication, distributor and solvent.

Drug compound	Abbr.	Indication	Distributor	Solvent
5-fluorocytosine	5-FC	Antifungal (pyrimidine analogue)	Sigma	DMSO
Alexidine dihydrochloride	ALX	Antibacterial/Anticancer	Sigma	DMSO
Anidulafungin	ANF	Antifungal (echinocandin)	Sigma	DMSO
Amphotericin B	AMB	Antifungal (polyene)	Sigma	DMSO
Caspofungin	CAS	Antifungal (echinocandin)	Sigma	MQ
Ciclopirox ethanolamine	CPX	Antibacterial/Antifungal	Selleckchem	DMSO
Chlorhexidine	CHX	Antibacterial	Sigma	DMSO
5,7-Diiodo-8-hydroxyquinoline	DHQ	Antiprotozoal	Sigma	DMSO
Ebselen	EBS	Anti-inflammatory	Sigma	DMSO
Fluconazole	FLU	Antifungal (azole)	Sigma	MQ
Geldanamycin	GEL	Anticancer	Sigma	DMSO
Ketoconazole	KTO	Antifungal (azole)	Sigma	DMSO
Micafungin	MCA	Antifungal (echinocandin)	Sigma	MQ
Nikkomycin Z	NKZ	Antifungal	Sigma	MQ
Nitroxoline	NIT	Antibacterial	Sigma	DMSO
Oleylphosphocholine	OPC	Antiparasitic (anti-leishmanial)	Dafra pharma	MQ
Posaconazole	POS	Antifungal (azole)	Sigma	DMSO
Pyrvinium pamoate salt hydrate	PAM	Antiparasitic (antihelmintic)	Sigma	DMSO
Suloctidil	SLC	Antiplatelet	Selleckchem	DMSO
Terbinafine hydrochloride	TRB	Antifungal	Sigma	DMSO

3.3 Antifungal drug susceptibility testing

MIC_{50} values were determined through BDA. Additionally, amphotericin B susceptibility was determined by ETEST® strips (bioMérieux).

3.3.1 Broth Dilution Assay (BDA)

The BDA protocol was adapted from the reference method suggested by CLSI [156] and used to determine the MIC_{50} of drugs. Drug dilutions were prepared ranging from 0.06 μg/mL to 16 μg/mL in a two-fold dilution series (or 0.004% to 1% for CHX and 0.125 μg/mL to 64 μg/mL for GEL) in maximum 1% DMSO in 96-well microtiter plates with layout depicted in Figure 11.

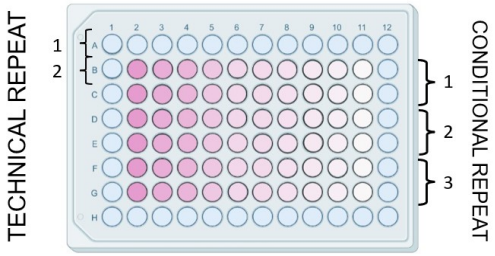

Figure 11: 96-well plate layout for BDA. The layout allows for 3 conditional repeats, with 2 technical repeats for each of them. The drug concentrations range from 0.0625-16 μg/mL (except for CHX: 0.004-1 μg/mL, GEL: 0.125-64 μg/mL).

Cell suspensions containing 100-500 cells were added into the wells in a final volume of 200μL. Plates were incubated at 37°C for 48 hours. Additionally, controls of the cell suspensions were made by plating out 20 μL on YPD agar and incubating them at 37°C for 48 hours. This was done to check for contamination and confirm correct cell dilutions (20-100 colony forming units (CFUs) per 20μL). Growth of the strains in the BDA plates was determined based on spectrophotometric (OD_{600}) determination using Synergy H1 (Biotek™). Furthermore, approximately 1μL of culture in each well was spotted onto YPD agar using a 96-well plate replicator.

3.3.2 ETEST® strips (bioMérieux)

Cell suspensions of $5x10^6$ cells were prepared in PBS 1X. Two different strains could be applied on round YPD agar plates by using cotton swabs. The ETEST® strip was then placed in the middle of the plate, touching both cell streaks. After an incubation period of 48 hours at 37°C, the intersection of the growth inhibition zone indicates the MIC.

3.4 Determine parameters of evolutionary responses

Relative growth of the evolved strains, based on BDA read-outs, was calculated after 48 hours. For each drug concentration, the following calculation was performed (1). The numerator and denominator are each subtracted by 0.04, which accounts for the OD_{600} of RPMI-MOPS:

$$Relative\ growth(\%) = \frac{OD_{600,\text{ in drug (0.0625-16 } \mu\text{g/mL)}} - 0.04}{OD_{600,\text{ no drug}} - 0.04} * 100 \quad (1)$$

The minimal drug concentration at which a relative growth of $\leq$ 50% was recorded, was used as MIC_{50} value. MFC_{99}, which is the minimal drug concentration that results in no CFU growth, was obtained from the BDA spotted YPD plates (see 3.3.1. Broth dilution assay). The resistance ratio (RR) based on MIC_{50} was calculated as followed (2) and indicates the level of resistance development relatively to the wild type. The same is done for MFC_{99} by performing calculation (3) and the SR stands for the susceptibility ratio to the drug, relatively to the wt.

$$MIC_{50}\ RR = \frac{MIC_{50,\text{ evolved strain}}}{MIC_{50,\text{ wt}}} \quad (2)$$

$$MFC_{99}\ SR = \frac{MFC_{99,\text{ evolved strain}}}{MFC_{99,\text{ wt}}} \quad (3)$$

Similarly, the area under the curve (AUC) was determined. This was based on plotting the graph of the relative growth of an evolved strain after 48 hours in a BDA experiment in PRISM. On the x-axis, the drug concentration range of 0.0625-16 μg/mL was depicted for each strain and on the y-axis the relative growth in percentages was illustrated. The RR based on AUC_{BDA} was determined accordingly (4).

$$AUC_{\text{BDA}}\ RR = \frac{AUC_{\text{BDA, evolved strain}}}{AUC_{\text{BDA, wt}}} \quad (4)$$

3.5 *In vitro* experimental evolution assay

3.5.1 Monotherapy

Wild type strains were evolved *in vitro* for nine antifungals and two repurposed drugs in a 16-days long evolution experiment in 1x, 2x, 4x, and 8x $MIC_{50,\text{ wt}}$ drug concentrations in maximum 1% DMSO. The evolution assay was performed in 96-well microtiter plates with plate layout presented in Figure 12a, which allowed for three replicates per drug condition. $5x10^6$ cells were added to each well in a final volume of 200μL. A plate transfer took place every 48 hours after incubation at 37°C.

20 μL cell culture was transferred to a new plate with the same layout and drug concentrations. Consequently, approximately 1μL of culture in each well was spotted onto YPD agar (2% glucose) to assess survival using a 96-well plate replicator. 75 μL of 75% glycerol was added to the old plate and stored at -80°C. At the end of the evolution, six strains per condition were taken, as displayed in Figure 12b, and single colony (SC) isolates were obtained.

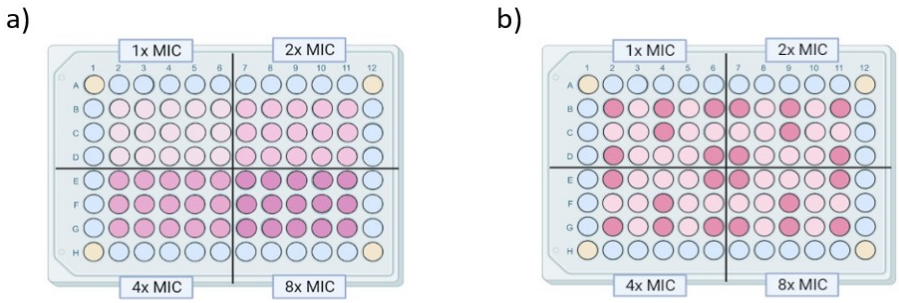

Figure 12: a) 96-well microtiter plate layout for monotherapy experimental evolution *in vitro* and b) selected strains from monotherapy. Experimental evolution is performed in a 96-well plate, divided into four different sections, each containing a different drug concentration as displayed in a) from top left to bottom right: 1x, 2x, 4x, and 8x $MIC_{50, wt}$. After monotherapy, six evolved strains per drug concentration were selected, as displayed in b) in dark pink, and tested for drug sensitivity in BDA.

3.5.2 Drug cycling

The same steps as in monotherapy were performed for drug cycling. However, cell cultures were transferred differently. Two different plate layouts (one for each drug used in the cycling scheme), depicted in Figure 13, were prepared by using two different drug concentrations: low (1x MIC_{50}) and high (2x MIC_{50}). The concentrations of the drugs of interest are depicted in Table 2. The experiment follows the schedule depicted in Figure 14, which includes 3 cycling steps (switch of drug) and four transfer steps (same drug).

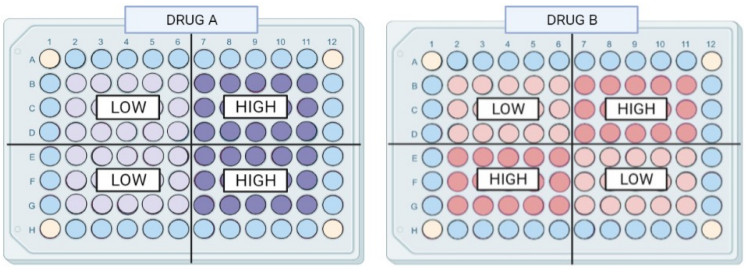

Figure 13: 96-well microtiter plate layouts for CS-based drug cycling evolution experiment. (Left) Plate layout of drug A, which exhibits collateral sensitivity towards drug B and (Right) Plate layout of drug B.

Table 2: Concentrations of drugs of interest used in cycling schemes. For each drug, 2 different drug concentrations were used to perform the cycling experiments: a low (1x MIC_{50}) and a high (2x MIC_{50}) concentration.

Drug compound	[Low] (μg/mL)	[High] (μg/mL)
AMB	1	2
CAS	0.5	1
CPX	1	2
GEL	1	2
NIT	0.5	1
POS	0.25	0.5

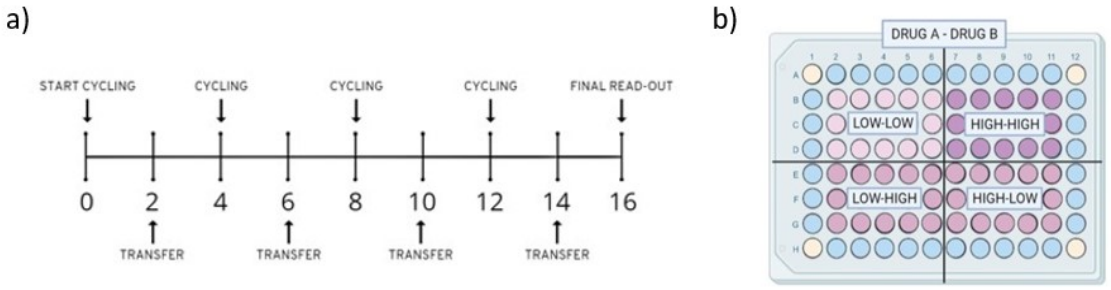

Figure 14: a) Drug cycling schedule. Transfers are performed by bringing the strains to a new growth medium with the same drug (same plate layout). Cycling steps involve a switch of the drug and strains are brought into a different plate layout. **b) Evolution conditions of CS-based drug cycling.** Wild type B8441 was eventually evolved in four different conditions: (from top left to bottom right) low-low, high-high, low-high, high-low of drugs A and B respectively.

Accordingly, on days 4, 8, and 12, cells were transferred to a plate with a different layout and thus a different drug, and on days 2, 6, 10, and 14, cells were transferred to a plate with the same plate layout and thus the same drug. Consequently, all strains were evolved in one drug for 96 hours, before cycling to the other drug. Upon cycling, cultures were pelleted by centrifugation for 5 min at 14000 rpm, washed in PBS to remove the drug, spun down again, and resuspended in RPMI-MOPS. Eventually, strains were grown in 4 different growth conditions: low-low, low-high, high-low, and high-high drug conditions of drugs A and B respectively, as depicted in Figure 14b. Relative growth was tracked every 48 hours by measuring OD_{600} using Synergy H1 (Biotek^{TM}) and resistance development was analyzed by performing BDA on the strains for the drugs they were cycled for. The same steps as in monotherapy were performed with the old plates afterwards.

3.6 DNA sequencing

3.6.1 gDNA isolation and ethanol precipitation

Cells were dissolved in 2 mL screw cap tubes containing 400 μL 1x TE buffer (10 mM Tris (pH 1), 1 mM EDTA, 100 mM NaCl, 1% SDS, and 2% Triton X-100), 400 μL PCI (phenol pH 6.7-chloroform-isoamylalcohol (25:24:1)) and small glass beads for lysis. The tubes were vortexed in FastPrep®-24 (MP Biomedicals) for 30 seconds twice. Extracts were centrifuged for 10 minutes at 14000 rpm. DNA was then precipitated by adding 300 μL of the aqueous phase together with 30 μL NaAc 3M (pH 5,2) and 900 μL 100% ethanol in an Eppendorf tube, incubated at -20°C for 20 minutes and centrifuged for 10 minutes at 14000 rpm. The DNA pellet was washed with 500 μL of 70% ethanol and dried at 30-37°C to allow evaporation of the ethanol. The DNA pellet was dissolved in 50 μL MQ and stored at -20°C.

3.6.2 Selection of genes to be sequenced and primer design

Primers were designed with CLC Main Workbench (QIAGEN) and annealing temperatures (T_m) of PCR primer pairs were calculated with NEB Tm Calculator [157]. PCR primers annealed to the upstream and downstream region of the open reading frame (ORF) and amplified the whole region, whereas sequencing primers targeted 500-1000 bp regions of interest in the ORF. Resistant strains were sequenced for genes of interest (GOI), in which resistance mutations previously have been found in *C. auris* or other *Candida spp*. These were displayed in Table 3. The primers for the PCR- and sequencing reactions for each gene were presented in Tables 4 and 5 respectively.

Table 3: Selection of genes to be sequenced in resistant strains. Resistant strains were sequenced for genes that have been associated with LOF/GOF mutations upon acquisition of resistance in *C. auris* and/or other *Candida spp.*

Drug compound	*ERG3*	*ERG6*	*ERG11*	*FCY1*	*FCY2*	*FKS1*	*FUR1*	*NCP1*	*TAC1b*
5-FC									
AMB									
KTO									
FLU									
POS									
ANF									
CAS									
MCA									

Table 4: PCR primer pairs that were used to amplify the GOI, depicted with their primer sequence.

PCR		
Gene	**Primer name**	**Sequence**
ERG3	CauERG3_PCR/Seq1_F	GTTTAGAGCTCGTTTTCAG
	CauERG3_PCR/Seq2_R	TACCATTGAATTTGGCTGC
ERG6	CauERG6_1F	CACTTCAACTGTTCCAAC
	CauERG6_4R	GGTTATCGTGAATGGCAT
ERG11	CauERG11_PCR/Seq1_F	TCGCGTAAATACAATGCCC
	CauERG11_PCR/Seq2_R	TGGTTTGGTGAAGAATTCGG
FKS1 HS1-2	CauFKS_B1120_Seq2.2.F	ATTTCAGAAGGAACCTGG
	CauFKS1_ASPCR_F	TACACTGCTTACAACTCGCCT
	CauFKS1_B11220_Seq2_R	TTCTTCGCTATCATGCCTTT
FKS1 HS2	CauFKS1_B8441_HS2_F	AGCAGATGTTGTCCAGAGAA
	CauFKS1_B8441_HS2_RF	AGATTGAGAACGGAATACGAGAA
FUR1	CauFUR1_F primer	CTCGTAATCTTTCCTCCAGG
	CauFUR1_R primer	TATGCTGAAAACCCCGATTG
FCY1	FCY1_US_F	GAGATCAAGCTGCAAAAAGA
	FCY1_DS_R	CACCACCTCGTCAACTATA
FCY2 (B9J08_002435)	FCY2_2435_US_F	CAAATACCCCGAATTGCTA
	FCY2_2435_DS_R	TCCAGGTCATTGGTTAACA
FCY2 (B9J08_002402)	FCY2_2402_US_F	CTCAATGGTTGCAAAACTC
	FCY2_2402_DS_R	TCGGGAGTCTATGATCAAA
NCP1	NCP1_US_F	CAAAAACATCGCAGACTCA
	NCP1_DS_R	CTTTTGCAAGCTCTTCATC
TAC1b	CauTAC1b_B11220_Seq4_F	GCCTCCTGCGCCTTCC
	CauTAC1b_B11220_PCR/Seq1_R	AGGTGGCAAAGAAAGTCAACATG

Table 5: Sequencing primers that were used to amplify the regions of interest in GOI, depicted with their primer sequence. The PCR products are sent for Sanger sequencing by TubeSeq (Eurofins).

Sequencing		
Gene	**Primer name**	**Sequence**
ERG3	CauERG3_PCR/Seq2_R	TACCATTGAATTTGGCTGC
ERG6	CauERG6_1F	CACTTCAACTGTTCCAAC
ERG11	CauERG11_PCR/Seq1_F	TCGCGTAAATACAATGCCC
	CauERG11_Seq1_R	GACCTCCCATCAAAACACC
	CauERG11_Seq2_F	AACGAGAGAAGAAAGACCG
	CauERG11_PCR/Seq2_R	TGGTTTGGTGAAGAATTCGG
FKS1 HS1-3	CauFKS_B1120_Seq2.2.F	ATTTCAGAAGGAACCTGG
FKS1 HS2	CauFKS1_B8441_HS2_F	AGCAGATGTTGTCCAGAGAA
FUR1	CauFUR1_R primer	TATGCTGAAAACCCCGATTG
FCY1	FCY1_seq_F	GAGGTGCTGAGTATGTTG
FCY2 (B9J08_002435)	FCY2_2435_ORF_F	CCATTTTCATTGCCATCATC
	FCY2_2435_ORF_R	GAAAAAGATACGGTATGCG
FCY2 (B9J08_002402)	FCY2_2402_ORF_F	CCATGGCAAAGACCTTTA
	FCY2_2402_ORF_R	CAAGATGCCAAAGAAAATCC
NCP1	NCP1_ORF_F	CCGTTCTGATTCCATTTCC
	NCP1_ORF_R	GACTGTCTGGAAATGGGA
TAC1b	CauTAC1b_B11220_Seq4_F	GCCTCCTGCGCCTTCC
	CauTAC1b_B11220_PCR/Seq3_F	CGCTGCTCAAGTCAGGTAAGG
	CauTAC1b_B11220_Seq2_F	CCATGCCTATCGAGCAGC
	CauTAC1b_B11220_Seq1_F	GATGAGCAGCGTCAATGA
	CauTAC1b_B11220_PCR/Seq1_R	AGGTGGCAAAGAAAGTCAACATG
	CauTAC1b_B11220_Seq3_R	GCACAGTAGCCATGCCTTC

3.6.3 PCR, gel electrophoresis and targeted sequencing

Regions of interest were amplified through PCR by using the Q5® High-Fidelity DNA Polymerase (New England Biolabs Inc). The annealing temperature (T_m) and amplicon length of each primer pair are depicted in Table A2 (Addendum). Every PCR reaction contains the following components, depicted in Table 6. PCR was conducted in a Labcycler Basic thermocycler (Bioké) as followed: an initial denaturation period of 30 seconds at 98°C, followed by 35 cycles consisting of 3 steps (98°C for 15 seconds, T_m for 30 seconds, and 72°C for 30 seconds/kb), finishing with a 2 minute elongation step at 72°C and finally paused at 10°C. The PCR products were stored at 4°C. To

ensure successful PCR reactions, gel electrophoresis was performed for 25 minutes at 165V. Agarose 1% gel was made with 0.5X TAE buffer (Tris-acetate-EDTA) and 5μL/100mL SYBR™ Safe DNA Gel Stain (Invitrogen) to visualize the fragments under UV light (Safe Imager 2.0, Invitrogen). After verifying the presence of adequate PCR products, the PCR products were sent for Sanger sequencing by TubeSeq (Eurofins) [158], along with their designated sequencing primers. Sequences were trimmed, aligned, and screened for mutations in CLC Main Workbench 21 (QIAGEN).

Table 6: Components of a PCR reaction. Each PCR reaction contains F- and R-primer, dNTPs, Q5 Reaction buffer, Q5 polymerase and Milli-Q, in the volumes depicted below.

Component	for every reaction (50 μL
DNA template	1 μL
10 mM Forward primer	4 μL
10 mM Reverse primer	4 μL
10 mM dNTPs	5 μL
5x Q5 Reaction buffer	10 μL
Q5 polymerase	0.5 μL
Milli-Q	add until 50 μL

3.6.4 Functional analysis of mutations

SNAP2 was used to predict the functional effects of single amino acid substitutions on the protein. The algorithm is based on "neural network", a machine learning device that differentiates neutral and effect variants based on the evolutionary information obtained from multiple sequence alignment and other features such as solvent accessibility and secondary structure of the protein. A prediction score, depicted in Figure 15, is assigned to each substitution, ranging from - 100 (strong neutral) to 100 (strong effect), which gives an estimate of the effect of the specific mutation on the protein function [159].

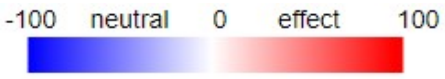

Figure 15: Range of prediction score generated by SNAP2. SNAP2 assigns a prediction score, ranging from -100 to 100, to every amino acid substitution in a protein sequence. A score of -100 to -50 stands for a strong neutral prediction (no drastic effects on protein function) or no effects, -50 $<$ score $<$ 50 stands for a weak effect, while a score between 50-100 represents a strong effect (drastic effect on protein function).

4. Results

4.1 Drug susceptibility of *C. auris* wild type B8441

MIC_{50} and MFC_{99} of wild type *C. auris* for various antifungal and repurposed drugs were determined by BDA and displayed in Table 7.

Table 7: Information on the selected antifungal and repurposed drugs used in this project.

Antifungal

Drug class	Drug compound	Abbrv.	MIC_{50}(μg/mL)	MFC_{99}(μg/mL)	Effect
Allylamine	**Terbinafine hydrochloride**	**TRB**	4	>16	Fungistatic
Azole	**Fluconazole**	**FLU**	1	>16	Fungistatic
	Itraconazole	**ITC**	4	>16	Fungistatic
	Ketoconazole	**KTO**	0.25	>16	Fungistatic
	Micoconazole	**MCO**	8	>16	Fungistatic
	Posaconazole	**POS**	0.25	16	Fungicidal
Echinocandin	**Anidulafungin**	**ANF**	1	4	Fungicidal
	Caspofungin	**CAS**	0.5	>16	Fungistatic
	Micafungin	**MCA**	1	4	Fungicidal
Nucleoside peptide	**Nikkomycin Z**	**NKZ**	>16	>16	Fungistatic
Polyene	**Amphotericin B**	**AMB**	1	1	Fungicidal
Pyrimidine analogue	**5-fluorocytosine**	**5-FC**	0.125	0.5	Fungicidal

Repurposed

Drug class	Drug compound	Abbrv.	MIC_{50}(μg/mL)	MFC_{99}(μg/mL)	Use
8-hydroxyquinoline	**5,7-Diiodo-8-hydroxyquinoline**	**DHQ**	0.5	1	Antiprotozoal
Biguanide	**Alexidine dihydrochloride**	**ALX**	1	8	Antimicrobial
Chlorobenzene	**Chlorhexidine**	**CHX**	0.0078(%)	0.03125(%)	Antibacterial
Pyridinone	**Ciclopirox ethanolamine**	**CPX**	1	2	Antifungal
Organoselenium	**Ebselen**	**EBS**	2	8	Anti-inflammatory
Benzoquinone	**Geldanamycin**	**GEL**	>64	>64	Anti-tumor
Nitroquinoline	**Nitroxoline**	**NIT**	0.5	2	Antibacterial (UTI)
Alkylglycerophosphocholine	**Oleylphosphocholine**	**OPC**	4	8	Anti-leishmanial
Naphthalene	**Pyrvinium pamoate salt hydrate**	**PYR**	4	16	Antihelmintic
Phenylpropane	**Suloctidil**	**SLC**	4	16	Antiplatelet

Within the range of **0.0625-16 μg/mL,** wild type *C. auris* is **susceptible** to **all of the selected drugs**, except NKZ and GEL. From the antifungals, a **fungistatic effect** (MFC: >16 μg/mL) is observed in CAS, FLU, KTO, NKZ, and TRB within that range. 5-FC, AMB, ANF, MCA, and POS exhibit **fungicidal effects** within that range. Furthermore, all **repurposed** drugs, except GEL, are shown to be fungicidal within this range. ITC and MCO will be left out in further experiments, as *C. auris* displays a relatively low susceptibility to these drugs (MIC_{50}: 4 μg/mL in ITC, 8 μg/mL in

MCO) compared to the other azoles. Additionally, the MIC of AMB is determined by ETEST® strips (bioMérieux), which was 0.25 μg/mL as displayed in Figure A1 (Addendum). Importantly, to facilitate calculations of resistance ratios based on MIC_{50}, an **MIC_{50} of an evolved strain that is >16 μg/mL is interpreted as 32 μg/mL.**

4.2 *In vitro* experimental evolution

4.2.1 Survival dynamics in monotherapy

The percentage and the relative number of surviving populations per drug and drug condition, based on MFC_{99}, are depicted in Figure 16. Generally, a **100% survival** is observed in all antifungal drugs, except **5-FC (91.67%)** and **AMB (16.67%)**. For the repurposed drugs, in **CHX, 26.67%** survival is reported and in **NIT 63.33%** survival. Noticeably, the highest survival in AMB is observed for strains evolved in 1x and 4x MIC_{50}. Furthermore, populations evolved in 8x MIC_{50} in NIT monotherapy on the one hand, and in 4x and 8x MIC_{50} in CHX monotherapy on the other hand, did not survive. Additionally, only one strain in 2x MIC_{50} CHX survived.

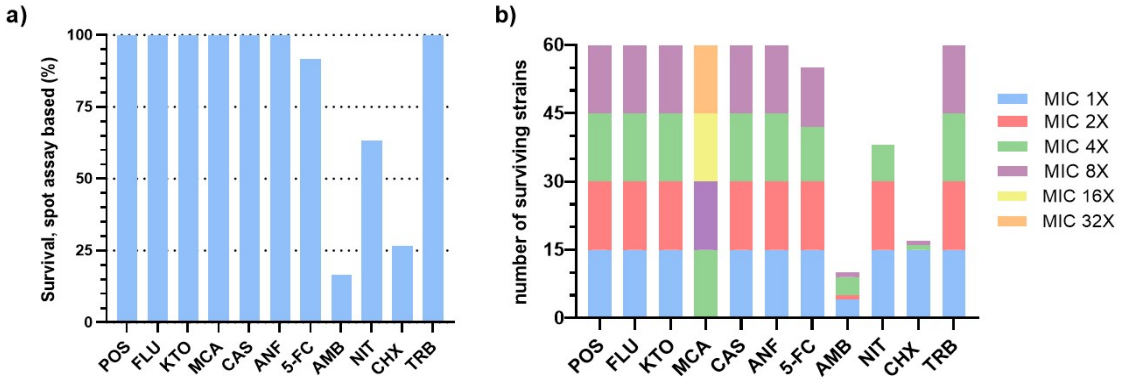

Figure 16: Survival of the populations, depicted in a) percentages and b) numbers, relative to the initial number of populations per drug condition, based on MFC_{99}. %-survival is calculated by dividing the total number of surviving populations (in all four drug conditions) by 60 and times 100. The distribution of surviving populations per drug condition is determined by calculating relative number of surviving populations out of 15 populations per drug condition.

As 5-FC, AMB, CHX and NIT monotherapy did not result in 100% survival, graphs are designed to track the relative percentage of survival of populations in each drug condition over time. This is done to estimate when the number of surviving populations might have decreased. This is depicted in Figure 17.

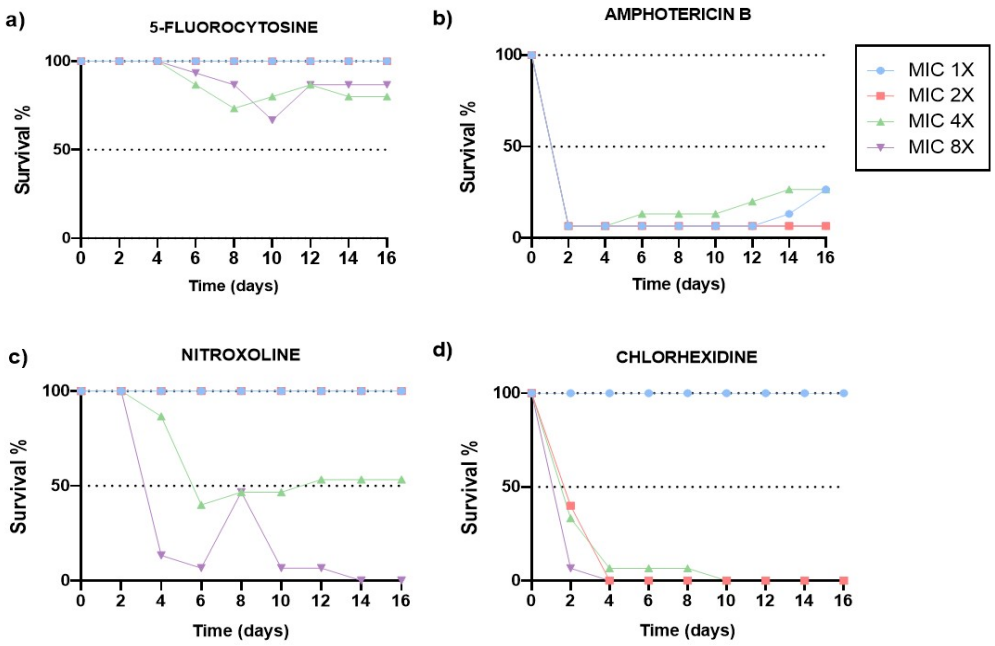

Figure 17: Relative percentage survival over time in a) 5-fluorocytosine, b) amphotericin B, c) nitroxoline and d) chlorhexidine monotherapy. Relative percentage of survival of populations in each drug condition (15 populations) is tracked over a period of 16 days, based on MFC_{99} of YPD spot assays of BDA plates.

In **5-FC** (Figure 17a), all populations evolved in 1x and 2x MIC_{50} showed 100% survival. On the other hand, the number of surviving populations in 4x and 8x MIC_{50} decrease, and on day 8 and 10 respectively, they increase and survival becomes stable. **In AMB** (Figure 17b), all populations drastically decrease in numbers in the first two days, as only one strain per condition (6.67%) survived the monotherapy. Populations in 2x MIC_{50} stabilize afterwards. Populations in 4x MIC_{50} start growing on day 6, while those in 1x MIC_{50} do not start growing until day 12. **In NIT** (Figure 17c), all populations in 1x and 2x MIC_{50} survived, whereas survival in 4x and 8x MIC_{50} decreased until day 6. After day 8, populations in 4x MIC_{50} increase and stabilize, whereas in 8x MIC_{50}, populations decrease and eventually go extinct. **In CHX** (Figure 17d), only in 1x MIC_{50} survival is 100% and populations in the other drug conditions steadily decrease and go extinct.

4.2.2 Resistance development in monotherapy

Resistance based on MIC_{50} is determined based on the **resistance ratio (RR)** which is described as the ratio:

$$RR\ MIC_{50} = \frac{MIC_{50,\ \text{evolved}}}{MIC_{50,\ \text{wt}}}$$

Accordingly, as we test 2-fold drug concentrations, **resistance** has developed if this **ratio is $\geq$2,** implying that the $MIC_{50,\ \text{evolved}}$ is at least twice as high as $MIC_{50,\ \text{wt}}$. Resistance acquisition for each

drug is displayed in percentages in Figure 18a. Additionally, the number of resistant/non-resistant strains, relative to the amount of surviving strains tested in BDA, is given in Figure 18b, to highlight that some populations did not survive the *in vitro* experimental evolution.

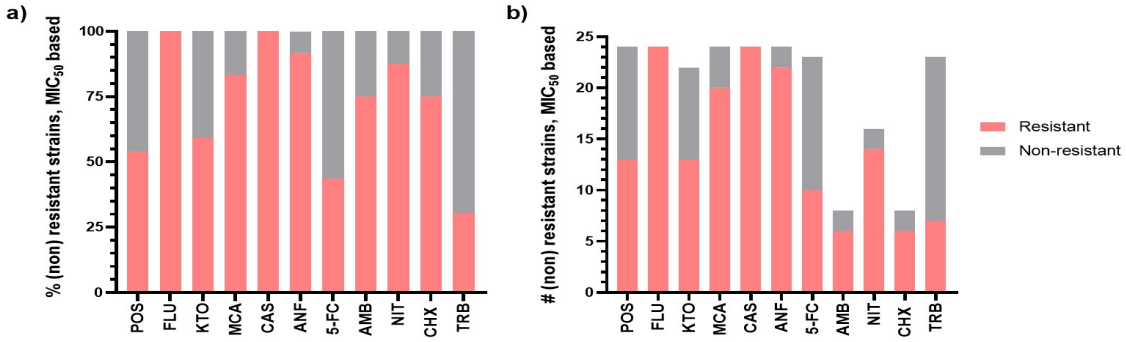

Figure 18: Based on MIC_{50} a) The percentage of surviving strains that acquired resistance (in red) and b) the relative number of resistant/non-resistant surviving strains per drug. %-(non)acquired resistance is determined by the relative percentage of (non-)resistant strains out of the 24 tested evolved strains per drug. The distribution of resistant/non-resistant strains is determined relative to the number of survived strains tested in BDA.

Regarding resistance emergence, 50% of the tested surviving strains in each drug acquired resistance, except for 5-FC and TRB. **FLU** exhibits 100% resistance emergence, whereas in **POS and KTO**, 13 strains acquired resistance, thus 54.16% and 59.05% of the surviving strains respectively. In **5-FC**, only 43.47% acquired resistance (10 strains). In echinocandins, 100% resistance in **CAS** is recorded, whereas for **MCA and ANF**, 83.33% (20 strains) and 91.67% (22 strains) respectively developed resistance. In **AMB and CHX**, resistance is recorded in 75% of the strains, as both drugs have 6 resistant strains out of 8. Lastly, 87.5% resistance (14 strains out of 16) is recorded in **NIT**.

Besides, for the **AMB-resistant strains**, based on MIC_{50}, resistance is double-checked with **ETESTs®**. For all strains, no halo is observed, as depicted in Figure A2 (Addendum), implying that MIC is higher than 32 μg/mL and resistance is acquired. However, substantial differences regarding the resistance determination can be commented as BDA results in three AMB-resistant strains with an MIC_{50} of 8 μg/mL and three AMB-resistant strains with an MIC_{50} >16 μg/mL. Therefore, to maintain consistency throughout the project, MIC_{50} values obtained from BDA will be used from now on as BDA is our preferred method to determine resistance.

4.2.3 Dose-dependency of resistance development

Dose-dependency of resistance acquisition for each drug **based on MIC_{50}** is explored by calculating the mean resistance ratios (RR) of six evolved strains in each drug condition. This

is depicted in Figure 19. For AMB, 2 strains in 1x MIC_{50}, 1 in 2x and 8x MIC_{50} and 4 in 4x MIC_{50} are used to estimate the RRs instead. For CHX, RRs in 4x and 8x MIC_{50} are determined based on one strain.

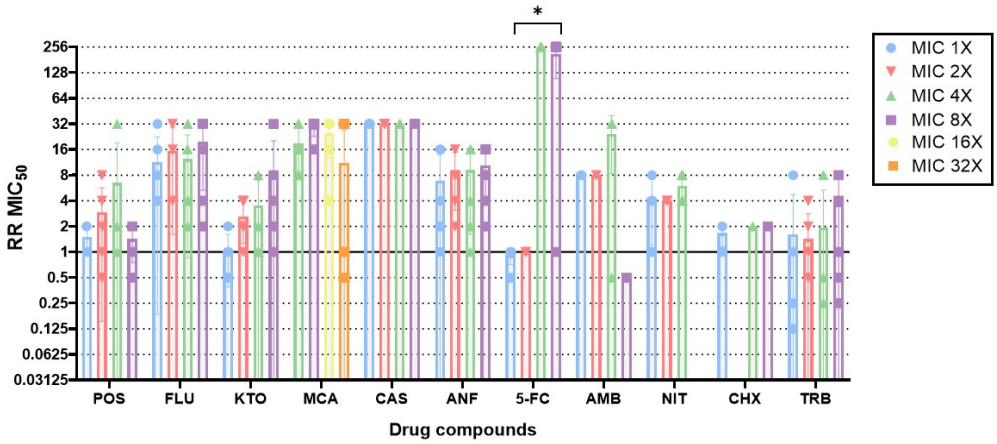

Figure 19: Distribution of mean RRs for each drug in each drug condition based on MIC_{50}. Bar plots indicate the mean RRs in each drug condition (1x, 2x, 4x, and 8x MIC_{50}, except for MCA which was 4x, 8x, 16x, 32x MIC_{50}). Data points indicate the individual RR MIC_{50} in each condition, error bars depict standard deviations. A significant difference between drug conditions is indicated by an *.

Only **in 5-FC,** resistance development was **significantly dose-dependent,** as only strains evolved in higher 5-FC concentrations (4x and 8x MIC_{50}) acquired resistance. In azoles, echinocandins and TRB, resistant strains in all four conditions are reported. No substantial differences are observed between the four conditions in azoles and echinocandins. In AMB, no resistant strains are retrieved in 8x MIC_{50} and the highest level of resistance is recorded in 4x MIC_{50} (mean RR: 24.125). In NIT, no surviving strains are reported in 8x MIC_{50}, and thus no resistance is present. Similarly in CHX, no resistance is acquired in 2x MIC_{50} as no surviving strains are retrieved in this drug condition. In TRB, the highest resistance level is recorded in 8x MIC_{50} (mean RR: 4).

In order to draw conclusions on the dose-dependent resistance development, an additional graph is made, depicted in Figure A3 (Addendum), in which only the resistant strains (RR MIC_{50} > 1) for each drug and drug condition are included. The only major differences regarding dose-dependency are observed for NIT and TRB. The highest levels of resistance in NIT monotherapy are recorded in 1x and 4x MIC_{50} NIT and in TRB monotherapy in 1x, 2x, and 8x MIC_{50} TRB.

Furthermore, **dose dependency of resistance development** is also explored **based on AUC_{BDA}.** Resistance acquisition is determined based on the AUC_{BDA} resistance ratio (RR), described by:

$$RR\ AUC_{\mathrm{BDA}} = \frac{AUC_{\mathrm{BDA,\ evolved}}}{AUC_{\mathrm{BDA,\ wt}}}$$

In the context of AUC_{BDA}, resistance has developed if this ratio > 1, implying that the $AUC_{BDA,\ evolved}$ is higher than $AUC_{BDA,\ wt}$. For each drug, the mean RRs for each drug in each drug condition is depicted in Figure 20. RRs are calculated based on six evolved strains per drug condition, except for AMB and CHX as previously described for MIC_{50}.

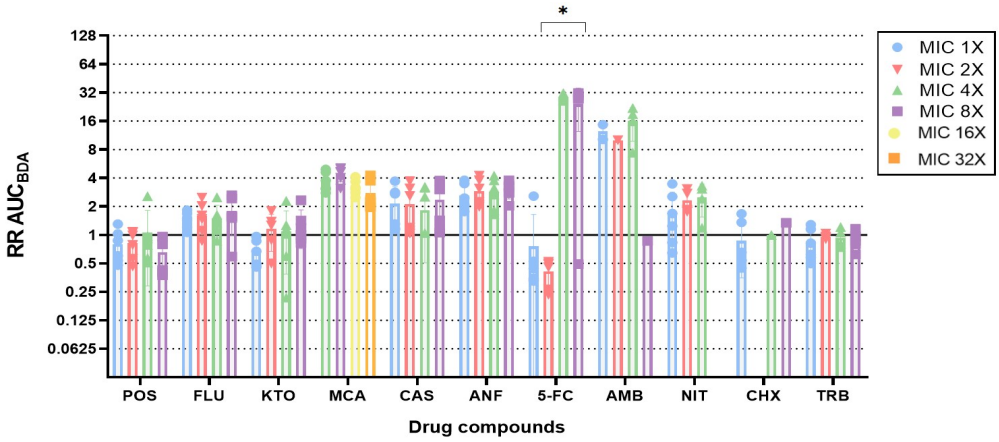

Figure 20: Distribution of mean RRs for each drug in each drug condition based on AUC_{BDA}. Bar plots indicate the mean RRs in each drug condition (1x, 2x, 4x, and 8x MIC_{50}, except for MCA which was 4x, 8x, 16x and 32x MIC_{50}). Data points indicate the individual RR AUC_{BDA} in each condition, error bars depict standard deviations. A significant difference between drug conditions is indicated by an *.

Similarly, as in MIC_{50}, resistance is significantly **dose-dependent in 5-FC based on AUC_{BDA}**, as resistance levels are significantly higher in higher 5-FC concentrations (4x and 8x MIC_{50}: 28.76 and 24.11 respectively). For the azoles, mean RRs in POS are ≤ 1, yet some strains still exhibit resistance as indicated by the data points. In FLU, KTO, and the echinocandins, low levels of resistance are reported but no substantial differences between the drug conditions are present. In AMB and NIT, only in 8x MIC_{50} resistance is not developed. In CHX, no resistant strains are retrieved in 2x MIC_{50}, as no strains survived the treatment.

Additionally, a graph is made based on AUC_{BDA}, in which only resistant strains (RR AUC_{BDA} > 1) of each drug are included, to draw conclusions on the dose-dependency of resistance development. This is depicted in Figure A4 (Addendum). For the azoles, POS acquired the most prominent resistance in 4x MIC_{50}, FLU developed resistance in all four conditions and in KTO, only in 1x MIC_{50} no resistant strains were retrieved. No major differences were recorded in the echinocandins, 5-FC, AMB, and NIT. In CHX, the highest level of resistance was recorded in 1x MIC_{50}, and in TRB only in 2x MIC_{50} no resistance was present.

4.2.4 Dynamics of resistance acquisition in monotherapy

For each antifungal, the average relative growth of the 15 populations in each drug condition, relative to the growth of wild type *C. auris*, is depicted in Figure 21. Through this, **trends regarding growth over time** in higher or lower concentrations may be distinguished and an average estimation of when resistance might have developed can be made.

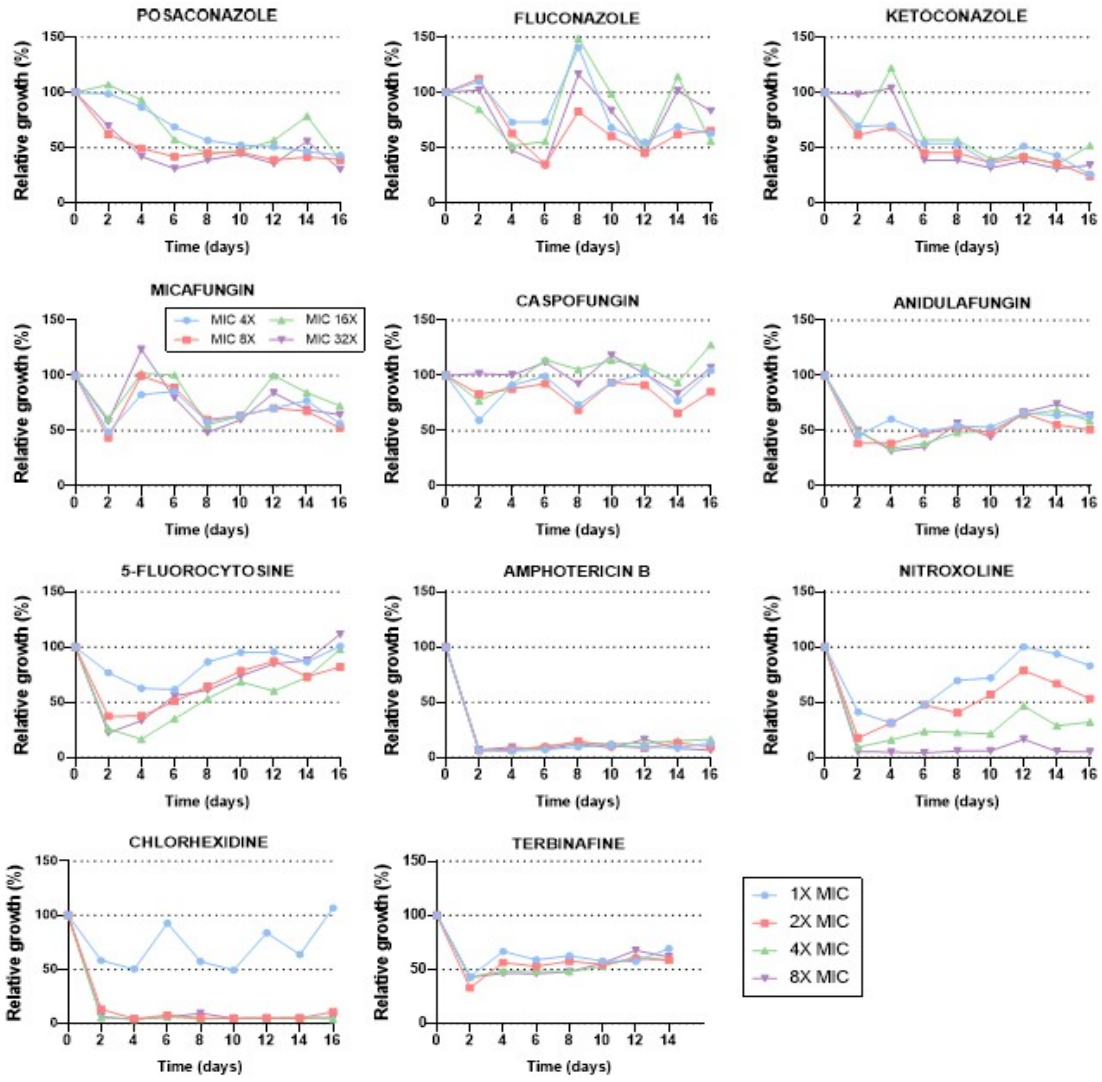

Figure 21: Average relative growth of drug evolved strains over time. Growth of the evolved strains in 1x, 2x, 4x and 8x MIC_{50} of their respective drugs, except for MCA which was evolved in 4x, 8x, 16x and 32x MIC_{50}, is tracked over a period of 16 days, relative to the wt control.

Overall, **no substantial trends** are distinguished as no major differences in average relative growth are observed between the four drug conditions, **except in CHX and NIT.** In CHX, only populations

in 1x MIC_{50} display growth and in NIT, populations in 1x and 2x MIC_{50} exhibit a higher growth rate than those in 4x and 8x MIC_{50} Nevertheless, the absence of distinct growth trends might be due to the averaging of the relative growth of the populations and therefore, this might not allow efficient prediction of when resistance exactly emerges. In order to estimate when resistance might have emerged and evaluate its dose dependency, the relative growth of an isolated resistant strain from each condition and each drug is plotted over time. This is depicted in Figure 22.

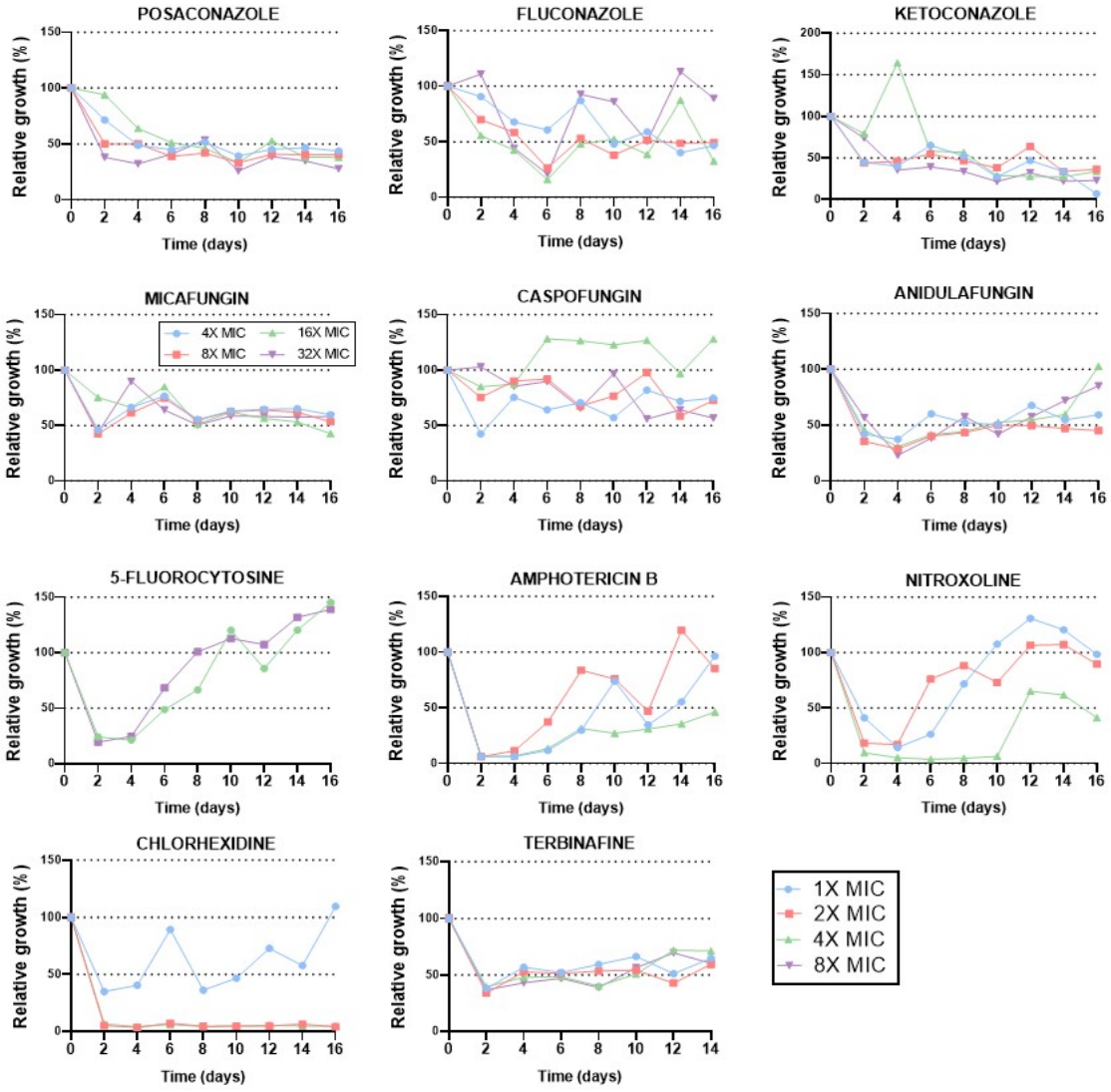

Figure 22: Relative growth of one resistant strain of each drug condition for each drug, depicted over time. Growth of single colony resistant strains, evolved in 1x 2x, 4x and 8x MIC_{50}, except for MCA which was evolved in 4x, 8x, 16x and 32x MIC_{50}, is tracked over a period of 16 days, relative to the wt control.

No substantial differences between the drug conditions are observed for the **azoles and the echinocandins, except in ANF,** in which a higher relative growth is observed in higher

concentrations (4x and 8x MIC_{50}). Furthermore, **in FLU and CAS,** growth is mostly random, while **in POS and MCA,** relative growth is stable after day 8. Noticeably, relative growth in 4x MIC_{50} CAS exceeds the growth of wild type strains, which might be caused by an experimental error. In **5-FC**, strains in 4x and 8x MIC_{50} show a steady increase in relative growth after day 4, and no resistant strains are obtained in 1x and 2x MIC_{50} 5-FC. **In AMB-resistant strains,** relative growth increases until day 8 for 2x and 4x MIC_{50}, and until day 10 for 1x MIC_{50}. Afterwards, relative growth initially declines and is recovered later. Furthermore, relative growth in all **NIT-resistant strains** decreases in the first four days. Afterwards, strains in 1x and 2x MIC_{50} NIT increase in relative growth, while strains in 4x MIC_{50} NIT continue to decline. After day 10, an increase in growth is recorded in all three NIT conditions. **In CHX,** relative growth is only observed in 1x MIC_{50} CHX, and strains in 2x and 4x MIC_{50} CHX decrease drastically in the first 2 days and never recover. Lastly, **TRB-resistant strains** decrease in growth in all four TRB conditions after day 2. Afterwards, populations in 1x and 2x MIC_{50} TRB on the one hand, and strains in 4x and 8x MIC_{50} TRB on the other hand follow a similar growth trend.

4.3 Genetic signature of resistance

4.3.1 Mutations in genes of interest

The resistant strains, based on RR MIC_{50}, are sequenced for their genes of interest and the number of mutations found in each gene for each drug are depicted in Table 8. Additionally, Figure A5 (Addendum) displays the ratio of resistant strains with/without mutations per gene, relative to the total number of sequenced strains. No mutations are noted in *ERG6, NCP1, FCY1*, and both *FCY2* genes. SNAP2 analyses are performed for every missense mutation found and heatmaps depicting the indicated regions in which mutations are found are given in Figure A6 (Addendum).

Table 8: Information on the total number of resistant strains sequenced for each specific gene and the number of mutations found.

Sequenced gene	Drug	total # strains sequenced	# mutations found
ERG3	ANF	22	0
	CAS	9	0
	MCA	16	0
	AMB	6	2
ERG6	AMB	6	0
ERG11	FLU	24	0
	KTO	13	0
	POS	13	0
	AMB	6	3
FCY1	5-FC	9	0
FCY2 (B9J08_002402)	5-FC	9	0
FCY2 (B9J08_002435)	5-FC	9	0
FKS1 (HS1,2 and 3	ANF	22	0
	CAS	15	0
	MCA	18	2
FUR1	5-FC	9	3
NCP1	AMB	6	0
TAC1b	FLU	24	2
	KTO	13	1
	POS	13	0

Four missense mutations are found in ***TAC1b*** and described in Table 9: three mutations in **FLU-resistant strains**, namely **G1620A/S540N** and **G1514A/S514N** in **Strain 60** and **T682A/F228I** in **Strain 63**, and one mutation in the **KTO-resistant strain 78**, namely **T1475G/V492G.** The latter two mutations are predicted to have a weak effect on the protein, as observed in the heatmaps depicted in Figures A7-A10 (Addendum), obtaining an effect score of -20 (57% accuracy) and 14 (59% accuracy) respectively.

Table 9: Summary of the mutations of azole resistant strains in *TAC1b*. The mutations are described, along with the strain number, drug and dose of monotherapy, RRs and SRs, and the SNAP2 effect score and prediction accuracy.

Strain #	Drug	Dose	RR AUC_{BDA}	RR MIC_{50}	SR MFC_{99}	Gene	Mutation	Effect score	Prediction accuracy
60	FLU	2x MIC	1.6078	4	1	*TAC1b*	G1620A/S540N	-61	82%
							G1541A/S514N	-67	82%
63	FLU	4x MIC	1.6266	4	1	*TAC1b*	T682A/F228I	-20	57%
78	KTO	8x MIC	1.1773	8	1	*TAC1b*	T1475G/V492G	14	59%

In ***FKS1*** **HS1**, the missense mutation **C1916A/S639Y** is found in **two MCA-resistant strains**, namely **Strains 151 and 152**, described in Table 10. No mutations are found in HS2 nor HS3. The SNAP2 analysis predicts an effect score of 51 with 75% accuracy, as depicted in Figure A12 (Addendum).

Table 10: Summary of the mutations of echinocandin resistant strains in *FKS1*. The mutations are described, along with the strain number, drug and dose of monotherapy, RRs and SRs, and the SNAP2 effect score and prediction accuracy.

Strain #	Drug	Dose	RR AUC_{BDA}	RR MIC_{50}	SR MFC_{99}	Gene	Mutation	Effect score	Prediction accuracy
151	MCA	1x MIC	3.7650	16	32	*FKS1 (HS1)*	C1916A/S639Y	51	75%
152	MCA	1x MIC	3.0642	8	32	*FKS1 (HS1)*	C1916A/S639Y	51	75%

Every **AMB-resistant strain** acquired a mutation, except for strain 52 (not displayed), in ***ERG3*** or ***ERG11***. These mutations are described in Table 11. We found one deletion in **Strain 48 (G1415del1)** and one missense mutation in **Strain 49 (G1512A/M504I)**, with a predicted effect of 44 (71% accuracy), depicted in Figure A13 (Addendum). Furthermore, we found three nonsense mutations in **Strain 47 (G490T/E164*), 50 (A473C/Y158*)** and **53 (G493T/E165*)**.

Table 11: Summary of the mutations of AMB-resistant strains in either *ERG3* or *ERG11*. The mutations are described, along with the strain number, drug and dose of monotherapy, RRs and SRs, and the SNAP2 effect score and prediction accuracy.

Strain #	Drug	Dose	RR AUC_{BDA}	RR MIC_{50}	SR MFC_{99}	Gene	Mutation	Effect score	Prediction accuracy
47	AMB	1X MIC	14.6514	8	32	*ERG3*	G490T/E164*	-	-
48	AMB	1X MIC	10.2140	8	32	*ERG3*	G1415del1	-	-
49	AMB	2X MIC	10.0551	8	32	*ERG11*	G1512A/M504I	44	71%
50	AMB	4X MIC	18.8920	32	32	*ERG11*	A473C/Y158*	-	-
53	AMB	4X MIC	21.8984	32	32	*ERG11*	G493T/E165*	-	-

In **5-FC** resistant strains, three mutations are found in ***FUR1***, which are described in Table 12. A nonsense mutation is found in **Strain 31**, namely **G202T/G68***. Furthermore, two missense mutations are found in **Strain 32 (G433T/G145C)** and **Strain 116 (G242T/C81F)**. SNAP2 predicted an effect of 86 and 81 for the mutations in strains 32 and 116 respectively, both estimated with 91% accuracy. Heatmaps, retrieved from SNAP2, that indicate these effect scores are depicted in Figures A14-A15 (Addendum).

Table 12: Summary of the mutations of 5-FC resistant strains in *FUR1*. The mutations are described, along with the strain number, drug and dose of monotherapy, RRs and SRs, and the SNAP2 effect score and prediction accuracy.

Strain #	Drug	Dose	RR AUC_{BDA}	RR MIC_{50}	SR MFC_{99}	Gene	Mutation	Effect score	Prediction accuracy
31	5-FC	4X MIC	29.0467	256	64	*FUR1*	G202T/G68*	-	-
32	5-FC	8X MIC	27.6874	256	64	*FUR1*	G433T/G145C	86	91%
116	5-FC	4X MIC	30.0304	256	64	*FUR1*	G242T/C81F	81	91%

In summary, Figure 23 depicts all mutations found in each gene. Four mutations are recovered for *TAC1b*: one is located between the DNA-binding domain (DBD) and the middle homology region (MHR), the others are situated next to the C-terminus of MHR. In *ERG11*, two nonsense mutations are noted in HS1 and one missense mutation next to HS3. *ERG3* acquired two mutations, closely located to each other. In *FKS1*, one mutation is found in HS1 and in *FUR1*, three mutations are acquired, including one nonsense mutation.

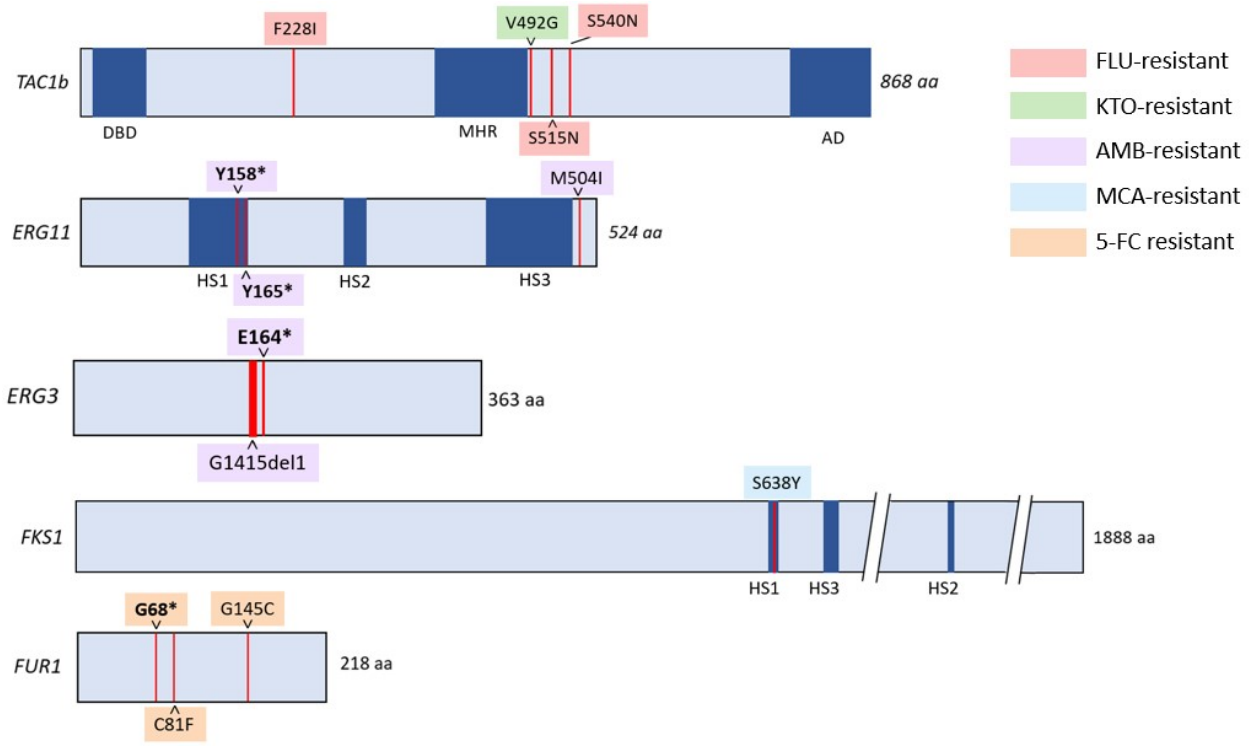

Figure 23: Summary of the mutations in the sequenced genes. (Top to bottom) *TAC1b, ERG11, ERG3, FKS1 and FUR1* are depicted with their important regions (dark blue) and the location of mutations found in our resistant strains (red). The drug-resistant strains in which mutations are found are depicted in colors: red (FLU-resistant), green (KTO-resistant), purple (AMB-resistant), blue (MCA-resistant), and orange (5-FC resistant).

4.3.2 Resistance dynamics of strains in which mutations were observed

Relative growth of the resistant strains with and without mutations in the genes we have sequenced and evolved in the same drug condition, is measured in drug concentrations ranging between 0.0625-16 μg/mL, relative to the growth in no drug. These graphs are displayed together with the wild type and control strain in the same drug in Figures 24-25.

FLU-resistant strains display higher MIC_{50} values ($\geq$4 μg/mL) than WT (MIC_{50}: 2 μg/mL) and CTRL (MIC_{50}: 8 μg/mL) strains, as observed in Figure 24a. On the other hand, the KTO-resistant strain without mutations exhibits a higher MIC_{50} (8 μg/mL) than the strain with mutations (MIC_{50}: 2 μg/mL), as illustrated in 24b. Nevertheless, the drug-resistant strains generally have higher MICs than WT and CTRL strains (MIC_{50}: 0.125-0.5 μg/mL).

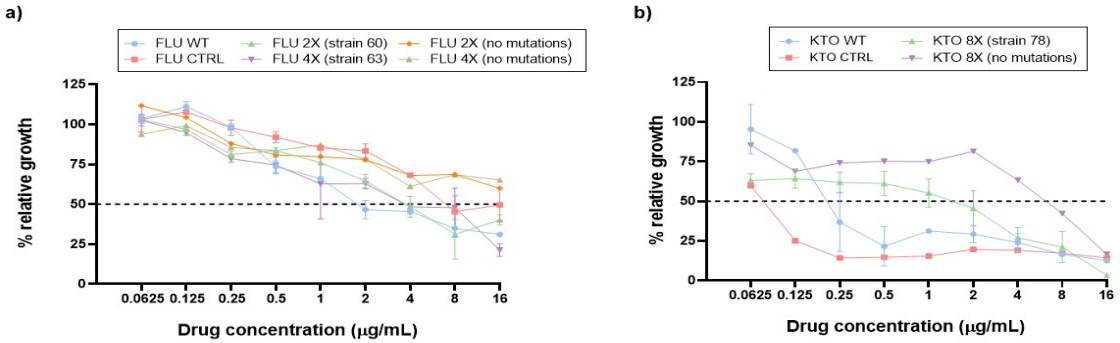

Figure 24: Relative growth of a) FLU-resistant and b) KTO-resistant strains with and without mutations in *TAC1B*, together with wild type (WT) and experimental control (CTRL) strains. Growth is measured at OD_{600} in concentrations ranging from 0.0625-16 μg/mL in a two-fold dilution series, relative to the $OD_{600, \text{ no drug}}$.

Next, in Figure 25, AMB-resistant strains with mutations in *ERG3* or *ERG11* exhibit higher MIC_{50} values ($\geq$16 μg/mL) than those without mutations (4 μg/mL), WT and CTRL strains (1 μg/mL).

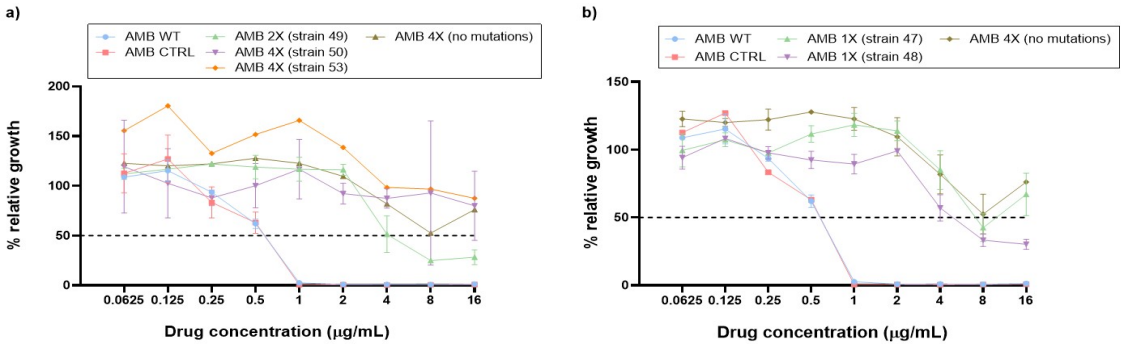

Figure 25: Growth of AMB-resistant strains with and without mutations in a) *ERG11* and b) *ERG3*, together with wild type (WT) and experimental control (CTRL) strain. Growth was measured at OD_{600} in concentrations ranging from 0.0625-16 μg/mL in a two-fold dilution series, relative to the $OD_{600, \text{ no drug}}$.

Lastly, depicted in Figure 26a, MCA-resistant strains with mutations exhibit lower MIC_{50} values (8-16 μg/mL) than the resistant strain without mutations (MIC_{50}: $\geq$ 16). Furthermore, the 5-FC-resistant strains, with and without mutations, all display MIC_{50} values higher than 16 μg/mL, as depicted in Figure 26b. Additionally, for both 5-FC and MCA-resistant strains, MIC_{50} is higher than those of WT and CTRL strains (5-FC: 0.125 μg/mL, MCA: 0.5-1 μg/mL).

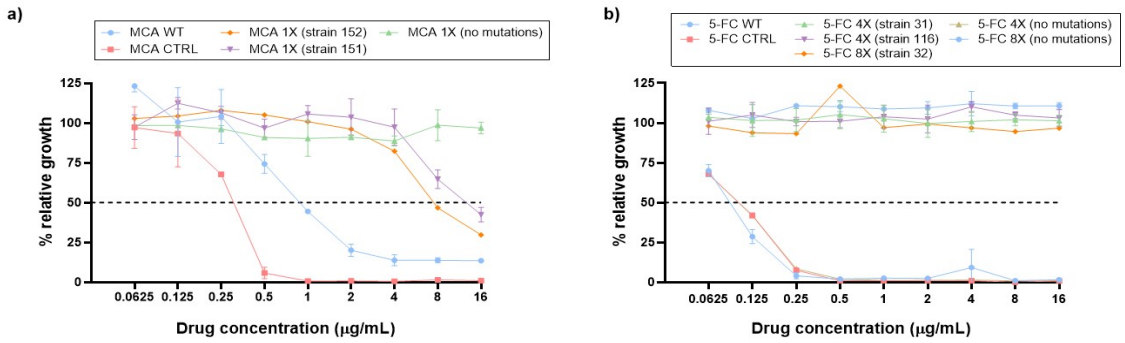

Figure 26: Relative growth of a) MCA-resistant and b) 5-FC-resistant strains with and without mutations in *FKS1* and *FUR1* respectively, together with wild type (WT) and experimental control (CTRL) strains. Growth is measured at OD_{600} in concentrations ranging from 0.0625-16 μg/mL in a two-fold dilution series, relative to the $OD_{600, \text{no drug}}$.

4.3.3 Resistance level of resistant strains with and without mutations in the GOI

As observed in Table 8 on page 42, some resistant strains did not obtain mutations in the GOI we sequenced, yet exhibit $MIC_{50} > 1$. Consequently, to evaluate if mutations in the sequenced GOI contribute to higher levels of resistance, violin plots are made, based on RR MIC_{50}, in which the resistance levels of the resistant strains (from the four conditions in monotherapy) are visualized, as depicted in Figure 27. From this, we could observe that resistant strains with mutations in the sequenced GOI do not necessarily exhibit higher resistance levels than those without mutations in the GOI. An exception however are 5-FC and AMB-resistant strains, for which strains with and without mutations in the GOI achieved equal levels of resistance. Yet as the 5-FC resistant strains all exhibit MIC_{50} >16 μg/mL, possible differences in resistance level could not be distinguished due to our measuring range (0.0625-16 μg/mL).

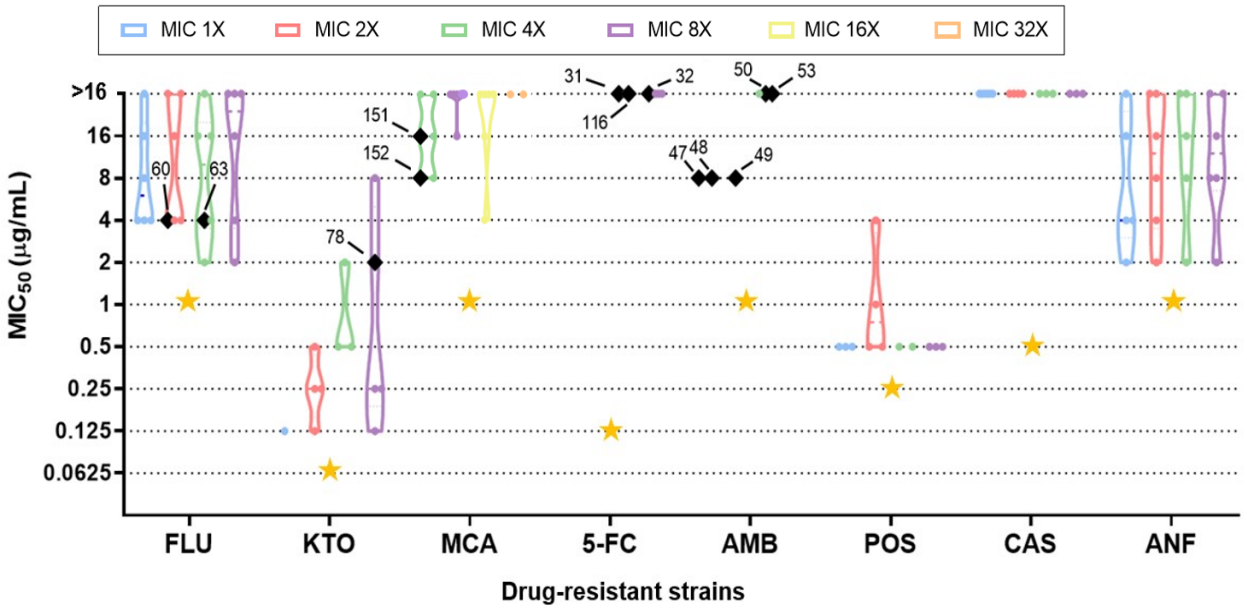

Figure 27: Violin plot of MIC_{50} values of all the resistant strains that are sequenced. Wild type *C. auris* is evolved in monotherapy in four conditions (1x, 2x, 4x and 8x MIC_{50}, depicted in blue, red, green and purple respectively) and $MIC_{50,\ wt}$ is depicted by a yellow star. Strains with elevated MIC_{50} values, relative to the wild type, in which mutations were found, are depicted by a black diamond and their unique strain number, which represents strains displayed in Tables 9-12.

4.4 Collateral sensitivity and cross resistance mapping

4.4.1 Collateral sensitivity and cross-resistance mapping based on AUC and MIC_{50}

In order to evaluate **collateral sensitivity (CS) and cross-resistance (XR)**, heatmaps based on RR AUC_{BDA} and MIC_{50} are generated and displayed in Figures 28-29. Data is retrieved from BDA experiments with three drug-resistant strains per drug condition (1x, 2x, 4x and 8x MIC_{50}, except for MCA which are 4x, 8x, 16x, and 32x MIC_{50}) against all antifungals and repurposed drugs. However, in some drugs, an insufficient amount of resistant strains is retrieved in some conditions. This was the case for POS 4x MIC_{50}, MCA 8x and 32x MIC_{50}, TRB 2x and 8x MIC_{50}, AMB 1x MIC_{50} and NIT 2x MIC_{50}, in which two strains are retrieved. Furthermore, in KTO 1x MIC_{50}, AMB 2x MIC_{50} and NIT 4x MIC_{50}, one strain is used each time. The heatmap generated from normalized mean AUC_{BDA} RR is displayed in Figure 28.

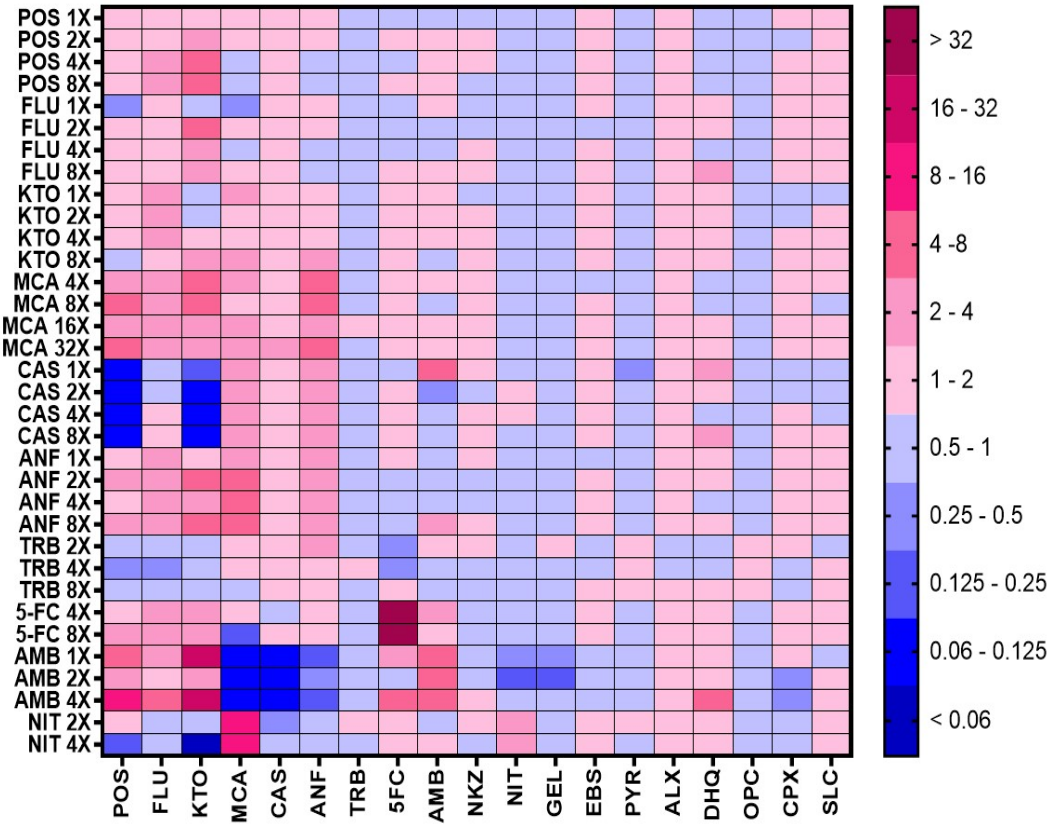

Figure 28: Heatmap of RRs based on normalized AUC_{BDA}. RRs are calculated by $AUC_{BDA,\ resistant}/AUC_{BDA,\ wt}$. Each row represents the average of three resistant strains indicated by the drug and drug dose in which it was evolved. Each column represent an antifungal or repurposed drug (for abbreviations and info see Table 7). A two-gradient colored scale visualizes the RR, ranging from >32 (pink) to <0.06 (blue), for which CS is displayed if RR < 1 (blue) and XR if RR > 1 (pink).

Generally, based on AUC_{BDA}, **XR** is observed in **azoles and echinocandins**, both **intra-** (against the drug it was evolved for) and **interclass** (within the same drug class). Besides, **5-FC, AMB, and NIT** display **intraclass XR** as well. Furthermore, XR is present in the **azole-resistant** strains to the echinocandins. Additionally, **5-FC, AMB-, ANF- and MCA-resistant** strains also exhibit XR against **azoles**. Lastly, 5-FC resistant strains exhibit XR against AMB, and NIT-resistant strains against MCA. No substantial trends are observed between the drug-resistant strains and the repurposed drugs. **CS** is reported for **CAS-resistant** strains to **POS** (0.07 - 0.19) and **KTO** (0.05- 0.48). Furthermore, **TRB-resistant** strains exhibit CS to the azoles, for which **POS and FLU** RRs are 0.27 - 0.80. Additionally, in **AMB-resistant** strains CS was prominently present against the echinocandins based on AUC_{BDA}: **MCA** (RR: 0.08 - 0.11), **CAS** (RR: 0.07 - 0.10) and **ANF** (RR: 0.20 - 0.26). Furthermore, AMB-resistant strains also exhibit CS to **NIT** (RR: 0.19 - 0.63), **GEL** (RR: 0.13 - 0.93), and **CPX** (RR: 0.29 - 0.99).

Furthermore, the heatmap generated from RR MIC_{50} is displayed in Figure 29.

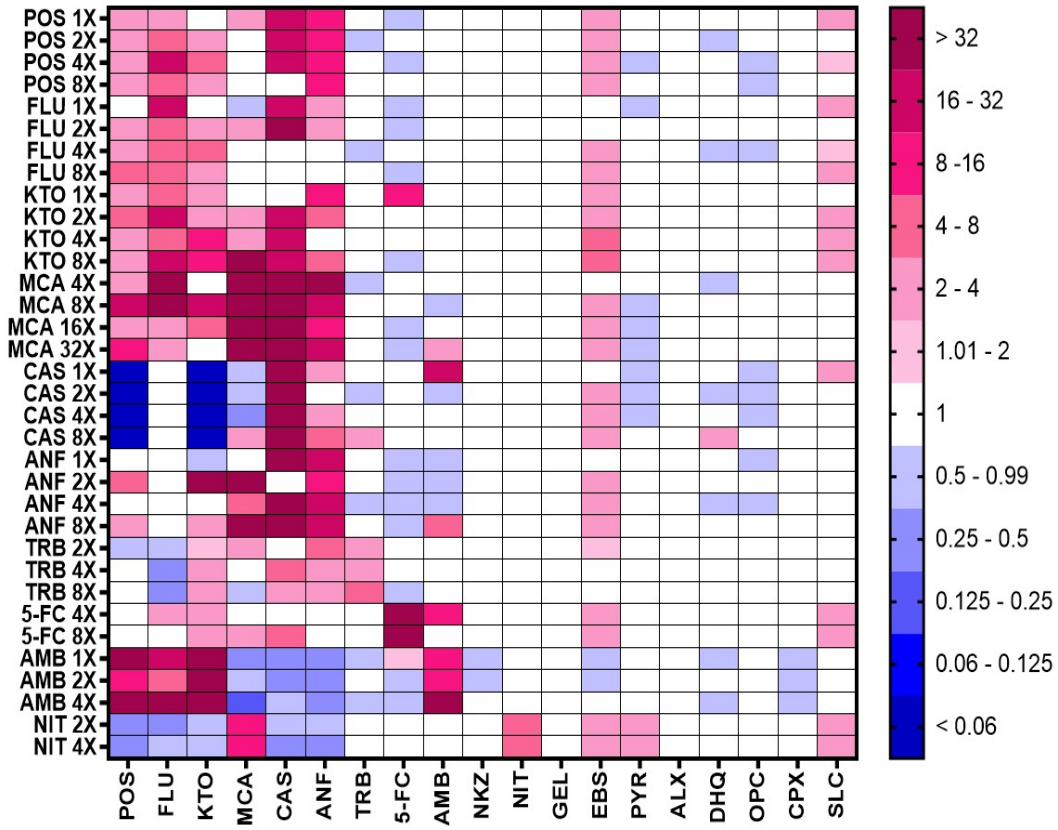

Figure 29: Heatmap of RR based on MIC_{50}. RRs are calculated by $MIC_{50,\ resistant}/MIC_{50,\ wt}$. Each row represents the average of three resistant strains indicated by the drug and drug dose in which it was evolved. Each column represents an antifungal or repurposed drug (for abbreviations and info see Table7). A two-gradient colored scale visualizes the RR, ranging from >32 (pink) to <0.06 (blue), for which CS is displayed if RR < 1 (blue), indifference if RR = 1 (white) or XR if RR > 1 (pink).

XR is observed within the **azoles and echinocandins**, both inter- and intraclass, except for CAS-resistant strains to MCA, which is unexpected. **Intraclass XR** is also present in **5-FC, AMB and TRB**. Furthermore, prominent XR is displayed in **AMB-resistant** strains against the **azoles**: POS (RR: 8-256), FLU (RR: 4-32) and KTO (RR: 64-192). XR is found in **TRB resistant** strains against **CAS and ANF** (RR: 1-8) and **NIT-resistant** strains display XR against **MCA** (RR: 8). In terms of **CS**, strong CS is observed in **CAS-resistant** strains to **POS** (RR MIC: 0.002) and **KTO** (RR: 0.002-0.0039). Furthermore, **AMB-resistant** strains display an increased sensitivity towards the **echinocandins**: MCA (RR: 0.125-0.5), CAS (RR: 0.25-0.5) and ANF (RR: 0.25). Lastly, **NIT-resistant** strains exhibit CS to the **azoles**, POS (RR: 0.25-0.375), FLU (RR: 0.375-0.5) and KTO (RR: 0.5), and to **CAS** (RR: 0.25-0.5) and **ANF** (RR: 0.25-0.75). No general trends are found for the drug resistant strains to the repurposed drugs.

As CS is important for designing drug cycling schemes, CS trends are compared between RRs of AUC_{BDA} and MIC_{50} to visualize which drug combinations are the most favorable to prevent resistance emergence. In AMB-, CAS-, TRB- and NIT-resistant strains, CS to other drugs is most evidently present. The heatmap in Figure 30 indicates the mean MIC_{50} and AUC_{BDA} of all four conditions and Table A3 (Addendum) includes the exact ranges in which CS occurs.

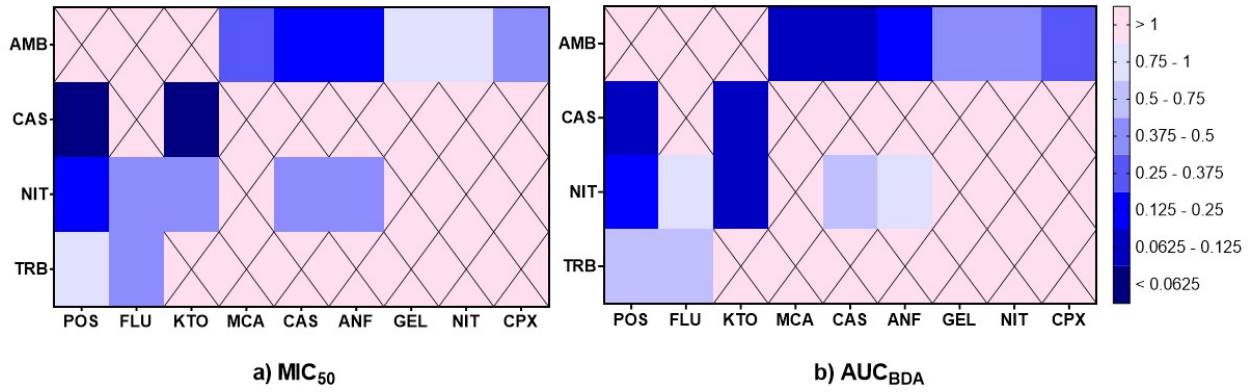

Figure 30: Collateral sensitivity ranges between resistant strains (y-axis: AMB, CAS, NIT and TRB) and antifungal/repurposed drugs (x-axis) based on mean RR values of a) MIC_{50} and b) AUC_{BDA}. Mean RRs MIC_{50} and mean RRs AUC_{BDA} of strains in all four conditions (1x, 2x, 4x and 8x MIC_{50}) are calculated for drug combinations in which CS is prominently present. These values were depicted based on a gradient from <0.0625-1 (blue) when CS is present and ≥1 when no CS is present (red).

The MIC_{50} and AUC_{BDA} heatmaps are easily distinguishable. A possible explanation for this are the different approaches on how resistance ratios are obtained. On the one hand, MIC_{50} describes resistance very robustly as it determines resistance at the cut-off of 50% growth, relative to the growth in no drug. AUC_{BDA}, on the other hand, is more subtle and takes more into account about the relative growth differences in BDA. Although differences are present, mutual trends regarding CS between AUC_{BDA} and MIC_{50} are present, as observed in Figure 30. CS is observed between CAS-resistant strains to POS and KTO. Furthermore, AMB-resistant strains display prominent sensitivity to the echinocandins and CPX. Additionally, TRB-resistant strains exhibit prominent CS to FLU as well, and NIT-resistant strains are more sensitive to the azoles, CAS and ANF.

4.4.2 CS and XR networks

CS and XR networks are constructed based on prominent CS and XR trends in both the AUC_{BDA} and MIC_{50} heatmaps in Figures 28-30 on pages 48-50. These networks are presented in Figure 31. In Figure 31a, CAS exhibits CS to POS and KTO. Furthermore, NIT displays CS to the azoles and the echinocandins (specifically CAS and ANF), and TRB shows CS to FLU. Lastly, AMB expresses

CS to the echinocandins and some repurposed drugs, such as CPX, GEL, and NIT. On the other hand, in Figure 31b, intra- and interclass XR in the azoles and the echinocandins are present, as well as XR in azoles against echinocandins. Additionally, AMB-resistant strains express increased resistance against the azoles and NIT displays XR against MCA as well.

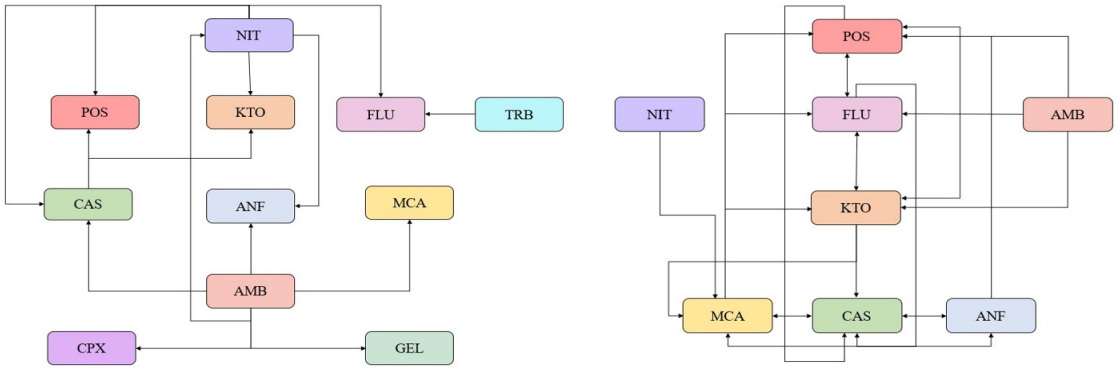

Figure 31: a) CS and b) XR networks. Networks are designed based on RR AUC_{BDA} and MIC_{50} data. Arrows indicate for which drugs the resistant strains have acquired a) sensitivity or b) resistance.

4.4.3 Survival dynamics in CS and XR

Although **MFC_{99}** is not a measure for resistance and is mostly biased, it allows for estimating the **susceptibility and survival dynamics** of drug-resistant strains against other drugs. Therefore, the **Susceptibility Ratio (SR)** of the strains used to generate the AUC_{BDA} and MIC_{50} heatmaps, is calculated. SR is based on YPD spot assays of BDA plates and is described as the ratio:

$$SR\,MFC_{99} = \frac{MFC_{99,\,\text{evolved}}}{MFC_{99,\,\text{wt}}}$$

From these ratios, the mean of three resistant strains per drug and drug condition against antifungals and repurposed drugs is calculated and a heatmap is generated, which is depicted in Figure 32.

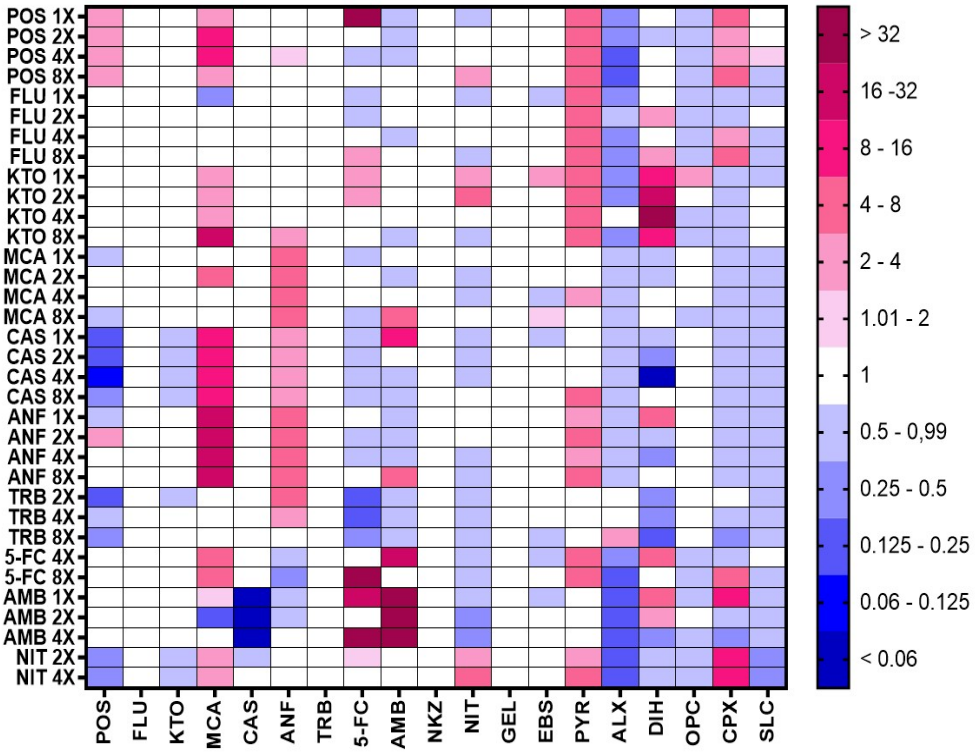

Figure 32: Heatmap of Susceptibility Ratio (SR) based on MFC_{99}. SRs are calculated of strains with RR MIC_{50} > 1. Each row represents the average of three resistant strains indicated by the drug and drug dose in which it was evolved. Each column represents an antifungal or repurposed drug (for abbreviations and info see Table 7). A two-gradient colored scale visualizes the SR, ranging from >32 (pink) to <0.06 (blue), for which an increased sensitivity to the drug is displayed if RR < 1 (blue), indifference if RR = 1 (white) and less susceptibility to the drug if RR > 1 (pink).

Prominently, POS-, ANF-, 5-FC and AMB-resistant strains show reduced susceptibility to their respective drugs. Furthermore, POS-resistant strains exhibit 2- to 8-fold reduced susceptibility to MCA. In the echinocandins, the most evident trends are CAS-resistant strains with an 8-fold increased insensitivity to MCA and ANF-resistant strains with a 16-fold decreased sensitivity to MCA. In AMB-resistant strains (1x and 4x MIC_{50}), 16- to 32-fold reduced susceptibility to 5-FC is observed. Nevertheless, similarly as in AUC_{BDA} and MIC_{50}, an increased susceptibility is observed in CAS-resistant strains to POS (4- to 16-fold) and KTO (2-fold), as well as TRB-resistant strains to POS (2- to 8-fold). In AMB-resistant strains, a 32-fold increased susceptibility is noted to CAS, implying that CAS may even act fungicidal in these strains. NIT-resistant strains also display a 4-fold increased sensitivity to POS. Lastly, TRB-resistant strains exhibit a 3- to 4-fold increased sensitivity to 5-FC.

4.5 Collateral sensitivity based drug cycling

4.5.1 Average relative growth in drug cycling schemes

In all five drug cycling schemes, a 100% survival is reported in each condition. YPD spot assays of the experimental evolution plates are displayed in Figure A18 (Addendum). **The average relative growth** in the cycling schemes is tracked based on **six random populations** per condition, of which single colony isolates were isolated and tested for their drug susceptibility. These are depicted in Figures 33-35. Additionally, **the average relative growth** in the cycling evolution experiments based on all **15 populations per condition** are displayed in Figures A19-A21 (Addendum). As the differences between these two types of graphs are minor, we will only discuss the relative growth based on six populations. The relative growth in **a) AMB-CAS and b) AMB-GEL** based on six populations is depicted in Figure 33

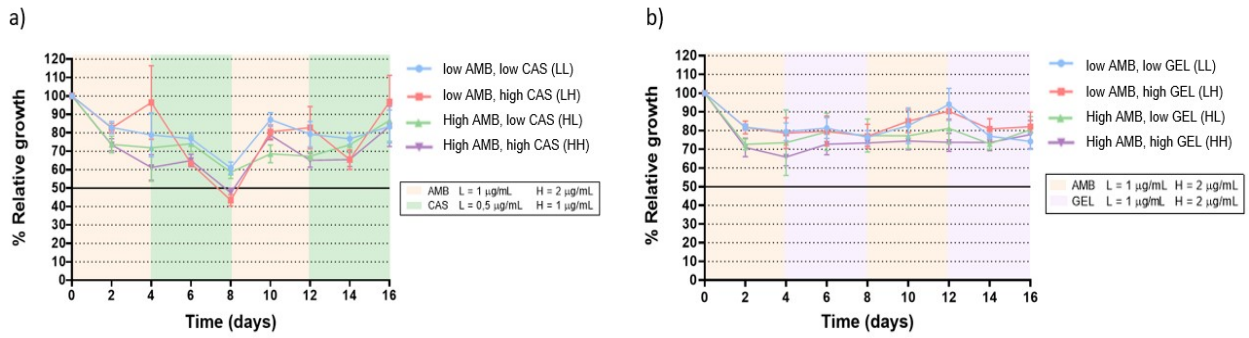

Figure 33: Average relative growth in a) AMB-CAS and b) AMB-GEL cycling. The average relative percentage of growth based on six populations per condition, relative to the controls without drug, is measured at OD_{600} in function of time. The following colors represent relative growth in LL (blue), LH (red), HL (green) and HH (purple). Background colors indicate at which point in time the drugs are switched. Error bars indicate the variation of data points in each condition.

Generally, no substantial differences are observed between the four conditions. In **AMB-CAS** (Figure 33a), populations decrease until day 8, except for populations in LH, before increasing in growth in the second AMB dose on day 10. Afterwards, relative growth is mostly random between all populations Furthermore, in **AMB-GEL**, the populations in HL and HH display a decrease in relative growth until day 4 and populations remain stable afterwards. This is also the case in LL and LH, except from day 8 onwards, populations increase and after day 12, they decrease.

Additionally, the average relative growth was also tracked in **a) AMB-NIT** and **b) AMB-CPX cycling** and displayed in Figure 34.

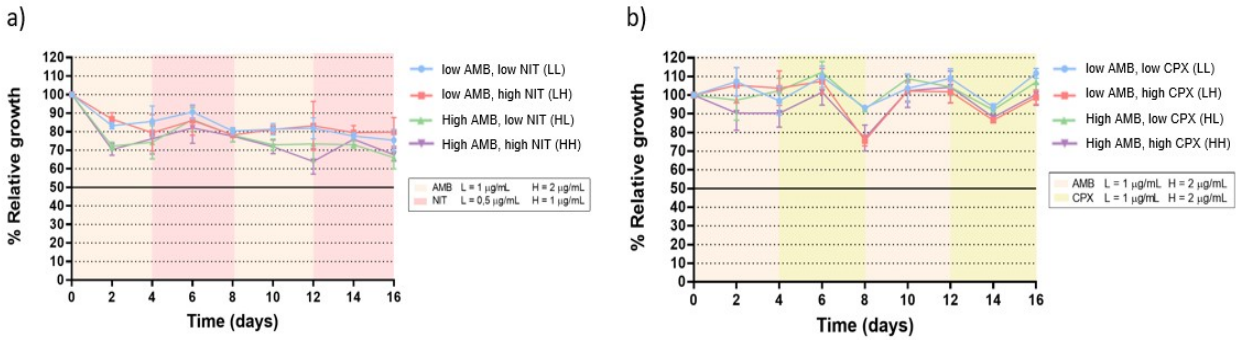

Figure 34: Average relative growth in a) AMB-NIT and b) AMB-CPX cycling. The average relative percentage of growth based on six populations per condition, relative to the controls without drug, is measured at OD_{600} in function of time. The following colors represent relative growth in LL (blue), LH (red), HL (green) and HH (purple). Background colors indicate at which point in time the drugs are switched. Error bars indicate the variation of data points in each condition.

In **AMB-NIT**, displayed in Figure 34a, populations evolved in low AMB on one the hand, and in high AMB on the other hand, seem to follow similar growth trends throughout the cycling evolution experiment. On day 16, lower population densities in high AMB than in low AMB are recorded (±10% difference). Furthermore, cycling between **AMB-CPX** delivered ambiguous results, as the relative growth of some populations surpassed the growth of wt populations, as depicted in Figure 34b. Growth in AMB appeared to be rather random, whereas in CPX, populations in low CPX on the one hand, and populations in high CPX on the other hand, follow comparable growth trends.

Lastly, the average relative growth in **CAS-POS** cycling, depicted in Figure 35, displays distinctive population densities. Relative growth in this cycling scheme was mostly random.

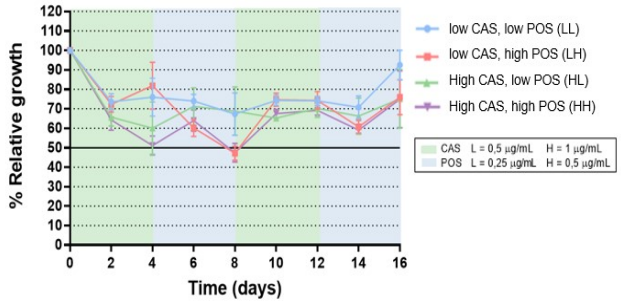

Figure 35: Relative growth in CAS-POS cycling experiment. The average relative percentage of growth based on 6 populations per condition, relative to the controls without drug, is measured at OD_{600} in function of time. The following colors represent relative growth in LL (blue), LH (red), HL (green) and HH (purple). Background colors indicate at which point in time the drugs are switched. Error bars indicate the variation of data points in each condition.

4.5.2 Resistance development and susceptibility in drug cycling

4.5.2.1 Relative percentage of resistance development in drug cycling and monotherapy

The percentage of resistance, based on AUC_{BDA} and MIC_{50}, and susceptibility levels, based on MFC_{99}, are determined in monotherapy and drug cycling, depicted in Table 13. Additionally, comparison between monotherapy and drug cycling RRs based on AUC_{BDA}, MIC_{50} and SRs based on MFC_{99} are displayed in Figure 36.

Table 13: Relative percentage of strains from monotherapy (MONO) and cycling (CYC) that acquired resistance based on AUC_{BDA} and MIC_{50} (RR > 1) or reduced susceptibility based on MFC_{99} (SR > 1). Column "Cycling scheme" describes in which cycling scheme the strains were evolved and "tested for" shows to which drug the strains were tested for susceptibility determination. **For each monotherapy column, only the "tested for" column is relevant.** Strains are evolved in low (1x MIC_{50}, blue) or high (2x MIC_{50}, red) concentrations of the drug in monotherapy or both drugs in drug cycling. Percentages are calculated relative to six strains per condition in monotherapy (except AMB, for which n=1 in 1x MIC_{50} and n=1 in 2x MIC_{50}). In drug cycling, the percentage of resistance or susceptibility is determined relative to 12 strains per condition, except for NIT (n=9 in 2x MIC_{50}).

		AUC		MIC		MFC	
Cycling scheme	**Tested for**	**MONO**	**CYC**	**MONO**	**CYC**	**MONO**	**CYC**
AMB-CAS	**AMB**	100	0	100	0	100	0
		100	0	100	0	100	0
	CAS	100	0	100	0	0	0
		100	0	100	0	0	0
AMB-CPX	**AMB**	100	0	100	0	100	0
		100	0	100	0	100	0
	CPX	/	0	/	0	/	0
		/	0	100	0	/	0
AMB-NIT	**AMB**	100	0	100	0	100	0
		100	0	100	0	100	0
	NIT	66.66	8.33	100	0	100	8.33
		100	8.33	100	0	100	25
AMB-GEL	**AMB**	100	0	100	0	100	0
		100	8.33	100	0	100	16.67
	GEL	/	41.67	/	0	/	0
		/	0	/	0	/	0
CAS-POS	**CAS**	100	8.33	100	0	0	0
		100	50	100	0	0	0
	POS	33.33	0	50	0	0	0
		33.33	0	66.67	0	0	0

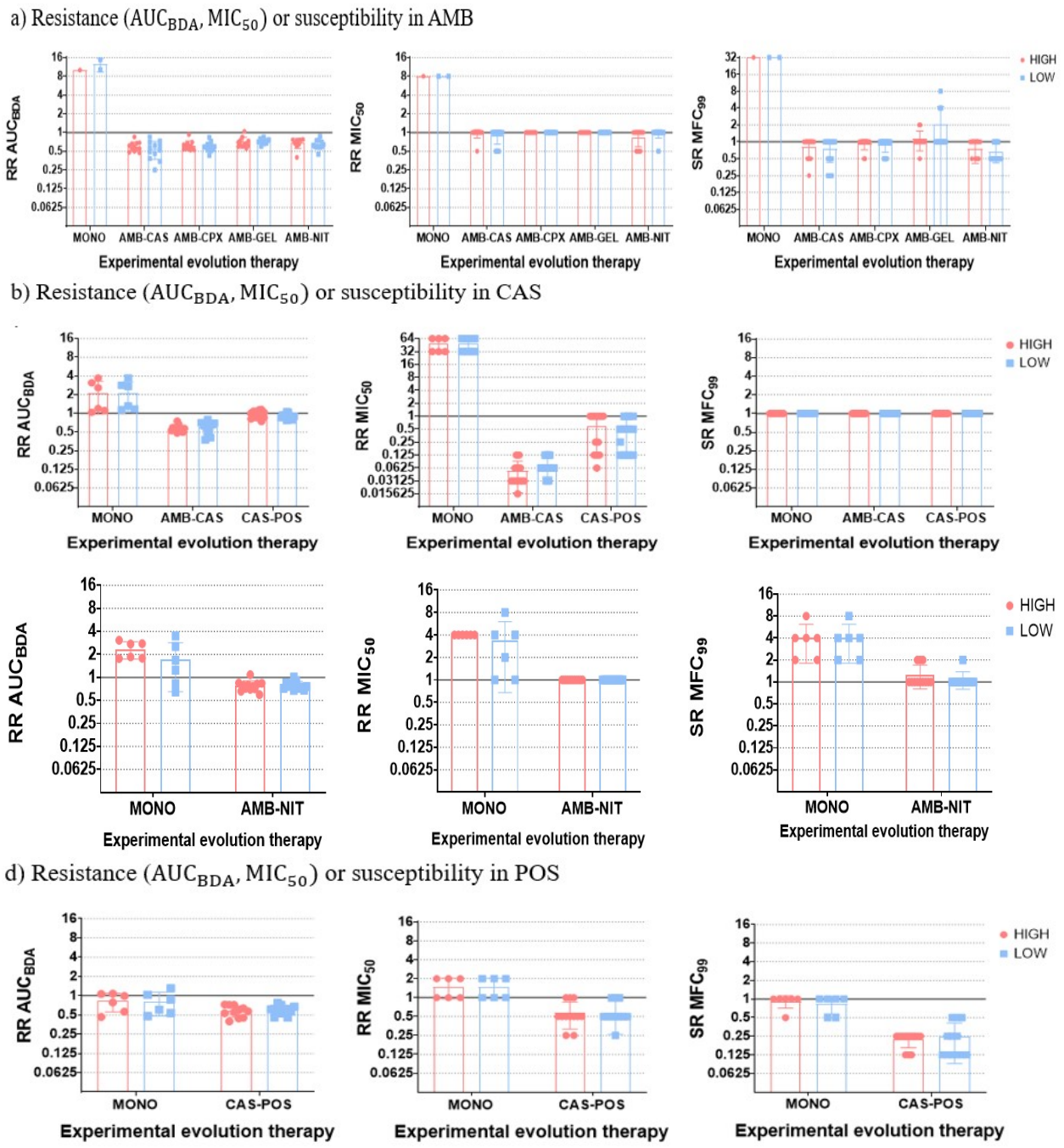

Figure 36: Comparison of RRs based on AUC_{BDA}, MIC_{50} and MFC_{99} in monotherapy and drug cycling schemes. The following graphs display RRs and SRs of drug evolved strains in high (red) and low (blue) conditions: a) AMB (low-high: 1-2 μg/mL), b) CAS (low-high: 0.5-1 μg/mL), c) NIT (low-high: 0.5-1 μg/mL) and d) POS (low-high: 0.25-0.5 μg/mL).

In drug cycling, **based on MIC_{50}**, we do not observe resistance development in any drug cycling scheme, as depicted in Table 13. In contrast, 100% resistance is acquired in both conditions of

monotherapy in AMB (RR: 8, Figure 36a), CAS (RR: 32, Figure 36b) and NIT (RR low: 4-8, high: 4, Figure 36c), but not in POS monotherapy, as only 50% resistance is developed here (RR low: 2, high: 2-8), Figure 36d).

As MIC_{50} is a robust measure, resistance development is also analyzed **based on AUC_{BDA}**. In monotherapy, 100% resistance is determined in **AMB** (RR low: 10.21-14.65, RR high: 10.05) and **CAS** (RR low: 1.14-3.71, RR high: 1.04-3.70) as depicted in Figures 36a-b. On the other hand, in 1x MIC_{50} NIT, 66.67% resistance is observed with resistance levels equal to RR low: 1.24-3.47 and RR high: 1.78-3.06 (Figure 36c), and in **POS** (33.33% resistance in both 1x and 2x MIC_{50}) with RR low: 1.03-1.30 and RR high: 1.07 (Figure 36d). In the case for **drug cycling**, in **AMB-GEL cycling**, resistance to AMB (RR: 1.04) is observed for one strain evolved in 2x MIC_{50} AMB (8.33%), which is shown in Figure 36a. Furthermore, resistance to CAS is recorded in 8.33% of strains evolved in 1x MIC_{50} CAS (RR: 1.03) and 50% of strains in 2x MIC_{50} CAS (RR: 1.01-1.15) in **CAS-POS cycling**, described in Figure 36b. Additionally, resistance to NIT is observed in 8.33% of strains in both conditions of **AMB-NIT cycling**, displayed in Figure 36c (RR low: 1.01, RR high: 1.08).

4.5.2.2 Resistance and susceptibility levels in drug cycling

Resistance development in cycling is analyzed by selecting six strains per condition (LL, LH, HL and HH) and test their susceptibility to the two drugs they were interchangeably evolved for.

In **AMB-CAS**, resistance nor reduced susceptibility is acquired, as displayed in Figure 37.

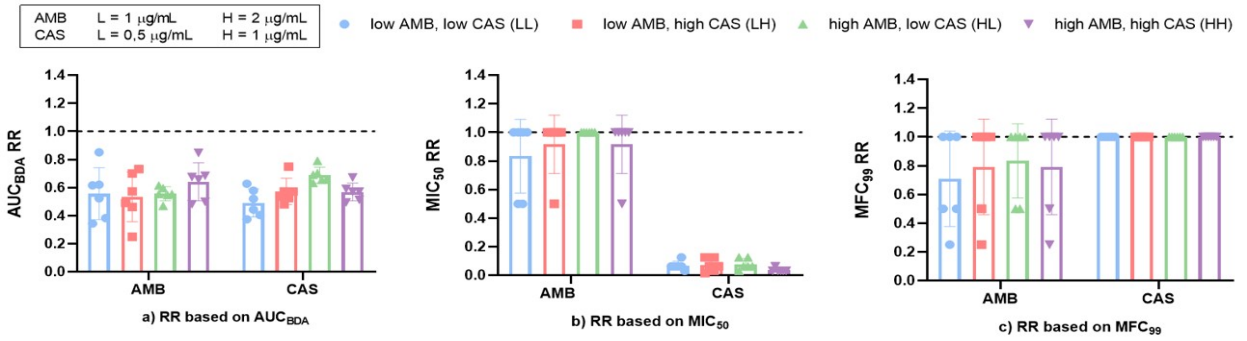

Figure 37: Resistance development in AMB-CAS cycling, investigated through a) RR based on AUC_{BDA}, b) RR based on MIC_{50} and susceptibility profiles are studied through c) SR based on MFC_{99}. Bars depict the mean RR or SR of six strains per condition, distinguished by colors. The legend displays which color is assigned to each condition and data points represent individual strains.

Judging from Figure 37a, **based on AUC_{BDA}**, no substantial differences regarding resistance

development between the four conditions are observed in both AMB (RR: 0.34-0.85) and CAS (0.37-0.79). Regarding RRs **based on MIC_{50}** depicted in Figure 37b, susceptibility of the strains in AMB (RR: 0.8-1) is lower compared to those in CAS (RR: 0.015625-0.2). Lastly, susceptibility of the strains is examined in Figure 37c by determining **SRs** in both drugs. In CAS, an indifference in susceptibility is noted in all strains, whereas in AMB, nine strains exhibit an increased sensitivity to the drug: 3 strains in LL, 2 in LH, 2 in HL and 2 in HH.

Besides, in **AMB-GEL** cycling, depicted in Figure 38, one HH strain acquired resistance to AMB, while two LL strains and one HL strain developed resistance to GEL, based on AUC_{BDA} (Figure 38a). Furthermore, two HH strains exhibit reduced susceptibility based on MFC_{99} in Figure 38c.

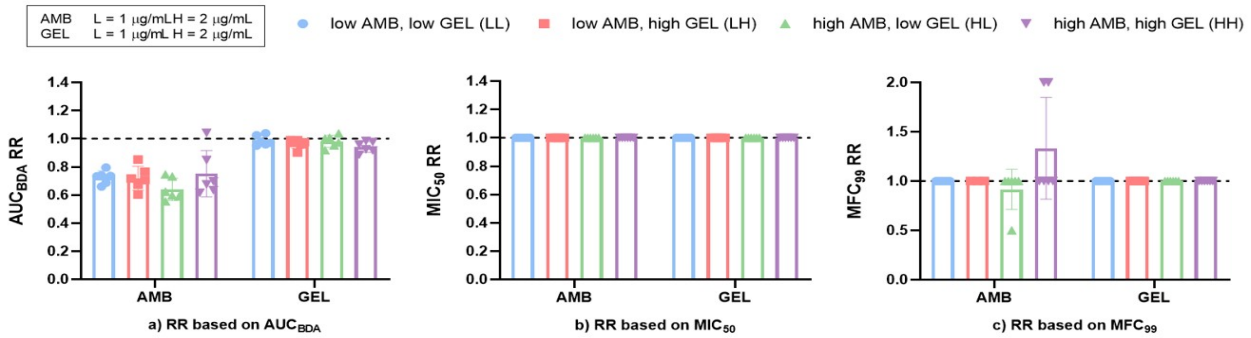

Figure 38: Resistance development in AMB-GEL cycling evolution experiment is investigated through a) RR based on AUC_{BDA}, b) RR based on MIC_{50} and susceptibility profiles are studied through c) SR based on MFC_{99}. Bars depict the mean RR or SR of six strains per condition, distinguished by colors. The legend displays which color is assigned to each condition and data points represent individual strains.

In Figure 38a, all strains, aside from those that exhibit resistance towards AMB or GEL, display an increased sensitivity towards both drugs, based on AUC_{BDA}, for which a higher level of sensitivity to AMB is observed (RR: 0.55-0.85 in AMB) compared to GEL (RR: 0.92-0.98). Generally, based on MIC_{50} in Figure 38b, RRs in both drugs show an indifference in all conditions. Lastly, in Figure 38c, in all conditions except HH and HL in AMB, susceptibility towards both drugs is indifferent. For a HL strain, an increased sensitivity to AMB is shown (SR: 0.5).

Furthermore, in **AMB-NIT** cycling in Figure 39, only one strain from LH acquired NIT resistance, based on AUC_{BDA} in Figure 39a, Additionally, from LL, LH and HH conditions, one strain of each condition shows a 2-fold reduced susceptibility to NIT in Figure 39c.

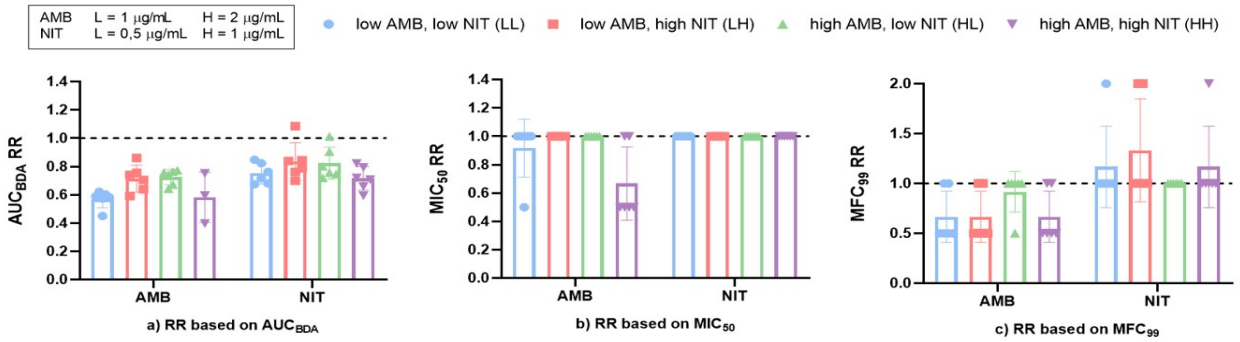

Figure 39: Resistance development in AMB-NIT cycling evolution experiment is investigated through a) RR based on AUC_{BDA}, b) RR based on MIC_{50} and susceptibility profiles are studied through c) SR based on MFC_{99}. Bars depict the mean RR or SR of six strains per condition, distinguished by colors. The legend displays which color is assigned to each condition and data points represent individual strains.

In Figure 38a, an increased sensitivity to both AMB and NIT in all four conditions is recorded based on AUC_{BDA} (RR: 0.40-0.86 in AMB, 0.59-0.90 in NIT). Yet, based on MIC_{50} in Figure 39b, resistance is indifferent for all conditions in NIT, and for LH and HL conditions in AMB. In addition, one LL strain and four HH strains display increased sensitivity to AMB (RR: 0.5). Lastly, in all four conditions, the strains generally became more sensitive to AMB (SR: 0.5-1), but less sensitive to NIT (RR: 1-2), except for strains in HL condition, which exhibit indifference.

Furthermore, RRs and SRs in **AMB-CPX** cycling are depicted in Figure 40. No strains acquired resistance or reduced susceptibility towards AMB nor CPX.

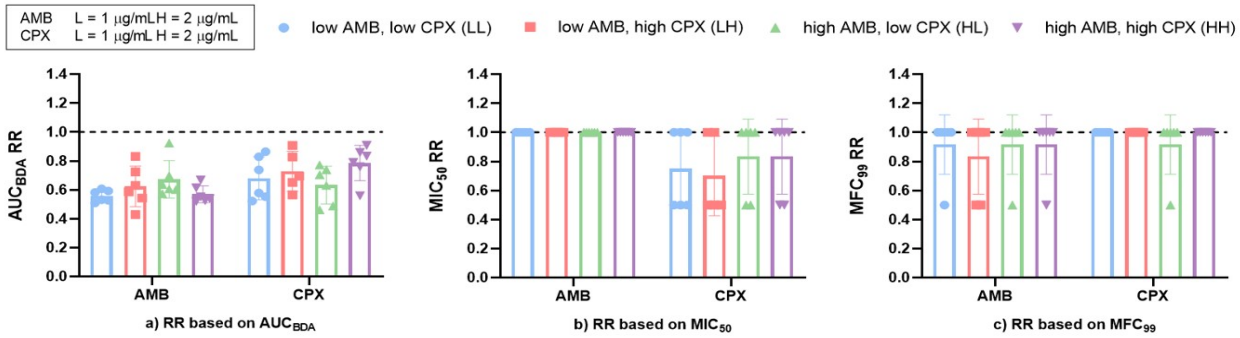

Figure 40: Resistance development in AMB-CPX cycling evolution experiment is investigated through a) RR based on AUC_{BDA}, b) RR based on MIC_{50} and susceptibility profiles are studied through c) SR based on MFC_{99}. Bars depict the mean RR or SR of six strains per condition, distinguished by colors. The legend displays which color is assigned to each condition and data points represent individual strains.

All strains exhibit an increased sensitivity to both AMB and CPX, based on AUC_{BDA} in Figure 40a. The strains exhibit RRs between 0.42-0.92 in AMB and between 0.46-0.91 in CPX, thus no substantial differences regarding susceptibility between the drugs are present. Yet, in Figure 40b,

resistance to AMB is indifferent, whereas strains of LL (3), LH (3), HL (2) and HH (2) display an increased sensitivity towards CPX (RR: 0.5), and the rest are indifferent. Lastly, susceptibility of the strains based on MFC_{99} in Figure 40c is mostly indifferent, except for one strain of LL, HL and HH, and two strains of LH in AMB, and one strain of HL in CPX (SR: 0.5).

Lastly, in **CAS-POS**, depicted in Figure 41, only seven CAS-resistant strains are observed based on AUC_{BDA}: one strain from LL and HL, and five strains from HH, displayed in Figure 41a.

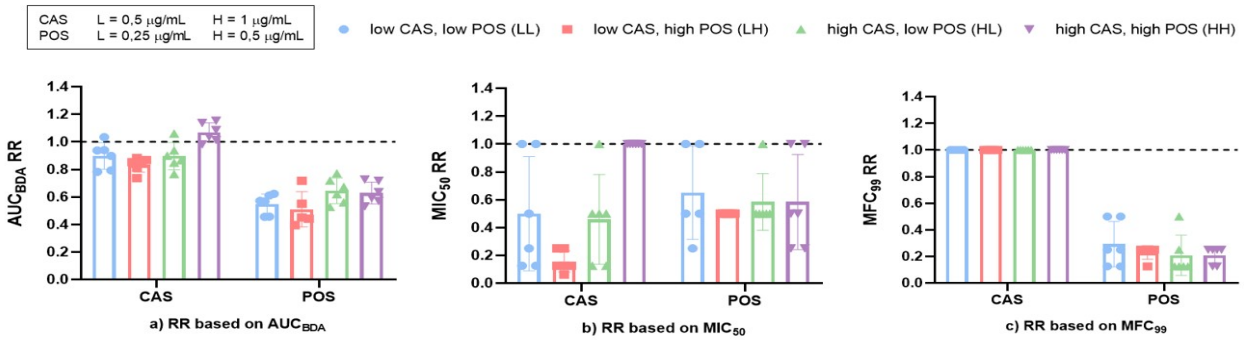

Figure 41: Resistance development in CAS-POS cycling evolution experiment is investigated through a) RR based on AUC, b) RR based on MIC_{50} and susceptibility profiles are studied through c) SR based on MFC_{99}. Bars depict the mean RR or SR of six strains per condition, distinguished by colors. The legend displays which color is assigned to each condition and data points represent individual strains.

Aside from those resistant strains, increased sensitivity to CAS and POS is observed for all strains, based on AUC_{BDA}, yet the level of susceptibility is different between CAS and POS. Disregarding the resistant strains, RRs are 0.73-0.98 in CAS and 0.40-0.72 in POS. Regarding determination of resistance based on MIC_{50} in Figure 41b, in CAS and POS, two LL strains and one HL strain exhibit indifference. Additionally, six HH strains in CAS and two HH strains in POS are indifferent to their respective drugs. The other strains display an increased sensitivity (RR: 0.125-0.5 in CAS, 0.25-0.5 in POS). Lastly, susceptibility to CAS is indifferent for all strains, whereas in POS, all strains display an increased susceptibility to POS (SR: 0.125-0.5), as displayed in Figure 41c.

4.5.2.3 Growth dynamics of resistant cycling evolved strains

As observed in the previous section (4.5.2.1 Resistance and susceptibility in drug cycling), some strains, isolated from cycling evolved populations, exhibit RR AUC_{BDA} >1 against their respective drugs, as depicted in Figures 37-41 on pages 57-60, implying that resistance might have developed. The relative growth of the populations from which these strains were isolated is tracked over a 16-day period and depicted in Figures A16-A17 (Addendum).

In Figure A16a (Addendum), the relative growth of an AMB-resistant population in high concentrations of AMB and GEL is depicted. The graph describes a decrease in population density on day 2, followed by a stable growth until the end of the experiment On the other hand, two different populations in low concentrations of AMB and GEL and one population in high AMB and low GEL concentrations developed resistance against GEL. Their relative growth is displayed in Figure A16b (Addendum). The LL populations show a rather random growth, whereas growth of the HL population decreases until day 4 and is stable afterwards.

Furthermore, the relative growth of a NIT-resistant population in low-high or high-low concentrations of AMB and NIT respectively is displayed in Figure A17a (Addendum). The population density decreased until day 4, increased on day 6 and stabilized afterwards. In Figure A17b (Addendum), for the CAS-resistant population in low concentrations of CAS and POS (depicted by a circle), relative growth decreased until day 8 and increased afterwards. For CAS-resistant populations evolved in high concentrations of CAS and POS (described by a triangle), the relative growth was random. Lastly, for the population in high CAS and low POS (depicted by a triangle), the population declined until day 2 and small differences in growth are recorded up until day 14, followed by an increase in growth at the end of the experiment on day 16.

5. Discussion

5.1 *In vitro* experimental evolution

5.1.1 Survival and resistance development in *C. auris* is mostly linked to the fungicidal or fungistatic nature of the drugs

No extinction of *C. auris* is observed in **azoles, echinocandins, and TRB** as these drugs, except ANF and MCA, act fungistatic in doses 1-8x MIC_{50} used during *in vitro* experimental evolution. **Lower survival** rates are distinguished for **5-FC, AMB, NIT, and CHX** (Figure 16, page 34), which most likely results from their fungicidal nature (Table 7, page 33). Furthermore, after experimental evolution, **resistant strains** are obtained for **nine antifungals** and two repurposed drugs (Figure 18, page 36). For strains evolved in azoles, 59.09% in KTO, 100% in FLU, and 54.16% in POS developed resistance against their respective drugs. In the case of echinocandins, 91.67% in ANF, 100% in CAS, and 83.33% in MCA acquired resistance to their drugs. For drugs such as AMB, NIT, and CHX, resistance development is respectively 75%, 87.50%, and 75%. A smaller fraction of strains in 5-FC and TRB monotherapy developed resistance: 43.48% and 30.43% respectively (Figure 18, page 36).

High percentages of **survival** (100%) and **resistance** to the **azoles**, and especially to FLU (100%) are observed in monotherapy. This observation is supported by the study of Chowdhary et al. (2018), as they observed FLU resistance (MIC: 32 to >64 μg/mL) in up to 90% of the isolates. This led us to believe that azole resistance is easily acquired in *C. auris*. A plausible explanation is that resistance to azoles can be induced through various mechanisms, such as drug efflux, target alteration, genomic alterations [88].

Furthermore, in **echinocandins** experimental evolution, **high** percentages of **survival** (100%) **and resistance** are observed. 100% of the isolated CAS-evolved strains display resistance against CAS. On the other hand, in ANF and MCA monotherapy, which are fungicidal drugs (MFC_{99}: 4 μg/mL), 91.67 % and 83.33% resistance is displayed respectively. However, echinocandins resistance has been reported to a lesser extent in the clinic, as the highest percentage of resistance to CAS recorded was 37% [160]. In line with this and our data, we could conclude that C. auris might acquire echinocandin resistance more easily *in vitro* than in a clinical setting [160].

In **5-FC monotherapy, survival** is relatively **high** (91.67%) (Figure 16, page 34), and MIC_{50} and MFC_{99} values are 0.125 μg/mL and 0.5 μg/mL respectively (Table 7, page 33). Therefore, wild type cells were exposed to 5-FC concentrations of at most 2x MFC_{99} during evolution, which

might explain the high survival. On the other hand, only **43.48%** of the isolated strains developed **resistance** to 5-FC (Figure 18, page 36). This percentage is similar to data observed in the clinic, as Chowdhary et al. (2014) observed 47% 5-FC resistance in *C. auris* isolates [100].

In **AMB monotherapy**, **low survival** is reported (16.67%) (Figure 16, page 34), which might be due to the fungicidal nature of AMB. Additionally, wild type *C. auris* in AMB displays an MIC_{50} and MFC_{99} of 1 μg/mL (Table 7, page 33). Therefore, *C. auris* is exposed to AMB concentrations of maximum 8x MFC_{99}, which is too high for the survival of non-resistant strains. Furthermore, strains evolved for AMB exhibit fitness trade-offs such as impeded growth, as described by Vincent et al. (2013), resulting in strains that might be too crippled to retain their viability [113]. This was also observed by us, as smaller colonies could be distinguished (Figure A2, Addendum). Besides, **75%** of the surviving AMB-evolved strains acquired **resistance** to AMB. However, taking into account that only six strains developed resistance to AMB, we can assume that AMB resistance occurs less frequently. Unlike azoles and echinocandins that target enzymes in biosynthesis pathways in *C. auris*, polyenes bind to the essential component ergosterol and directly disrupt the cell membrane. Therefore, AMB has effective antifungal activity and the lower occurrence of AMB resistance might be due to the low percentage of surviving populations in AMB monotherapy (Figure 18, page 36).

For both **NIT and CHX, lower survival** is recorded, 63.33% and 26.67% respectively (Figure 16, page 34). A plausible explanation is that these repurposed drugs exhibit effective antifungal activity as MIC_{50} is 2 μg/mL for NIT and 0.03125% for CHX (Table 7, page 33). Nevertheless, relatively high percentages of resistance are observed for both drugs (NIT: 87.5%, CHX: 75%) (Figure 18, page 36). However, as far as we know, cases of resistance to NIT or CHX in fungal pathogens, let alone *C. auris*, have not been reported in the clinic yet. Besides, resistance to CHX might not have been acquired at all, as MIC_{50} resistance ratios (RR) are maximum 2, and dilution errors occur more often at low drug concentrations, which is the case for CHX (0.004-1%). Lastly, **100% survival** is observed in **TRB monotherapy** (Figure 16, page 34), which is expected as TRB acts fungistatic. However, only **30.43%** developed **TRB resistance** (Figure 18, page 36). Similar to NIT and CHX, TRB resistance has not been reported in the clinic yet, but Chowdhary et al. (2018) reported little to no antifungal activity of TRB against *C. auris* isolates (MIC: 2-32 μg/mL) [34].

5.1.2 Resistance development in *C. auris* shows dose-dependent trends in 5-FC

Resistance is acquired in all four drug conditions in azoles, echinocandins and TRB monotherapy. Additionally, no substantial differences in resistance levels are observed between the conditions.

Furthermore, no resistant strains are obtained in 8x MIC_{50} of AMB and NIT monotherapy, and 2x MIC_{50} of CHX monotherapy. Remarkably, statistical tests reveal that only **in 5-FC monotherapy, significant trends regarding drug dose-dependent resistance development** are present. Accordingly, 5-FC resistance is only reported in **4x and 8x MIC_{50}** of 5-FC monotherapy, in which **high levels of resistance** are acquired as well (RR MIC_{50}: 256) (Figure 19, page 37).

Nevertheless, dose-dependency in resistance development is not a new concept as studies in bacteria and tumors have acknowledged this. Resistance to doxorubicin or epirubicin in breast cancer cells was only acquired when a certain threshold dose of these drugs was achieved. Additionally, resistance levels increased progressively at increasing drug doses [161]. Furthermore, in the bacterium *Salmonella typhimurium*, high streptomycin concentrations selected for strains carrying rpsL mutations, which cause high levels of resistance (>1024 μg/mL). These rpsL mutations were also associated with growth defects. Therefore, in low streptomycin concentrations, rpsL mutations are usually not favored [162, 163, 164]. Accordingly, resistance can be dose-dependent as heterogeneity within a population can induce selection of strains that are intrinsically resistant. Additionally, high drug concentrations might also stimulate the acquisition of rescue mutations. This was demonstrated by Van den Bosch et al. (2014), who performed theoretical and experimental studies on agricultural fungicides and observed that high drug doses will speed up resistance development [165]. Furthermore, two phases are generally distinguished during resistance development. In the emergence phase, a few cells acquire resistance mutations. In the selection phase, selection pressure of the drug is high, causing the resistant cells to thrive and the drug-sensitive cells to go extinct [166, 167, 168].

5.1.3 Resistance development in monotherapy in *C. auris* displays drug-dependent trends

By evolving wild type *C. auris* in monotherapy *in vitro*, resistant strains with distinct ranges of resistance, based on MIC_{50}, are obtained for nine antifungals and two repurposed drugs.

For the **azoles**, FLU-resistant strains exhibit an MIC_{50} range between 2 to >16 μg/mL (Figure 19, page 37), whereas Chowdhary et al. (2018) observed an MIC range of 32 to > 64 μg/mL in their FLU-resistant *C. auris* isolates. Although our strains did not acquire a similar resistance range as in the clinic, our data might provide further evidence for the intrinsic resistance to FLU in *C. auris*. Besides, in POS and KTO ($MIC_{50,\,wt}$: 0.25 μg/mL), resistance development is less pronounced than in FLU, as MIC_{50} values are situated between 0.5-16 μg/mL for POS and 0.5-8 μg/mL for KTO (Figure 19, page 37). In a study conducted by Killburn et al. (2022), POS-resistant strains exhibited MIC_{50} between 0.5-1 μg/mL [169], which is comparable to our results as the majority

of our POS-resistant strains have an MIC_{50} of 0.5 μg/mL (not mentioned).

As for the **echinocandins**, all CAS-resistant strains exhibit an MIC_{50} of >16 μg/mL, whereas MIC_{50} ranged between 2 to >16 μg/mL in ANF-resistant strains, and between 4 and >16 μg/mL in MCA-resistant strains (Figure 19, page 37). The tentative breakpoints recommended by the CDC are $\geq$2 μg/mL for CAS, and $\geq$4 μg/mL for both ANF and MCA [170]. Additionally, MIC resistance ranges in the clinic include 4-8 μg/mL for ANF and MCA, and 2-$\geq$16 μg/mL for CAS [169]. Notably, our resistance ranges slightly deviate from those in the clinic, as our resistant strains exhibit higher MIC_{50} values. Yet, Carolus et al. (2021) reported MIC_{50} of $\geq$64 μg/mL for their CAS-resistant strains in CAS. These strains were associated with mutations in genes such as *FKS1, ERG3*, but also in *PEA2* and *CIS2* genes [99].

Furthermore, **5-FC resistant** strains exhibit MIC_{50} of >16 μg/mL (Figure 19, page 37) while $MIC_{50,\,wt}$ is 0.125 μg/mL (Table 7, page 33). Similarly, Chowdhary et al. (2014) observed 47% 5-FC resistance in 15 clinical isolates with MIC: $\geq$64 μg/mL [100]. Furthermore, Kathuria et al. (2015) reported 5-FC resistance in 11 out of 105 isolates, with elevated MICs of $\geq$32 μg/mL [160]. This is in accordance with our observations.

As for **polyenes**, MIC_{50} of wild type *C. auris* and AMB-resistant strains were evaluated by both BDA and ETEST®. Distinct variability between these methods is observed in our results and in the clinic, as higher MIC endpoints are obtained in BDA compared to ETEST®, yet both methods are reliable [160]. These discrepancies might be caused by the differential method of conducting these assays, as ETEST® involves the use of solid agar, whereas CLSI susceptibility testing is performed in liquid media. In BDA, three AMB-resistant strains exhibit an MIC_{50} of 8 μg/mL, whereas three other AMB-resistant strains display an MIC_{50} of >16 μg/mL (Figure 19, page 37). On the other hand, in ETESTs®, all these strains display MIC_{50} >32 μg/mL (Figure A2, Addendum). Thus, MIC_{50} of AMB-resistant strains are atleast 8 times higher than wt *C. auris* in AMB (MIC_{50}: 1 μg/mL, Table 7, page 33). Clinical isolates in the literature indicate resistance to AMB at MICs $\geq$2 μg/mL [34, 171]. Nevertheless, Rybak et al. (2022) described a case in which a patient with azole-resistant *C. auris* was treated with AMB and developed resistance to the drug as well, of which isolates exhibited MICs higher than 32 μg/mL [172].

Lastly, **TRB monotherapy** yields resistant strains with MIC_{50} between 8 and >16 μg/mL (Figure 19, page 37), while $MIC_{50,\,wt}$ of *C. auris* is 4 μg/mL (Table 7, page 33). On the contrary, Chowdhary et al. (2018) observed a wider range of MICs of TRB-resistant strains, namely 2-32 μg/mL [34]. **In NIT monotherapy,** an MIC_{50} range of 2-4 μg/mL is reported in the resistant strains (Figure 19, page 37), whereas wt *C. auris* exhibit MIC_{50} of 0.5 μg/mL (Table 7, page

33). In concordance with our data, Fuchs et al. (2021) reported a NIT MIC range of 0.125-1 μg/mL [173]. No records of NIT resistance in *C. auris* have been defined yet in the literature, thus acquired resistance and its mechanisms are still a knowledge gap. At last, wt MIC_{50} **in CHX** was 0.0078 μg/mL (Table 7, page 33) and six CHX-resistant strains are obtained in monotherapy (MIC_{50}: 0.01563 μg/mL) (Figure 19, page 37). However, CHX-resistant strains did not display high levels of resistance as their MIC_{50} is only two-fold higher than $MIC_{50,\,wt}$. Consequently, it is unclear whether this is actual CHX resistance or whether it is technical variation or tolerance based adaptation to the drug. In the literature, MIC_{80} was reported to range between 2-8 μg/mL and cases of CHX resistance in fungi have not been reported yet [174].

5.2 Acquired resistance mutations

5.2.1 Azole resistance is linked to four missense mutations in *TAC1b*

In **Strain 60, 63** and **78**, **four missense mutations** are found in ***TAC1b***, namely **F228I, V492G, S514N** and **S540N** (Table 9, page 42). These have not been described in the literature. Three mutations in *TAC1b* were reported by Rybak et al. (2020) from *in vitro* evolution experiments, namely F214S, R495G, and A640V. These mutations contributed to FLU resistance, and additionally were characterized in clinical FLU-resistant *C. auris* isolates. Several other mutations found by Rybak et al. [91], Carolus et al. (2020) [99] and Li et al. (2021) [92] are displayed in Table 14.

Table 14: *TAC1b* mutations that have been reported in the literature

Paper	Mutations in *TAC1b*
Rybak et al. (2021) [91]	A15T, S192N, S195C, F214S, K247E, R495G, A583S, P595L/H, A640V, A651T, M653V, A657V, F862_N866del
Carolus et al. (2021) [99]	F191Δ, F15 (codon deletion), [i(5L)]
Li et al. (2021) [92]	F214L, S611P

Mutations S514N and S540N (strain 60), and V492G (strain 78) are located near the middle homology region (MHR) of ***TAC1b*** (Figure 23, page 44), a transcription factor that positively regulates the expression of ***CDR1*** and ***CDR2***, which encode **drug transporters Cdr1** and **Cdr2** respectively [42, 89]. In line with this, Rybak et al. (2020) found an enhanced expression of *CDR1* in strains with GOF mutations F214S, R495G, and A640V in *TAC1b*, associated with FLU resistance [91]. Consequently, our mutations might be GOF mutations as they are located near these

GOF mutations found by Rybak et al. Additionally, **azole resistance** is observed in our strains as well, which further supports this hypothesis. FLU-resistant strain 60 (*TAC1b*, S514N and S540N) and strain 63 (*TAC1b*, F288I) display RR MIC_{50} of 4 to FLU (Table 9, page 42). Additionally, susceptibility of strain 63 to POS and KTO is also tested, which reveals RRs MIC_{50} of 2 to POS (not mentioned) and 4 to KTO (not mentioned). For KTO-resistant strain 78 (*TAC1b*, V492G), RR MIC_{50} is 8 to KTO (Table 9, page 42), 2 to POS, and 16 to FLU (not mentioned).

Additionally, the missense mutations in *TAC1b* have either a neutral effect (S514N: -67, S540N: -61) or a weak effect (F228I: -20, V492G: 14) (Table 9, page 42), which is reasonable as they are substituted for similar amino acids. Furthermore, as they are most likely GOF mutations in *TAC1b* due to their association with FLU- and KTO resistance, the effect score does not necessarily have to be high as GOF mutations are small and subtle by nature. Evidence for this is provided by running SNAP2 analysis on the A640V mutation in *TAC1b* found by Rybak et al. (2020) [91]. SNAP2 predicted a neutral effect of -37 with 66% accuracy (Figure A11, Addendum), which was paired with an 8-fold increase in MIC when this mutation was introduced into the native *TAC1b* locus of a FLU-susceptible strain [91]. Remarkably, V492G is the only mutation with a positive effect score (14). This might be due to the extra isopropyl group carried by Valine (V) compared to Glycine (G). This group may introduce additional bulkiness, which would disappear when substituted for G, and might be important for the protein structure as it is favored in β-sheets [175].

5.2.2 Mutation S639Y in *FKS1* HS1, corresponding to a mutation in *C. albicans*, is associated to echinocandin resistance

Mutation **S639Y** is found in **HS1 of *FKS1*** in **two MCA-evolved strains** (Table 10, page 43). *FKS1* encodes the catalytic subunit of the **β-(1,3)-D-glucan synthase,** which is the target of echinocandins. As a consequence, mutations in *FKS1*, and especially in HS regions, may lead to **echinocandin resistance** due to the reduced binding of the drug to the protein [45, 102, 103].

Mutations at the same location in *FKS1* in *C. auris*, but not the same amino acid substitution, have been reported in the clinic. Chowdhary et al. (2018) found mutation S639F in HS1 of *FKS1* in four isolates (n=38). These isolates exhibited pan-echinocandin resistance with elevated MICs of $\geq$8 μg/mL to ANF, CAS, and MCA, compared to isolates without mutations in echinocandins (MIC: 0.125-1 μg/mL) [34]. In addition, Kordalewska et al. (2018) evaluated this mutation *in vivo* by challenging BALB/c mice (Charles River Laboratories), a murine neutropenic model for disseminated candidiasis, with the *fks1* S639F mutant and treating them with CAS. Correspondingly, mutant mice failed to respond to CAS and kidney burden did not decrease [45].

Furthermore, a different substitution in *C. auris* was reported by Berkow and Lockhart (2018) in the same position, namely S639P, which was linked to resistance against CD101, a novel echinocandin under development [176]. In line with our data and previous reports in the clinic, amino acid substitutions in *FKS1* at position 639 (HS1) are associated with echinocandin resistance. By performing SNAP2 analysis for position S639 in *FKS1*, it is predicted that our mutation as well as those found in the literature have a strong effect on the protein (Figure A12, Addendum).

Furthermore, our mutation S639Y in *FKS1* in *C.auris* is equivalent to mutation S645Y reported in *C. albicans* in *FKS1* by Garcia-Effron et al. (2009). They observed 8 to >100-fold MIC increases in isolates with substitutions at position S645. Further analyses of kinetic properties of β-(1,3)-D-glucan synthase showed lower V_{max} values in *fks1* mutants compared to wt. In addition, CAS, ANF, and MCA showed noncompetitive inhibition of the enzyme and in fks1 mutants with S645P, S645F or S645Y mutations, a $\geq$100-fold increase of K_i (inhibition constant) was observed for the three echinocandins [102], which implies a weaker binding of echinocandins. V_{max} describes the reaction rate of the enzyme when fully saturated by the substrate and is dependent on the enzyme structure [177]. As a result, the amino acid substitution S645Y in *FKS1* may alter the structure of β-(1,3)-D-glucan synthase, as Serine (S) is a neutral amino acid, containing a reactive hydroxyl group, while Tyrosine (Y) is partially hydrophobic and has an aromatic ring as a side chain, which is linked to a reactive hydroxyl group [175]. Consequently, a similar mechanism might be at play for our mutation as well, causing MCA resistance.

5.2.3 *ERG3* and *ERG11* mutations are linked to polyene (AMB) resistance

Five AMB-resistant strains acquired mutations: **strains 47 (E164*) and 48 (G1415del1)** obtained mutations in ***ERG3*** and **strains 49 (M504I), 50 (Y158*) and 53 (E165*)** acquired mutations in ***ERG11***. *ERG3* encodes for **sterol desaturase** [178] and *ERG11* encodes for **14α-lanosterol demethylase** [179]. Both are important enzymes in the ergosterol biosynthesis pathway (Figure A22, Addendum) [40].

These mutations have not been covered in previous studies and potentially confer reduced sensitivity to AMB (Table 11, page 43). LOF mutations in *ERG3* and *ERG11* can cause the incorporation of alternative sterols into the fungal cell membrane [40], with lower ergosterol levels as a result [47, 113, 115]. Consequently, the mutant strains are less susceptible to polyenes as these selectively bind to ergosterol [53]. In our case, **one-nucleotide (frameshift) deletion** and **three nonsense mutations** are reported. These usually have more **drastic effects** on the protein function and structure. One or two-nucleotide deletions cause a frameshift and may alter the protein function,

while nonsense mutations introduce a premature stop codon, resulting in a truncated protein that is usually dysfunctional. In our case, the nonsense mutations result in a premature stop codon in one of the first 200 amino acids of *ERG3* (ORF: 364 amino acids) or *ERG11* (ORF: 525 amino acids) and thus, will most likely result in a non-functional protein. In accordance with this, the susceptibility to AMB is compared between strain 49, which has a missense mutation in *ERG11*, and strains 50 and 53, which have nonsense mutations in *ERG11*. Strains 50 and 53 have a lower susceptibility to AMB (MIC_{50}: >16 μg/mL) compared to strain 49 (MIC_{50}: 8 μg/mL) (Figure 25, page 45). This result could be explained by the truncated Erg11 as a result of the nonsense mutations, affecting the activity of Erg11 and possibly resulting in reduced ergosterol biosynthesis. This might further prove the more drastic effect of nonsense mutations compared to missense mutations.

Furthermore, SNAP2 predicted a functional effect of 44, with 71% accuracy, for the amino acid substitution M504I. Generally, amino acid substitutions at this position are predicted to be important, as any substitution seemed to have an effect at this position (Figure A13, Addendum).

5.2.4 5-FC resistance is associated with high MIC_{50} and linked to LOF mutations in *FUR1*

5-FC resistance is observed in three strains with mutations in ***FUR1***: **strain 31** with **nonsense mutation G68***, and **strains 32 (G145C)** and **116 (C81F)** with missense mutations. *FUR1* encodes a **uracil phosphoribosyl transferase (UPRT)**, which catalyzes the conversion of 5-fluorouracil (5-FU), derived from 5-FC, to 5-fluorouridine monophosphate (FUMP) [180, 181]. Presumably, *FUR1* mutations reduce the production of FUMP, ultimately hindering the integration of FUDP into RNA, thus allowing protein synthesis to occur efficiently [182]. Thus, LOF mutations in *FUR1* will eliminate the inhibiting effect of 5-FC on the protein synthesis, resulting in 5-FC resistance. Our *FUR1* mutants also exhibit high RR MIC_{50} values of 256 (Table 12, page 44).

5-FC resistance in *C. auris* has not been frequently screened for, identified, or studied in the clinic yet. As we know from other species, besides *FUR1*, other genes linked to the metabolism and absorption of 5-FC can induce 5-FC resistance. *FCY1* encodes cytosine deaminase, which converts 5-FC into 5-FU [183] and *FCY2* encodes purine-cytosine permease, which transports cytosine [184]. Rhodes et al (2019) found missense mutation F211I in *FUR1* in *C. auris* that was associated with reduced susceptibility to 5-FC (MIC: $\geq$ 64 μg/mL) [185]. Furthermore, Jacobs et al. (2022) recently found two mutations in *FUR1*, e.g. S84L and 1Δ33 in strains that exhibited elevated MICs (>512 μg/mL) against 5-FC [186]. Wild type MICs in both studies were not specified. In conclusion, mutations in *FUR1* are associated with high levels of 5-FC resistance, as observed in both our data and in the clinic. Additionally, Jacobs et al. (2022) also found mutations S70R in

FCY1, which was not important regarding 5-FC resistance, and M128frameshift in *FCY2* which was associated with 5-FC resistance (MIC: 256 μg/mL) [186]. However, no mutations in these genes were present in our 5-FC resistant strains.

Hypothetically, we assume that the nonsense mutation G68* (strain 31) has a detrimental effect on the protein, as premature transcription termination results in only 10% of *FUR1* being transcribed. Furthermore, mutations C81F (strain 116) and G145C (strain 32) are predicted to have a high impact (effect: 81, Table 12, page 44). In C81F, Cysteine (C) has a sulfide group as side chain, allowing it to participate in disulfide bonds, which are important for binding metals and the overall enzyme activity. Consequently, C prefers to be substituted with a small aa with a sulfide group as well, yet phenylalanine (F) has an aromatic ring and is bulky. The G145C mutation, on the other hand, might have introduced an additional disulfide bond, and thus might alter the catalytic site of the enzyme.

5.2.5 Resistant isolates with mutations in the GOI do not necessarily exhibit higher levels of resistance than those without mutations in the GOI

FLU-, KTO- and MCA-resistant strains with mutations in the GOI that we have sequenced display lower MIC_{50} values than those without mutations in the GOI, evolved in the same conditions (Figures 24 and 26a, pages 45-46) and in other conditions in monotherapy (Figure 27, page 47). This could be appointed to **mutations in genes that we have not sequenced.** Therefore, through targeted sequencing of other important genes, we could reveal resistance mutations. In addition, through WGS we might even elucidate **novel resistance mechanisms** that have not been considered earlier. Furthermore, the FLU control strain shows higher resistance to FLU (MIC_{50}: 8 μg/mL) than some FLU-resistant strains (Figure 24a, page 45), which is most probably the result of an experimental error or cross-contamination with resistant strains during the evolution experiment.

No difference in resistance levels is observed between 5-FC resistant strains with and without mutations in the sequenced GOI from the same condition and the strains exhibit similar growth trends (Figure 26b, page 46). Additionally, the degree of resistance development is independent of the drug dose received (Figure 27, page 47). Yet, taking into consideration that MIC_{50} is >16 μg/mL, differences in resistance are beyond the measuring range. Lastly, AMB-resistant strains, evolved in 4x MIC_{50} AMB, with (strains 50 and 53, *ERG11*) and without mutations in *ERG11* display similar susceptibility levels to AMB (Figure 25a, page 45). However, mutant strains evolved in 1x (strains 47 and 48, *ERG3*) and 2x (strain 49, *ERG11*) MIC_{50} AMB display lower MIC_{50} values compared to the AMB-resistant strain without mutations in *ERG3* (Figure 25b, page 45). Although strains 49, 50 and 53 have a mutation in *ERG11*, strain 49 has a lower MIC_{50} than

the other strains. This might be due to the nature of the mutation, as previously explained in 5.2.3. Strain 49 has a missense mutation (M504I), whereas strains 50 and 53 have nonsense mutations (Y158* and E165* respectively), which have a more detrimental effect on Erg11. Furthermore, we observed that mutations in *ERG11* seem to confer higher levels of resistance than mutations in *ERG3* (Table 11, page 43). This might be due to the activity of the genes in the ergosterol biosynthesis pathway, as Erg11 catalyzes a reaction more upstream in the pathway than Erg3 (Figure A22, Addendum). Therefore, LOF mutations in *ERG11* might have more impact than in *ERG3*.

5.2.6 Experimentally evolved strains with stable MIC_{50} might exhibit tolerance

The lack of resistance mutations in presumably resistant strains might be attributed to reduced susceptibility that is not defined as resistance by genetic change but rather as a result of **epigenetic alterations** or **transcriptomic rewiring** and thus (transient) **tolerance**. Berman and Krysan (2020) defined antifungal tolerance as "the ability of a drug-susceptible fungal strain to grow in the presence of an antifungal drug at concentrations above the MIC" [187]. Tolerance, which is most prominent in fungistatic drugs and reversible, should not be disregarded as it might result in a subpopulation of persister cells that are able to survive antifungal drug therapy. These isolates may exhibit phenotypic heterogeneity, resulting in different degrees of tolerance that are described as trailing growth [187, 188]. This phenomenon refers to the variable residual growth of tolerant strains in supra MIC concentrations [188]. Dudiuk et al. (2019) suggested the **ratio MFC:MIC**, which we will call the **tolerance ratio (TR)**, as a measure of tolerance. If TR is $\geq$32, the strain is considered tolerant to the drug. Thus, through MFC_{99} and MIC_{50} measurements, these subpopulations of tolerant cells can be distinguished. Additionally, MFC_{99} can be quantified from the same *in vitro* assay as MIC_{50} (e.g. BDA), which is extremely beneficial in the clinic [187].

In line with this, from the azoles 22 POS-evolved strains and 19 KTO-evolved strains display TR $\geq$ 32 (not mentioned), which suggests tolerance. Consequently, these strains that were deemed as resistant based on MIC_{50} might actually be (transiently) tolerant to the drugs. This might also explain why RR MIC_{50} and RR AUC_{BDA} were considerably lower in POS and KTO monotherapy compared to FLU monotherapy. TRs of all FLU-evolved strains are <32, thus these strains might have developed actual resistance to FLU. Additionally, the KTO-evolved strain 78 with a mutation in TAC1b has a TR of 16, which implies that the *TAC1b* mutation might have conferred KTO resistance. Furthermore, for the echinocandins, 4 MCA-evolved strains and one ANF-evolved strain display TR $\geq$32 (not mentioned), suggesting tolerance to these drugs. Remarkably, the MCA-evolved strains with mutations in *FKS1* (strains 151 and 152) have TRs of 2 and 4 respectively.

Thus, the *FKS1* mutations possibly conferred MCA resistance in these strains.

Although we mainly focus on CS in resistant strains, the observation of strains that might have developed drug tolerance has made us wonder if CS is present at the level of tolerance. Berman and Krysan (2020) suggested that tolerant subpopulations exhibit elevated thresholds in stress responses, which is often attributed to epigenetic changes that affect their growth in the presence of the drug [187]. Furthermore, it has been shown in *C. albicans* that epigenetic changes are inheritable [187, 189]. Thus, hypothetically, epigenetic changes that induce tolerance to one drug might exhibit trade-off mechanisms that confer increased sensitivity to another drug.

5.2.7 Experimentally evolved strains might exhibit resistance or tolerance on the basis of random variability

The possibility exists that some of these strains are not resistant nor tolerant, but have been selected and analyzed on the premise of an increase in RR due to **random variability.** In this case, strains with only a **slight (e.g. 2-fold) increase in MIC_{50}, MFC_{99}, or AUC_{BDA},** which we will call **indifferent strains**, have to be differentiated from those with significant alterations in their susceptibility profile. In six CHX-evolved isolates with indifferent MIC_{50}, 4 out of 6 strains exhibit RR MFC_{99} of 1 μg/mL and two strains have MFC_{99} of 2 μg/mL (not mentioned). In addition, the RR AUC_{BDA} range of these strains includes 0.45 - 1.67 (Figure 20, page 38). As these strains lack clear signs of possible resistance or tolerance development, the interplay between CHX resistance/tolerance and CS to other drugs in these strains might be invalid. Thus CHX-evolved strains will be excluded from CS and XR analyses.

5.3 Cross resistance and collateral sensitivity in *C. auris*

5.3.1 Azoles and echinocandins display intra- and interclass XR

Intraclass XR is prominent for the azoles and the echinocandins (Figure 28, page 48), which is expected as modes of action are similar within the same drug class. As a result, resistance might be conferred through similar mechanisms. Pristov and Ghannoum (2019) argued that overexpression of drug efflux pumps contributes to XR between azoles in *C. albicans*, both *in vitro* and in the clinic [190]. Besides, upregulation of *CDR1* and *CDR2* was observed in FLU-resistant *C. glabrata* isolates in the clinic and treatment with itraconazole, ketoconazole and voriconazole was discouraged as XR was observed [191, 192]. Accordingly, our FLU-resistant (strain 63) and KTO-resistant (strains 78) strains with a mutation in *TAC1b* exhibit decreased susceptibility to the other

azoles. Strain 63 displays a 2- to 4-fold higher resistance to POS and KTO, whereas in strain 78, susceptibility to POS and FLU decreased by 2- to 16-fold (not mentioned). Furthermore, echinocandins act through the same MOA, which is the inhibition of β-(1,3)-D-glucan synthase [46]. Therefore, XR might develop through similar resistance mechanisms for these drugs, such as the acquisition of mutations in HS regions in *FKS1*, which reduces the enzyme's susceptibility to echinocandins [103]. This is observed in our MCA-resistant strain 151 with an *FKS1* mutation (Table 10, page 43) that exhibits MIC_{50} of >16 μg/mL to both CAS and ANF (not mentioned), while wt MIC_{50} is 1 μg/mL for both drugs (Table 7, page 33). Previous findings in the clinic support this observation, as in CAS-resistant *C. albicans* with *FKS1* mutations in HS1, XR against MCA and ANF was observed [47]. In addition, alterations in HS regions of Fks1 in *C. glabrata* conferred XR against all three echinocandins [105]. Nevertheless, intraclass XR in azoles and echinocandins is as prominently found in strains without mutations as strains with mutations.

Furthermore, XR is also exhibited in azole-evolved strains to the echinocandins and to a lesser degree vice-versa (Figure 28, page 48). Schuetzer-Muehlbauer et al. (2003) observed this in *C. albicans*, as they collected clinical azole-resistant isolates (e.g. FLU, KTO), which expressed high levels of *CDR1* and *CDR2*. This seemed to contribute to CAS resistance, which was confirmed by constitutively overexpressing *CDR2* in a drug-sensitive *C. albicans* strain, resulting in CAS resistance [193]. Pham et al. (2014) observed XR between these drug classes as well in *C. glabrata*, as 36% of the echinocandin-resistant strains (n=371) were resistant to FLU [194]. In our case, FLU-resistant strain 63 with a mutation in *TAC1b* (Table 9, page 42) shows reduced susceptibility to CAS (RR MIC_{50}: 32) and ANF (RR MIC_{50}: 4) (not mentioned. Conversely, the MCA-resistant strain 151 with a mutation in *FKS1* (Table 10, page 43) displays RR MIC_{50} of 2 to FLU (not mentioned).

5.3.2 Mutations in *ERG11* and *ERG3* might be associated with XR to azoles in AMB-resistant strains

Our AMB-resistant strains display reduced susceptibility to azoles (Figure 28, page 48). AMB resistance can be caused by LOF mutations in *ERG11*, which encodes 14α-lanosterol demethylase, the target of azoles. Therefore, mutations in *ERG11* might confer XR between AMB and azoles [113, 195]. This was confirmed in *C. glabrata* [196], *C. auris* [99], and in *C. tropicalis*, in which a defect Erg11 resulted in the production of a toxic 3,6-diol derivative in the presence of functional Erg3 [195]. Furthermore, mutations in *ERG3* were also proven to cause XR between azoles and AMB in the clinic [99, 115]. This is in line with our data as the AMB-resistant strains with mutations in *ERG3* (strains 47 and 48) and *ERG11* (strains 49, 50, and 53) display RRs MIC_{50} ranging from

8 to 32 (Table 11, page 43). Furthermore, we observed slightly lower levels of XR in strains with *ERG3* mutations than strains with *ERG11* mutations, except for strain 49 (Figure 28, page 48). This might be due to the nature of the enzyme activity, encoded by these genes, and the stage at which they act in the ergosterol biosynthesis pathway. Erg11 acts upstream in the pathway, relatively to Erg3 (Figure A22, Addendum) and therefore, LOF mutations in *ERG11* induce higher levels of resistance, resulting in a presumably larger interplay between AMB resistance and XR to azoles. Remarkably, strain 49 exhibits lower XR to the azoles than strains 50 and 53, even though they all have mutations in *ERG11*. Yet, strains 50 and 53 have nonsense mutations, whereas strain 49 has a missense mutation, which has a lower impact on the *ERG11* gene.

5.3.3 Prominent trends of collateral sensitivity could be distinguished in *C. auris*.

As far as we know, CS has not been explored in pathogenic fungi. Correspondingly, knowledge on this topic is lacking. We observed CS in CAS-resistant strains to azoles, especially POS and KTO. Furthermore, AMB-resistant strains eminently exhibit increased susceptibility to MCA, CAS, ANF, CPX, NIT, GEL and TRB (Figure 28, page 48). Survival dynamics based on the MFC_{99} values of the CAS- and AMB-resistant strains in BDA provide further evidence for the increased sensitivity of these strains to POS and CAS respectively. CAS-resistant strains exhibit a 2- to 16-fold increase in susceptibility to POS (RR MFC_{99}: 0.0625 - 0.5) and CAS exhibits a fungicidal effect on the AMB-resistant strains, as susceptibility to CAS, based on MFC_{99}, is shown to have increased by >16-fold (Figure 32, page 52).

5.3.4 Collateral sensitivity might be associated to the mode of action of drugs

The combination of the different modes of action of antifungal drugs might induce CS due to their underlying resistance mechanisms. Almost all CS trends we observed are based on AMB resistance. This is most likely attributed to the altered sterol homeostasis and reduced cell fitness associated with AMB resistance.

AMB-resistant strains exhibit CS to the echinocandins, which is most likely attributed to the effect of AMB resistance on the cell membrane. Ergosterol maintains the cell membrane integrity and lipid rafts, which predominantly consist of ergosterol and sphingolipids, and house many important enzymes [37, 38]. As resistance to AMB is most often associated with reduced ergosterol levels [43, 53], these lipid rafts might become disturbed. As Fks1 is a cell membrane enzyme [197], disruption of the lipid rafts might affect the mobilization and functioning of Fks1, possibly making it more accessible to CAS, which might explain CS of AMB-resistant strains to CAS.

Furthermore, AMB-resistant strains show CS to GEL. GEL inhibits the heat shock protein Hsp90, which is a chaperone important for proper folding and stabilization of proteins [198]. As a result, by stabilizing protein kinase C (PKC) and calcineurin, which are important signal transduction proteins that regulate stress responses, Hsp90 could promote drug resistance as it alleviates drug-induced membrane stress [89, 199]. Consequently, the inhibition of Hsp90 by GEL could prevent resistance development [124, 199, 200, 201, 202]. Likewise, calcineurin and PKC are essential to alleviate AMB resistance-induced stress [113]. Therefore, in the presence of GEL, Hsp90 is inhibited and AMB-resistant strains might become more vulnerable to the resistance-induced stress [113].

Besides, AMB-resistant strains also exhibit CS to CPX, which has the ability to chelate polyvalent metal cations (e.g. iron), and thus, it can inhibit iron-dependent enzymes which are important for various cellular processes, such as catalases [203]. In AMB-resistant strains with a reduced fitness, catalases are important enzymes as they alleviate oxidative stress, preventing cell death [52, 121, 122]. Therefore, treatment with CPX might reduce or prevent AMB resistance development.

CS was also observed in CAS-resistant strains to azoles, especially POS. Resistance to CAS is associated with an impeded glucan biosynthesis, resulting in the instability of the fungal cell wall [46]. Consequently, the penetration of POS into the cell might be facilitated, resulting in POS having a higher efficacy [204]. Furthermore, as POS targets 14α-lanosterol demethylase, ergosterol production will be impeded and the membrane environment will be altered. As Fks1 is a cell membrane enzyme, alterations in the membrane might induce more accessibility of the protein or make Fks1 more sensitive to inhibition by CAS [204].

Lastly, AMB-resistant strains also exhibit CS to NIT, for which the mechanism of its antifungal activity is still poorly understood. Yet chelation-like activity had been described in the past [173, 205, 206]. Accordingly, NIT inhibits the correct functioning of metal-dependent enzymes such as catalases, as NIT has the ability to chelate polyvalent metal cations (e.g. iron). Consequently, as AMB-resistant strains often exhibit fitness defects such as oxidative stress [52, 53], these enzymes presumably can no longer alleviate this stress, resulting in cell death.

5.3.5 Resistance might be accompanied by fitness trade-offs, possibly resulting in CS

Remarkably, whenever resistance to a drug develops, it may induce evolutionary fitness trade-offs that could result in CS [137]. Imamovic et al. (2018) observed *in vitro* that evolving resistance to specific antibiotics in *P. aeruginosa* led to a distinct phenotypic state, associated with mutations in specific genes, that exhibit CS to other antibiotic classes. Accordingly, in *C. auris*, resistance to AMB is often accompanied by fitness trade-offs [99]. Vincent et al. (2013) linked mutations

in *ERG2, ERG3, ERG6, and ERG11* in AMB-resistant *C. albicans* isolates to hypersensitivity to various stresses (high temperature, oxidative stress, iron deprivation) [113]. In line with our data, five AMB-resistant strains acquired mutations in either *ERG3* or *ERG11* (Table 11, page 43). Consequently, we observed evident CS trends in these AMB-resistant strains to several drugs (CAS, CPX, GEL, NIT) (Figure 28, page 48). In conclusion, AMB resistance possibly conferred by mutations in the *ERG* genes might alter the sterol composition in the membrane [53]. Consequently, these alterations in the membrane could reduce the fitness of the resistant strains and thus leave them more vulnerable to other antifungals.

5.3.6 Repurposed drugs show promising CS trends

Susceptibility testing of antifungal-resistant strains against repurposed drugs reveals promising CS trends that might translate into potentially effective drug cycling schemes. Based on AUC_{BDA} (Figure 28, page 48), high levels of CS in AMB-resistant strains to NIT and GEL are observed (RR AUC_{BDA}: 0.13-0.47). Remarkably, AMB-resistant strains exhibit a high degree of CS against CPX (RR AUC_{BDA}: 0.29-0.33). Consequently, the combinations of AMB-NIT, AMB-GEL and AMB-CPX were taken into consideration and drug cycling schemes were designed accordingly.

Furthermore, to pyrvinium pamoate salt hydrate (PYR), oleylphosphocholine (OPC), alexidine dihydrochloride (ALX) and 5,7-diiodo-8-hydroxyquinoline (DHQ) an increase in susceptibility is observed in several antifungal-resistant strains (Figure 28, page 48). Remarkably, ALX and DHQ exhibit $MIC_{50,\,wt}$ between 0.5-1 μg/mL, while OPC and PYR have $MICs_{50,\,wt}$ of 4 μg/mL (Table 7, page 33). Therefore, they exhibit antifungal activity against *C. auris* and might be potential candidate drugs to fight (resistant) *C. auris*. Considering that CPX [207], DHQ [208] and NIT [209] are ion chelators, further investigation of the efficacy of these drugs could culminate a new approach to fight *C. auris*. ALX and FLU are found to interact synergistically in *C. albicans*, highlighting the prospective antibiofilm activity of ALX, which could be of use in the clinic [210]. Furthermore, OPC is an analog of miltefosine, which is thought to bind ergosterol in *C. krusei* and induce apoptosis, exerting its antifungal activity accordingly. [211]. Additionally, synergy was recorded between AMB and miltefosine [211, 212], which refers to the greater effect of the combined activities of the two drugs compared to the sum of their individual activities [213, 214].

5.4 Collateral sensitivity-based drug cycling schemes

Based on the CS phenomena mentioned above, drug cycling schemes were designed accordingly. Imamovic and Sommer (2013) suggested that CS-based drug cycling schemes might be effective to

circumvent drug resistance development in bacteria. To prove this, they developed *E. coli* strains resistant to antibiotics, selected two-drug combinations that exhibit reciprocal CS, and designed two drug cycling schemes for each combination. Each cycling scheme is initiated by one of the drugs, implying that resistance is developed to the first drug, and CS is exhibited towards the second drug [128]. However, no signs of reciprocal CS are present in our data (Figure 28, page 48), thus drug cycling in our case is based on one-directional CS. Remarkably, Aulin et al. (2021) built a mathematical model and suggested that one-directional CS, in which cells only exhibit CS for the second drug, was as sufficient in impeding resistance development as reciprocal CS between two drugs [149]. In line with this, the following drug combinations were chosen, in which every first noted drug is the first drug administered in the cycling evolution experiment: AMB-CAS, AMB-CPX, AMB-GEL, AMB-NIT and CAS-POS.

5.4.1 Resistance development in *C. auris* is generally reduced in drug cycling therapy compared to monotherapy

We selected six strains from six different populations per condition (LL, LH, HL, HH) and tested these in BDA against their respective drugs. Resistance development based on AUC_{BDA} and MIC_{50}, and susceptibility to the drug based on MFC_{99} are determined. As drug cycling schemes are designed based on CS trends, we could theorize that resistance development would not occur as prominently as in monotherapy due to the underlying mechanisms regarding CS. This theory could be confirmed by our data (Table 13, page 55 and Figure 36, page 56).

In monotherapy based on MIC_{50} (Figure 36, page 56) resistance is observed in 1x and 2x MIC_{50} conditions of AMB (RR MIC_{50}: 8), CAS (RR MIC_{50}: 32), POS (RR MIC_{50}: 2-8), and NIT ((RR MIC_{50}: 4-8). In drug cycling, however, no resistance is developed based on MIC_{50}. However, as MIC_{50} has a strict cut-off, we also evaluate resistance development based on AUC_{BDA}.

Based on AUC_{BDA} (Figure 36, page 56), some cycling evolved strains developed resistance against one or both of their respective drugs. However, resistance ratios based on AUC_{BDA}, in these strains do not indicate high resistance levels and therefore, no actual resistance might have developed. During **amphotericin B and geldanamycin** cycling, one strain evolved in high drug conditions of AMB and GEL (HH) shows a RR AUC_{BDA} of 1.04 to AMB. Furthermore, three strains, evolved in either low-low drug concentrations or high-low drug concentrations of AMB and GEL respectively, show a RR AUC_{BDA} range of 1.01-1.04 to GEL (Figure 38a, page 58). Therefore, no actual resistance to AMB nor GEL might have been acquired. In **amphotericin B and nitroxoline** cycling, one strain evolved in low-high concentrations, and one strain evolved in high-low drug

concentrations of AMB and NIT respectively, display a RR AUC_{BDA} range of 1.01-1.09 to NIT (Figure 39a, page 59). Similarly as in AMB-GEL cycling, resistance levels to NIT in these strains are low and thus actual resistance to NIT might not have been developed. Lastly, in **caspofungin and posaconazole** cycling, RR AUC_{BDA} of 1.01-1.15 to CAS is observed in one strain evolved in low-low, one strain evolved in high-low and five strains evolved in high-high concentrations of CAS and POS respectively. However, as these strains exhibit low RRs based on AUC_{BDA}, CAS resistance might not have been developed at all (Figure 41a, page 60).

Furthermore, MFC_{99} is worth analyzing as it is an interesting parameter for susceptibility, especially in conjunction with MIC_{50}. Accordingly, a TR of >32 might indicate the presence of drug tolerance. However, in our data, no indications of tolerance were observed in our cycling evolved strains.

5.4.1.1 Enhanced drug susceptibility in drug cycling in *C. auris* might be linked to underlying CS mechanisms and interactions between drugs

In **amphotericin B and caspofungin cycling**, no resistance to either drug is observed. In fact, our data suggests that our AMB-CAS cycling strains became even more susceptible to the drugs, as observed from AUC_{BDA} RR (AMB: 0.25-0.85, CAS: 0.37-0.79) and MIC_{50} RR data (AMB: 0.5-1, CAS: 0.03125-0.125) (Figure 37a-b, page 57). In addition, MFC_{99} RR values were ≤ 1 (Figure 37c, page 57), which further proves the increase in susceptibility (except when RR=1, which implies indifference in susceptibility). Therefore, we can suggest that AMB and CAS might be a promising drug pair to explore in future studies regarding CS, as we observed increased susceptibility to both AMB and CAS in AMB-CAS cycling. Additionally, the use of this drug pair is supported in several papers. Olsen et al. (2005) demonstrated the increase in efficacy of the sequential therapy of AMB, followed by CAS in *C. glabrata*. They reported a reduction in fungal kidney burden when given AMB first, followed by CAS in C57BL/6N females that were challenged with the fungal pathogen [215]. Similarly, in *C. parapsilosis*, the combined use of AMB and CAS was associated with lower MICs compared to both drugs in monotherapy *in vitro* and *in vivo* [216]. Recently, Caballero et al. (2021) reported fungicidal activity in *C. auris* when isolates were treated with combinations of AMB (1 μg/mL) and CAS ($\geq$0.5 μg/mL) [44]. However in the same conditions (low AMB and low/high CAS concentrations), fungicidal activity is not observed in our strains. Yet, our determination of MFC_{99} values is usually biased, whereas Caballero et al. (2021) performed time-kill assays, which are more accurate in defining fungistatic and fungicidal activity [44, 217].

Furthermore, no resistance is acquired during **amphotericin B and ciclopirox cycling** (Figure 40, page 59). Strains confer increased sensitivity to AMB, based on AUC_{BDA} (RR: 0.43-0.93),

yet show indifference based on MIC_{50}. Enhanced susceptibility to CPX is also observed, based on AUC_{BDA} (RR AUC_{BDA}: 0.46-0.91) and MIC_{50} (RR MIC_{50}: 0.5-1) (Figure 40a-b, page 59). MFC_{99} data mostly indicates indifference as well (Figure 40c, page 59). All things considered, AMB and CPX might be a promising drug pair to study further, regarding CS. However, as some cycling evolved populations of AMB-CPX exceed the growth of wt populations (Figure 34b, page 54), which points to an experimental error or cross-contamination, we cannot say with certainty that the results of the AMB-CPX cycling evolution experiment are correct. The effect of CPX on AMB in *Candida* has not been studied so far. An indifferent effect of the combination of AMB and CPX has been described in *C. neoformans* [203] and *A. fumigatus* [218]. Nevertheless, we could still hypothesize how CS in AMB-resistant strains to CPX is developed. CPX is an iron chelator [203] and thus, it will inhibit catalase, which is an important enzyme to alleviate oxidative stress in AMB-resistant strains [52, 121, 122].

Remarkably, in drug cycling between **caspofungin and posaconazole**, higher susceptibility to POS is developed in all four conditions (RR AUC_{BDA}: 0.40-0.77, RR MIC_{50}: 0.25-1, SR MFC_{99}: 0.125-0.5). In addition, no substantial differences in susceptibility are observed between the four conditions (Figure 41, page 60). Previous studies suggested that this combination can induce synergy in *Aspergillus spp.* [219, 220, 221], *C. tropicalis* [220] and *C. glabrata* [220, 222]. This was further demonstrated in *C. albicans in vitro* and *in vivo* by treating CAS-resistant isolates with POS, which was effective [223]. Although we did not simultaneously combine CAS and POS in our cycling experiments, these studies do acknowledge the effect these drugs have on each other. Furthermore as CAS targets β-(1,3)-D-glucan synthase, impeding the glucan biosynthesis and causing destabilization of the cell wall [46], further use of POS, which targets 14α-lanosterol demethylase, causing the inhibition of the ergosterol production [53], will presumably damage the "outer layers" of fungal cells, making them less viable.

Generally, during **amphotericin B and geldanamycin cycling**, only pronounced sensitivity to AMB is observed (RR AUC_{BDA}: 0.55-0.85) (Figure 38a, page 58). Mycogab, a human recombinant antibody that inhibits Hsp90, in combination with AMB demonstrated pronounced synergy in several *Candida spp.* in the clinic. In addition, Mycogab reduced MICs for AMB to ≤ 0.5 μg/mL in *C. albicans* and *C. glabrata* [224]. Yet, we alternately cycled AMB and GEL, thus synergy is not applicable in our case. However, this mechanism might give us an idea of how this enhanced susceptibility to AMB is established during the cycling experiment. GEL, on the other hand, has little to no effect on the cycling evolved strains, as AUC_{BDA} resistance ratios range between 0.87-1.04, and RRs of MIC_{50} and MFC_{99} are 1 (Figure 38, page 58).

Lastly, in **amphotericin B and nitroxoline cycling**, aside from the two NIT-resistant strains, increased susceptibility to AMB (RR AUC_{BDA}: 0.45-0.86) and NIT (RR AUC_{BDA}: 0.59-0.90) is evident (Figure 39a, page 59). Nevertheless, the effect of NIT on AMB-resistant *C. auris*, or other fungal pathogens, has not been studied yet. However, the dual effect of AMB resistance, which induces oxidative stress, and NIT, which involves ion chelation and thus inhibition of metal-dependent enzymes, might provide a possible explanation for this CS trend.

5.4.2 Growth dynamics during drug cycling might reveal the effect of CS on resistance development in time

The average relative growth of six cycling evolved strains per condition is plotted over time (Figures 33-35, page 53-54). Through this, we could possibly link the lack of resistance development in drug cycling to underlying CS mechanisms between the drugs in a CS drug pair.

The absence of a prolonged increase in relative growth after a short initial decrease in relative growth in all the drug cycling schemes involving AMB might indicate that resistance is not developed. In AMB-CAS cycling, the relative growth decreased until day 8 and was mostly random afterwards (Figure 33a, page 53). Furthermore, in AMB-NIT (Figure 34a, page 54) and AMB-GEL (Figure 33b, page 53) cycling, the relative growth decreased until day 2 and day 4 respectively, and was stable afterwards. Lastly, relative growth in AMB-CPX cycling was mostly random (Figure 33b, page 54). Compared to AMB-resistant strains from AMB monotherapy from the same conditions as cycling (Figure 22, page 40), these strains exhibit an initial decrease in relative growth until day 2, followed by an increase in growth until day 8 (2x MIC_{50} AMB) and day 10 (1x $MIC_{50)}$. Furthermore, the average relative growth of CAS-POS cycling populations (Figure 35, page 54) and relative growth of resistant strains from CAS-monotherapy (Figure 22, page 40) was mostly random and thus indications of resistance development are difficult to distinguish.

6. Future perspectives

6.1 Discovery of novel resistance mechanisms: genomics and transcriptomics

Drug-resistant strains were sequenced for genes of interest, which were selected based on knowledge from literature. 13 out of 140 resistant strains in total exhibit a mutation in a gene of interest, as described in Table 8 on page 42, suggesting that drug resistance in other strains might have been acquired due to mutations in other genes or by other genomic alterations such as aneuploidies or genomic rearrangements.

A next step could be performing **targeted sequencing of genes that we have not sequenced** but either encode important proteins involved in the MOA of certain antifungals or contain resistance-conferring mutations that previously have been found in the literature. In the clinic, a GOF mutation (N647T) in ***MRR1***, encoding the transcription factor Mrr1, was associated with an upregulated expression of ***MDR1***. This gene encodes Mdr1 which is an MFS efflux pump and therefore, overexpression of *MDR1* induces **reduced susceptibility to azoles** [225]. Furthermore, GOF mutations in ***PDR1*** in *C. glabrata* lead to **high *CDR1/CDR2* levels**, and thus overexpression of drug efflux pumps [226, 227]. Furthermore, overexpression of ***UPC2 and NDT80***, which encode zinc cluster transcription factors, will induce **upregulation of *ERG* genes** [228, 229], affecting ergosterol biosynthesis. Therefore, sequencing these genes might elucidate novel resistance mutations in *C. auris* and could explain the elevated MIC_{50} levels in our azole-resistant strains. On the other hand, **hot spot regions in *FKS2*** could be checked for mutations, as this gene is often associated with **echinocandin resistance,** as observed in *C. glabrata* [230, 231, 232]. Furthermore, **other *ERG* genes** such as ***ERG5*** [113] and ***ERG2*** [233] could be sequenced as mutations in these genes resulted in AMB resistance in other *Candida spp.* Besides, a mutation in ***ADE17*** was associated with **5-fluorocytosine resistance** [186]. Lastly, as terbinafine targets squalene epoxidase, encoded by ***ERG1***, mutations in this gene were found to confer **TRB resistance** in *S. cerevisiae* [234].

Additionally, **targeted gene expression analyses** could be performed through **qPCR or RT-PCR** to check the expression of genes that are associated with drug resistance in *C. auris*. Accordingly, expression of *CDR1/CDR2*, *MDR1*, and *ERG11* can be checked as overexpression of these genes has shown to be linked to azole resistance in *C. auris* [14] and other *Candida spp.* [235, 236, 237]. Furthermore, Shivarathri et al. (2022) described distinct expression of genes associated with cell wall function **(*IFF4.1/2, PHR1, HYR3.1*)**, adhesion **(*ALS1/3/4*)**, ergosterol and lipid

biosynthesis ***ERG1/2/3/5/25/27*** and chromatin remodeling **(*HST3, GCN5, HAT2*)** [238] in AMB-resistant strains compared to AMB-susceptible strains. Therefore, expression levels of these genes could be checked, which might allow us to verify AMB resistance in AMB-evolved strains.

Resistance development could also involve **genomic rearrangements or aneuploidies**, which cannot be revealed through targeted sequencing but require **whole genome sequencing.** Carolus et al. (2020) discovered two aneuploidies in two experimentally evolved *C. auris* strains that conferred decreased susceptibility to azoles. In the fluconazole-resistant strain, a partial duplication of Chr1, which contains *ERG11*, was found to be associated with reduced susceptibility to AMB. Furthermore, a whole duplication of Chr5, in which *TAC1b* is located, was marked in a caspofungin-resistant strain which was exposed to fluconazole. This strain exhibited reduced susceptibility to fluconazole as well [99]. Bing et al. (2021) observed a lower growth rate in *C. auris* strains with the Chr5 aneuploidy, which might be the result of a fitness trade-off between growth and resistance. Remarkably, in the absence of FLU drug stress, the extra copy of Chr5 was lost, enforcing the idea of an unstable aneuploidy and plasticity in the *C. auris* genome [98].

6.2 Improved design of CS-based drug cycling schemes: evolutionary modeling

Our data suggest that collateral sensitivity-based drug cycling might be a promising treatment strategy to fight *C. auris*, as resistance development is presumably reduced compared to monotherapy and drug-susceptible strains are possibly selected for in drug cycling. Therefore, a next step could be the improvement of drug cycling schemes. For this, modeling of CS drug cycling could be introduced to guide future research into drug cycling. Such a particular model could navigate researchers in further validating CS schemes, possibly allowing them to predict which cycling schemes (which drugs, doses, and cycling intervals) are most promising to explore.

Aulin et al. (2021) developed a model framework, which was based on the deterministic PK-PD model generated by Udekwu and Weiss. The latter investigates the effect of PK-PD characteristics of antibiotics (AB) in cycling schemes on resistance development when CS is present [239]. The PK-PD traits of AB determine their impact on events that are concentration-dependent (growth, killing, and inhibition of bacteria) and thus are necessary to translate *in vitro* findings regarding CS to *in vivo* treatment strategies [149, 240, 241] They suggested the use of mathematical modeling which could incorporate resistance mutations (to simulate the stochasticity of resistance development) and other parameters (pathogen- and drug-specific parameters) to elucidate their effect on resistance emergence in multi-drug two-week treatment strategies that either consider

CS or not. They concluded that CS-based one-day cycling or simultaneous administration of drugs was effective in suppressing resistance. Furthermore, they suggested that the order in which drugs are administered is important for the efficacy of the cycling treatment, and that reciprocal CS is insignificant to suppress resistance [149]. Lastly, antibiotic-specific PK (e.g absorption, distribution, metabolism) and PD (e.g. drug activity) parameters as well as pathogen-specific properties (e.g. fitness) are taken into consideration to study their effects on different treatment strategies. As a result, effective dosing treatments could be explored, which might lead to reduced resistance emergence [149].

Consequently, this model may be applicable to our research to study CS-based cycling schemes and possibly achieve the most effective dosing strategy. In our case, PK and PD parameters of antifungals that exhibit one-directional CS to other drugs can be calculated using the mono-exponential PK model, developed by Aulin et al. (2021) [149], and the PD model, defined by Regoes at al. (2004) [241]. Furthermore, resistance mutations that we have discovered and those that are observed in the literature could be implemented in the model as well. Furthermore, pathogen- and drug-specific parameters should be taken into account. Eventually, the Probability of Resistance (PoR) is determined for each simulated treatment to evaluate the efficacy of the dosing strategy [149].

6.3 Exploring the mechanisms behind CS: fitness vs drug mode of action

As we observed that treatment strategies such as drug cycling, involving drug pairs that exhibit CS, possibly reduce resistance development, a next step could be to elucidate the underlying mechanisms of CS to expand our knowledge on this trade-off mechanism.

As we previously mentioned, CS might be induced by **fitness trade-offs** that derive from resistance mutations. Consequently, we could perform **competition experiments** in which a wild type strain is tagged with a selectable marker. We could opt for a NAT (Nourseothricin N-acetyl transferase)-tag in a neutral locus so that the fitness of these wild type strains is not affected. These NAT-tagged strains would confer resistance to nourseothricin (NTC), a broad spectrum antibiotic [242], allowing them to grow on agar containing this drug. Consequently, by mixing experimentally evolved resistant strains with these NAT-tagged wt strains in different ratios, drug concentrations, and/or drug combinations in both *in vitro* experiments or *in vivo* models such as a murine systemic infection model, we could observe the evolutionary and competition dynamics of these strains. The number of surviving NAT-wt and drug-resistant strains can be counted by growing them on NTC-containing agar and normal YPD agar. Through this, we could estimate how well the resistant

strains might compete against the NAT-wt strains and translate this to the fitness of the resistant strains.

Another way to investigate if CS is attributed to fitness trade-offs from resistance mutations is by testing the fitness of the AMB-resistant strains (CS to CAS, CPX, NIT, and GEL) and CAS-resistant strains (CS to POS). This can be done through **growth performance tests** in different stressors such as high febrile temperature (42°C), oxidative stress (H_2O_2), membrane stress (SDS), cell wall stress (Calcofluor White), and osmotic stress (NaCl). Indications of reduced fitness in these resistant strains might signify that CS is caused by fitness trade-offs induced by resistance.

Additionally, we mentioned earlier that CS might be associated to the **mode of action of drugs** as well. Therefore, by challenging the effects of CAS, CPX, NIT, GEL and POS, we might be able to elucidate if the mode of action of these drugs in combination with the effect of AMB- or CAS resistance attributes to CS observed in these resistant strains. As **NIT and CPX** are iron chelators, we could test the activity of iron-dependent enzymes such as catalase in the AMB-resistant strains in the absence and presence of NIT. Hypothetically, we assume that AMB-resistant strains in the presence of NIT or CPX exhibit a lower activity of the iron-dependent enzymes than in the absence of these drugs. Furthermore, **GEL** inhibits Hsp90, which stabilizes calcineurin that is essential for alleviating AMB resistance-induced membrane stress. Therefore by testing AMB-resistant strains in fitness tests with a cell membrane stressor (e.g. SDS) in the presence/absence of GEL, we could elucidate if the ability of GEL to inhibit Hps90 attributes to CS of AMB-resistant strains to GEL. Hypothetically, in the presence of GEL, AMB-resistant strains should have a weaker cell membrane. For **CAS**, it works through the inhibition of Fks1. As Fks1 is a cell membrane enzyme, we could hypothesize that ergosterol is a co-factor of Fks1. Therefore, by labelling Fks1 with a fluorophore, we could investigate the mobilization of the enzyme in AMB-resistant strains, in which lipid rafts are disturbed, and in POS-resistant strains, in which the membrane environment is altered, compared to wild-type *C. auris*. Additionally, by administering fluorescent derivatives of CAS to these fluorescently labeled Fks1 enzymes, we might be able to visualize the protein-drug interactions. Additionally, as CS in CAS-resistant strains to **POS** might also be explained by the facilitated uptake of POS due to the unstable cell wall, we could measure the drug uptake of POS.

7. Conclusions

Firstly, our ***in vitro*** **experimental evolution study** showed that **resistance can be acquired to all major antifungal drugs** and **drug specific trends are present.** Long term exposure to concentrations up to 8-fold MIC_{50} in our evolution experiments did not account for extinction of populations in azoles, echinocandins and terbinafine, which is most likely due to the fungistatic effect these drugs have in this concentration range. Furthermore, survival was lower in AMB (13%), 5-FC (91,67%), NIT (63.33%), and CHX (26.67%).

Furthermore, **only in 5-FC monotherapy, resistance development was significantly dose-dependent in the doses that were tested.** Accordingly, only in 4- to 8-fold MIC_{50}, five out of six strains in each condition achieved high levels of resistance. Overall, only a small subpopulation in 5-FC acquired resistance, which is most likely caused by the 8-fold difference between $MIC_{50,\,wt}$ and $MFC_{99,\,wt}$. In AMB and NIT monotherapy, 75% of the surviving strains exhibited resistance to their respective drugs, implying that mostly all survived strains might have developed resistance.

Targeted sequencing of GOI in our resistant isolates revealed several mutations known to confer drug resistance or that are similar to mutations described before. We found four missense mutations in ***TAC1b*** in FLU- and KTO-resistant strains, which were located near other GOF mutations in *TAC1b* found in the clinic and associated with **azole resistance** [91]. One missense mutation in ***FKS1*** **in HS1** was found in two MCA-resistant strains, which corresponds to an echinocandin resistance conferring mutation in *C. albicans*. Other substitutions on the same position have been found in the clinic in *C. auris* as well [34, 176], which were all associated with **echinocandin resistance**. Furthermore, in AMB-resistant strains, we found a nonsense mutation and a frameshift deletion in *ERG3*, and two nonsense mutations and one missense mutation in *ERG11*. These mutations have not been covered in the literature and might be LOF mutations that induce AMB resistance. Lastly, we found one nonsense and two missense mutations in *FUR1* that are closely located to other LOF mutations in the clinic, which are linked 5-FC resistance [15, 186].

Nevertheless, we observed that **resistant strains with mutations in the sequenced GOI do not exhibit higher levels of resistance than those without mutations in the sequenced genes.** By performing targeted expression analyses and/or whole genome sequencing, novel resistance mutations or resistance mechanisms can be elucidated. In addition, in isolates that do not have mutations in the sequenced GOI, for which the tolerance ratio (TR) is $\geq$32, tolerance to the drug might be exhibited. This was observed in some POS-, KTO-, MCA- and ANF-evolved strains.

Major XR and CS trends were observed in *C. auris*. We observed intra- and interclass XR in

azoles and echinocandins. Azoles and echinocandins exhibit XR reciprocally and AMB-resistant strains showed XR to azoles as well. Furthermore, CS was apparent in CAS-resistant strains to POS and KTO, but not to FLU. In addition, AMB-resistant strains showed prominent CS to CAS, CPX, NIT, and GEL. These CS trends might be the result of **resistance mutations that are associated with fitness-trade offs** that induce CS, or the **modes of action of the drugs** in a CS drug pair. Accordingly, CS in our AMB-resistant strains could be appointed to the mutations found in *ERG3* and *ERG11*. On the other hand, as no mutations were found in CAS-resistant strains, CS to POS might be attributed to the facilitated penetration of POS into the cell due to the unstable cell wall induced by CAS-resistance. Furthermore, CS in AMB-resistant strains might be appointed to the mechanisms of CAS, CPX, GEL and NIT as well. CS between AMB and GEL might be associated with Hsp90 and its ability to alleviate AMB resistance-induced stress [113]. Antifungal activity of NIT [205] and CPX [203] are still poorly understood, but were thought to include an iron chelation-like activity, inhibiting the activity of iron-dependent enzymes such as catalase that can reduce AMB resistance-induced oxidative stress. CS in AMB-resistance strains to CAS might be attributed to the disrupted lipid rafts and the cell membrane enzyme Fks1. All things considered, CS might work through both fitness trade-off mechanisms and the mode of action of drugs.

CS-based drug cycling significantly reduces resistance development in the tested schemes. Resistance ratios (RR) based on MIC_{50} did not show resistance development in any of the cycling schemes, while RR based on AUC_{BDA} in some strains in AMB-GEL, AMB-NIT and CAS-POS cycling were higher than 1. Yet, these ratios did not indicate high levels of resistance, thus actual resistance was most likely not developed. In each cycling scheme, we observed an enhanced susceptibility of the cycling evolved strains to either one or both drugs, e.g. AMB-CAS and AMB-CPX to both drugs, AMB-NIT and AMB-GEL to AMB, and CAS-POS to POS. This might be attributed to CS and/or interactions between the drugs.

As far as we know, this is the first study regarding CS in fungal pathogens. We chose to study CS and CS-based alternative treatment strategies in *C. auris* because of its rapid emergence and multi-drug resistance. Although we observed efficient prevention of resistance emergence in our drug cycling schemes, a multitude of experiments can be performed to further prove the presence and robustness of CS and the efficiency of alternative treatment strategies both in *C. auris* and in other species. Some of the most promising future perspectives include the **use of modeling to design CS-based treatment strategies**, the **validation of CS-based sequential treatment in *in vivo* models and other genetic backgrounds** and the use of **transcriptomics and genomics to investigate the mechanisms that cause CS.**

References

[1] Bodey, G. P., Mardani, M., Hanna, H. A., Boktour, M., Abbas, J., Girgawy, E., Hachem, R. Y., Kontoyiannis, D. P., & Raad, I. I. (2002). The epidemiology of *Candida glabrata* and *Candida albicans* fungemia in immunocompromised patients with cancer. *The American journal of medicine*, *112*(5), 380–385.

[2] Hasan, F., Xess, I., Wang, X., Jain, N., & Fries, B. C. (2009). Biofilm formation in clinical *Candida* isolates and its association with virulence. *Microbes and infection*, *11*(8-9), 753–761.

[3] Sardi, J. d. C. O., Silva, D. R., Mendes-Giannini, M. J. S., & Rosalen, P. L. (2018). *Candida auris*: Epidemiology, risk factors, virulence, resistance, and therapeutic options. *Microbial pathogenesis*, *125*, 116–121.

[4] Fidel Jr, P. L., Vazquez, J. A., & Sobel, J. D. (1999). *Candida glabrata*: Review of epidemiology, pathogenesis, and clinical disease with comparison to c. albicans. *Clinical microbiology reviews*, *12*(1), 80–96.

[5] Spivak, E. S., & Hanson, K. E. (2018). *Candida auris*: An emerging fungal pathogen. *Journal of clinical microbiology*, *56*(2), e01588–17.

[6] Satoh, K., Makimura, K., Hasumi, Y., Nishiyama, Y., Uchida, K., & Yamaguchi, H. (2009). *Candida auris* sp. nov., a novel ascomycetous yeast isolated from the external ear canal of an inpatient in a japanese hospital. *Microbiology and immunology*, *53*(1), 41–44.

[7] Lee, W. G., Shin, J. H., Uh, Y., Kang, M. G., Kim, S. H., Park, K. H., & Jang, H.-C. (2011). First three reported cases of nosocomial fungemia caused by *Candida auris*. *Journal of clinical microbiology*, *49*(9), 3139–3142.

[8] Corsi-Vasquez, G., & Ostrosky-Zeichner, L. (2019). *Candida auris*: What have we learned so far? *Current opinion in infectious diseases*, *32*(6), 559–564.

[9] Chybowska, A. D., Childers, D. S., & Farrer, R. A. (2020). Nine things genomics can tell us about *Candida auris*. *Frontiers in genetics*, *11*, 351.

[10] Ben-Ami, R., Berman, J., Novikov, A., Bash, E., Shachor-Meyouhas, Y., Zakin, S., Maor, Y., Tarabia, J., Schechner, V., Adler, A., et al. (2017). Multidrug-resistant *Candida haemulonii* and c. auris, tel aviv, israel. *Emerging infectious diseases*, *23*(2), 195.

[11] Guarie, M. (n.d.). *What is candida auris*. https://www.verywellhealth.com/candida-auris-4692475 (accessed: 02.06.2022)

[12] Nett, J. E. (2019). *Candida auris*: An emerging pathogen "incognito"? *PLoS pathogens*, *15*(4), e1007638.

[13] Casadevall, A., Kontoyiannis, D. P., & Robert, V. (2019). On the emergence of *candida auris*: Climate change, azoles, swamps, and birds. *MBio*, *10*(4), e01397–19.

[14] Lockhart, S. R., Etienne, K. A., Vallabhaneni, S., Farooqi, J., Chowdhary, A., Govender, N. P., Colombo, A. L., Calvo, B., Cuomo, C. A., Desjardins, C. A., et al. (2017). Simultaneous emergence of multidrug-resistant *Candida auris* on 3 continents confirmed by whole-genome sequencing and epidemiological analyses. *Clinical Infectious Diseases*, *64*(2), 134–140.

[15] Rhodes, J., & Fisher, M. C. (2019). Global epidemiology of emerging *Candida auris*. *Current opinion in microbiology*, *52*, 84–89.

[16] Chow, N. A., Gade, L., Tsay, S. V., Forsberg, K., Greenko, J. A., Southwick, K. L., Barrett, P. M., Kerins, J. L., Lockhart, S. R., Chiller, T. M., et al. (2018). Multiple introductions and subsequent transmission of multidrug-resistant *Candida auris* in the usa: A molecular epidemiological survey. *The Lancet Infectious diseases*, *18*(12), 1377–1384.

[17] Chow, N. A., Muñoz, J. F., Gade, L., Berkow, E. L., Li, X., Welsh, R. M., Forsberg, K., Lockhart, S. R., Adam, R., Alanio, A., et al. (2020). Tracing the evolutionary history and global expansion of *Candida auris* using population genomic analyses. *MBio*, *11*(2), e03364–19.

[18] Welsh, R. M., Sexton, D. J., Forsberg, K., Vallabhaneni, S., & Litvintseva, A. (2019). Insights into the unique nature of the east asian clade of the emerging pathogenic yeast *Candida auris*. *Journal of Clinical Microbiology*, *57*(4), e00007–19.

[19] Chow, N. A., de Groot, T., Badali, H., Abastabar, M., Chiller, T. M., & Meis, J. F. (2019). Potential fifth clade of *Candida auris*, iran, 2018. *Emerging infectious diseases*, *25*(9), 1780.

[20] Lone, S. A., & Ahmad, A. (2019). *Candida auris*—the growing menace to global health. *Mycoses*, *62*(8), 620–637.

[21] Szekely, A., Borman, A. M., & Johnson, E. M. (2019). *Candida auris* isolates of the southern asian and south african lineages exhibit different phenotypic and antifungal susceptibility profiles in vitro. *Journal of Clinical Microbiology*, *57*(5), e02055–18.

[22] Kohlenberg, A., Struelens, M. J., Monnet, D. L., Plachouras, D., et al. (2018). *Candida auris*: Epidemiological situation, laboratory capacity and preparedness in european union and european economic area countries, 2013 to 2017. *Eurosurveillance*, *23*(13), 18–00136.

[23] Gaitán, A. C. R., Moret, A., Hontangas, J. L. L., Molina, J. M., López, A. I. A., Cabezas, A. H., Maseres, J. M., Arcas, R. C., Ruiz, M. D. G., Chiveli, M. Á., et al. (2017). Nosocomial fungemia by *Candida auris*: First four reported cases in continental europe. *Revista iberoamericana de micologia*, *34*(1), 23–27.

[24] Calvo, B., Melo, A. S., Perozo-Mena, A., Hernandez, M., Francisco, E. C., Hagen, F., Meis, J. F., & Colombo, A. L. (2016). First report of *Candida auris* in america: Clinical and microbiological aspects of 18 episodes of candidemia. *Journal of Infection*, *73*(4), 369–374.

[25] Schwartz, I., & Hammond, G. (2017). Outbreak detection: First reported case of multidrug-resistant *Candida auris* in canada. *Canada Communicable Disease Report*, *43*(7-8), 150.

[26] Araúz, A. B., Caceres, D. H., Santiago, E., Armstrong, P., Arosemena, S., Ramos, C., Espinosa-Bode, A., Borace, J., Hayer, L., Cedeño, I., et al. (2018). Isolation of *Candida auris* from 9 patients in central america: Importance of accurate diagnosis and susceptibility testing. *Mycoses*, *61*(1), 44–47.

[27] Heath, C. H., Dyer, J. R., Pang, S., Coombs, G. W., & Gardam, D. J. (2019). *Candida auris* sternal osteomyelitis in a man from kenya visiting australia, 2015. *Emerging infectious diseases*, *25*(1), 192.

[28] Larkin, E., Hager, C., Chandra, J., Mukherjee, P. K., Retuerto, M., Salem, I., Long, L., Isham, N., Kovanda, L., Borroto-Esoda, K., et al. (2017). The emerging pathogen *Candida auris*: Growth phenotype, virulence factors, activity of antifungals, and effect of scy-078, a novel glucan synthesis inhibitor, on growth morphology and biofilm formation. *Antimicrobial agents and chemotherapy*, *61*(5), e02396–16.

[29] Ahmad, A., Spencer, J. E., Lockhart, S. R., Singleton, S., Petway, D. J., Bagarozzi Jr, D. A., & Herzegh, O. T. (2019). A high-throughput and rapid method for accurate identification of emerging multidrug-resistant *Candida auris*. *Mycoses*, *62*(6), 513–518.

[30] Wattal, C., Oberoi, J., Goel, N., Raveendran, R., & Khanna, S. (2017). Matrix-assisted laser desorption ionization time of flight mass spectrometry (maldi-tof ms) for rapid identification of micro-organisms in the routine clinical microbiology laboratory. *European Journal of Clinical Microbiology & Infectious Diseases*, *36*(5), 807–812.

[31] Bao, J. R., Master, R. N., Azad, K. N., Schwab, D. A., Clark, R. B., Jones, R. S., Moore, E. C., & Shier, K. L. (2018). Rapid, accurate identification of *Candida auris* by using a novel matrix-assisted laser desorption ionization–time of flight mass spectrometry (maldi-tof ms) database (library). *Journal of clinical microbiology*, *56*(4), e01700–17.

[32] Eyre, D. W., Sheppard, A. E., Madder, H., Moir, I., Moroney, R., Quan, T. P., Griffiths, D., George, S., Butcher, L., Morgan, M., et al. (2018). A *Candida auris* outbreak and its control in an intensive care setting. *New England Journal of Medicine*, *379*(14), 1322–1331.

[33] Ku, T. S., Walraven, C. J., & Lee, S. A. (2018). *Candida auris*: Disinfectants and implications for infection control. *Frontiers in microbiology*, *9*, 726.

[34] Chowdhary, A., Prakash, A., Sharma, C., Kordalewska, M., Kumar, A., Sarma, S., Tarai, B., Singh, A., Upadhyaya, G., Upadhyay, S., et al. (2018). A multicentre study of antifungal susceptibility patterns among 350 *Candida auris* isolates (2009–17) in india: Role of the *ERG11* and *FKS1* genes in azole and echinocandin resistance. *Journal of Antimicrobial Chemotherapy*, *73*(4), 891–899.

[35] Fromtling, R. A. (1988). Overview of medically important antifungal azole derivatives. *Clinical microbiology reviews*, *1*(2), 187–217.

[36] Bhattacharya, S., Sae-Tia, S., & Fries, B. C. (2020). Candidiasis and mechanisms of antifungal resistance. *Antibiotics*, *9*(6), 312.

[37] Kodedová, M., & Sychrová, H. (2015). Changes in the sterol composition of the plasma membrane affect membrane potential, salt tolerance and the activity of multidrug resistance pumps in *Saccharomyces cerevisiae*. *PLoS One*, *10*(9), e0139306.

[38] Mollinedo, F. (2012). Lipid raft involvement in yeast cell growth and death. *Frontiers in oncology*, *2*, 140.

[39] Dupont, S., Fleurat-Lessard, P., Cruz, R. G., Lafarge, C., Grangeteau, C., Yahou, F., Gerbeau-Pissot, P., Abrahão Júnior, O., Gervais, P., Simon-Plas, F., et al. (2021). Antioxidant properties of ergosterol and its role in yeast resistance to oxidation. *Antioxidants*, *10*(7), 1024.

[40] Bhattacharya, S., Esquivel, B. D., & White, T. C. (2018). Overexpression or deletion of ergosterol biosynthesis genes alters doubling time, response to stress agents, and drug susceptibility in *Saccharomyces cerevisiae*. *MBio*, *9*(4), e01291–18.

[41] Sanglard, D., Coste, A., & Ferrari, S. (2009). Antifungal drug resistance mechanisms in fungal pathogens from the perspective of transcriptional gene regulation. *FEMS yeast research*, *9*(7), 1029–1050.

[42] Francois, I. E., Cammue, B., Borgers, M., Ausma, J., Dispersyn, G. D., & Thevissen, K. (2006). Azoles: Mode of antifungal action and resistance development. effect of miconazole on endogenous reactive oxygen species production in *Candida albicans*. *Anti-Infective Agents in Medicinal Chemistry (Formerly Current Medicinal Chemistry-Anti-Infective Agents)*, *5*(1), 3–13.

[43] Delattin, N., Cammue, B. P., & Thevissen, K. (2014). Reactive oxygen species-inducing antifungal agents and their activity against fungal biofilms. *Future medicinal chemistry*, *6*(1), 77–90.

[44] Caballero, U., Kim, S., Eraso, E., Quindós, G., Vozmediano, V., Schmidt, S., & Jauregizar, N. (2021). In vitro synergistic interactions of isavuconazole and echinocandins against *Candida auris*. *Antibiotics*, *10*(4), 355.

[45] Kordalewska, M., Lee, A., Park, S., Berrio, I., Chowdhary, A., Zhao, Y., & Perlin, D. S. (2018). Understanding echinocandin resistance in the emerging pathogen *Candida auris*. *Antimicrobial agents and chemotherapy*, *62*(6), e00238–18.

[46] Grover, N. D. (2010). Echinocandins: A ray of hope in antifungal drug therapy. *Indian journal of pharmacology*, *42*(1), 9.

[47] Perlin, D. S. (2007). Resistance to echinocandin-class antifungal drugs. *Drug Resistance Updates*, *10*(3), 121–130.

[48] Cândido, E. d. S., Affonseca, F., Cardoso, M. H., & Franco, O. L. (2020). Echinocandins as biotechnological tools for treating *Candida auris* infections. *Journal of Fungi*, *6*(3), 185.

[49] Kovács, R., Tóth, Z., Locke, J. B., Forgács, L., Kardos, G., Nagy, F., Borman, A. M., & Majoros, L. (2021). Comparison of in vitro killing activity of rezafungin, anidulafungin, caspofungin, and micafungin against four *Candida auris* clades in rpmi-1640 in the absence and presence of human serum. *Microorganisms*, *9*(4), 863.

[50] Pfaller, M., Boyken, L., Hollis, R., Messer, S., Tendolkar, S., & Diekema, D. (2006). Global surveillance of in vitro activity of micafungin against *Candida*: A comparison with caspofungin by clsi-recommended methods. *Journal of clinical microbiology*, *44*(10), 3533–3538.

[51] Tóth, Z., Forgács, L., Kardos, T., Kovács, R., Locke, J. B., Kardos, G., Nagy, F., Borman, A. M., Adnan, A., & Majoros, L. (2020). Relative frequency of paradoxical growth and trailing effect with caspofungin, micafungin, anidulafungin, and the novel echinocandin rezafungin against *Candida* species. *Journal of Fungi*, *6*(3), 136.

[52] Carolus, H., Pierson, S., Lagrou, K., & Van Dijck, P. (2020). Amphotericin b and other polyenes—discovery, clinical use, mode of action and drug resistance. *Journal of Fungi*, *6*(4), 321.

[53] Gray, K. C., Palacios, D. S., Dailey, I., Endo, M. M., Uno, B. E., Wilcock, B. C., & Burke, M. D. (2012). Amphotericin primarily kills yeast by simply binding ergosterol. *Proceedings of the National Academy of Sciences*, *109*(7), 2234–2239.

[54] Kamiński, D. M. (2014). Recent progress in the study of the interactions of amphotericin b with cholesterol and ergosterol in lipid environments. *European biophysics journal*, *43*(10), 453–467.

[55] Anderson, T. M., Clay, M. C., Cioffi, A. G., Diaz, K. A., Hisao, G. S., Tuttle, M. D., Nieuwkoop, A. J., Comellas, G., Maryum, N., Wang, S., et al. (2014). Amphotericin forms an extramembranous and fungicidal sterol sponge. *Nature chemical biology*, *10*(5), 400–406.

[56] Dutcher, J. D. (1968). The discovery and development of amphotericin b. *Diseases of the Chest*, *54*, 296–298.

[57] Saravolatz, L. D., Ostrosky-Zeichner, L., Marr, K. A., Rex, J. H., & Cohen, S. H. (2003). Amphotericin b: Time for a new "gold standard". *Clinical Infectious Diseases*, *37*(3), 415–425.

[58] Duschinsky, R., Pleven, E., & Heidelberger, C. (1957). The synthesis of 5-fluoropyrimidines. *Journal of the American Chemical Society*, *79*(16), 4559–4560.

[59] Titsworth, E., & Grunberg, E. (1973). Chemotherapeutic activity of 5-fluorocytosine and amphotericin b against *Candida albicans* in mice. *Antimicrobial Agents and Chemotherapy*, *4*(3), 306–308.

[60] Tassel, D., & Madoff, M. A. (1968). Treatment of *Candida* sepsis and *Cryptococcus* meningitis with 5-fluorocytosine: A new antifungal agent. *Jama*, *206*(4), 830–832.

[61] Mayers, D. L., Sobel, J. D., Ouellette, M., Kaye, K. S., & Marchaim, D. (2009). *Antimicrobial drug resistance*. Springer.

[62] Vermes, A., Guchelaar, H.-J., & Dankert, J. (2000). Flucytosine: A review of its pharmacology, clinical indications, pharmacokinetics, toxicity and drug interactions. *Journal of Antimicrobial Chemotherapy*, *46*(2), 171–179.

[63] Polak, A., & Scholer, H. (1975). Mode of action of 5-fluorocytosine and mechanisms of resistance. *Chemotherapy*, *21*(3-4), 113–130.

[64] Waldorf, A. R., & Polak, A. (1983). Mechanisms of action of 5-fluorocytosine. *Antimicrobial Agents and Chemotherapy*, *23*(1), 79–85.

[65] INC, S. (n.d.). *Ibrexafungerp (formerly scy-078)*. https://www.scynexis.com/pipeline (accessed: 09.12.2021)

[66] Jallow, S., & Govender, N. P. (2021). Ibrexafungerp: A first-in-class oral triterpenoid glucan synthase inhibitor. *Journal of Fungi*, *7*(3), 163.

[67] Arendrup, M. C., Jørgensen, K. M., Hare, R. K., & Chowdhary, A. (2020). In vitro activity of ibrexafungerp (scy-078) against *Candida auris* isolates as determined by eucast methodology and comparison with activity against c. albicans and c. glabrata and with the activities of six comparator agents. *Antimicrobial agents and chemotherapy*, *64*(3), e02136–19.

[68] Berkow, E. L., Angulo, D., & Lockhart, S. R. (2017). In vitro activity of a novel glucan synthase inhibitor, scy-078, against clinical isolates of *Candida auris*. *Antimicrobial Agents and Chemotherapy*, *61*(7), e00435–17.

[69] Gamal, A., Chu, S., McCormick, T. S., Borroto-Esoda, K., Angulo, D., & Ghannoum, M. A. (2021). Ibrexafungerp, a novel oral triterpenoid antifungal in development: Overview of antifungal activity against *Candida glabrata*. *Frontiers in cellular and infection microbiology*, *11*, 126.

[70] Azie, N., Angulo, D., Dehn, B., & Sobel, J. D. (2020). Oral ibrexafungerp: An investigational agent for the treatment of vulvovaginal candidiasis. *Expert Opinion on Investigational Drugs*, *29*(9), 893–900.

[71] Sobel, R., Nyirjesy, P., Ghannoum, M. A., Delchev, D. A., Azie, N. E., Angulo, D., Harriott, I. A., Borroto-Esoda, K., & Sobel, J. D. (2022). Efficacy and safety of oral ibrexafungerp for the treatment of acute vulvovaginal candidiasis: A global phase 3, randomised, placebo-controlled superiority study (vanish 306). *BJOG: An International Journal of Obstetrics & Gynaecology*, *129*(3), 412–420.

[72] Masone, M. C. (2021). Ibrexafungerp to treat acute vulvovaginal candidiasis. *Nature Reviews Urology*, *18*(11), 638–638.

[73] Wiederhold, N. P., Najvar, L. K., Olivo, M., Morris, K. N., Patterson, H. P., Catano, G., & Patterson, T. F. (2021). Ibrexafungerp demonstrates in vitro activity against fluconazole-resistant *Candida auris* and in vivo efficacy with delayed initiation of therapy in an experimental model of invasive candidiasis. *Antimicrobial agents and chemotherapy*, *65*(6), e02694–20.

[74] Therapeutics, A. (n.d.). *A novel, broad spectrum, clinical stage antifungal to address severe and difficult-to-treat invasive fungal infections*. https://www.appilitherapeutics.com/ati-2307

[75] Mitsuyama, J., Nomura, N., Hashimoto, K., Yamada, E., Nishikawa, H., Kaeriyama, M., Kimura, A., Todo, Y., & Narita, H. (2008). In vitro and in vivo antifungal activities of t-2307, a novel arylamidine. *Antimicrobial agents and chemotherapy*, *52*(4), 1318–1324.

[76] Cohen, A., & Brown, S. (n.d.). *Appili therapeutics acquires clinical stage antifungal program from fujifilm toyama chemical*. https://www.businesswire.com/news/home/20191121005346/en/Appili-Therapeutics-Acquires-Clinical-Stage-Antifungal-Program-From-FUJIFILM-Toyama-Chemical

[77] Gerlach, E. S., Altamirano, S., Yoder, J. M., Luggya, T. S., Akampurira, A., Meya, D. B., Boulware, D. R., Rhein, J., & Nielsen, K. (2021). Ati-2307 exhibits equivalent antifungal activity in *Cryptococcus neoformans* clinical isolates with high and low fluconazole ic50. *Frontiers in Cellular and Infection Microbiology*, *11*.

[78] Nolan, E. (n.d.). *Pfizer acquires amplyx pharmaceuticals*. https://www.businesswire.com/news/home/20210428005147/en/Pfizer-Acquires-Amplyx-Pharmaceuticals (accessed: 10.12.2021)

[79] Petraitiene, R., Petraitis, V., Maung, B. B. W., Mansbach, R. S., Hodges, M. R., Finkelman, M. A., Shaw, K. J., & Walsh, T. J. (2021). Efficacy and pharmacokinetics of fosmanogepix (apx001) in the treatment of candida endophthalmitis and hematogenous meningoencephalitis in nonneutropenic rabbits. *Antimicrobial Agents and Chemotherapy*, *65*(3), e01795–20.

[80] Hoenigl, M., Sprute, R., Egger, M., Arastehfar, A., Cornely, O. A., Krause, R., Lass-Flörl, C., Prattes, J., Spec, A., Thompson, G. R., et al. (2021). The antifungal pipeline: Fosmanogepix, ibrexafungerp, olorofim, opelconazole, and rezafungin. *Drugs*, *81*(15), 1703–1729.

[81] Shaw, K. J., & Ibrahim, A. S. (2020). Fosmanogepix: A review of the first-in-class broad spectrum agent for the treatment of invasive fungal infections. *Journal of Fungi*, *6*(4), 239.

[82] Watanabe, N.-a., Miyazaki, M., Horii, T., Sagane, K., Tsukahara, K., & Hata, K. (2012). E1210, a new broad-spectrum antifungal, suppresses *Candida albicans* hyphal growth through inhibition of glycosylphosphatidylinositol biosynthesis. *Antimicrobial agents and chemotherapy*, *56*(2), 960–971.

[83] Kim, J. H., Cheng, L. W., Chan, K. L., Tam, C. C., Mahoney, N., Friedman, M., Shilman, M. M., & Land, K. M. (2020). Antifungal drug repurposing. *Antibiotics*, *9*(11), 812.

[84] De Oliveira, H. C., Monteiro, M. C., Rossi, S. A., Pemán, J., Ruiz-Gaitán, A., Mendes-Giannini, M. J. S., Mellado, E., & Zaragoza, O. (2019). Identification of off-patent compounds that present antifungal activity against the emerging fungal pathogen *Candida auris*. *Frontiers in Cellular and Infection Microbiology*, *9*, 83.

[85] Wall, G., Herrera, N., & Lopez-Ribot, J. L. (2019). Repositionable compounds with antifungal activity against multidrug resistant *Candida auris* identified in the medicines for malaria venture's pathogen box. *Journal of Fungi*, *5*(4), 92.

[86] Wall, G., Chaturvedi, A. K., Wormley Jr, F. L., Wiederhold, N. P., Patterson, H. P., Patterson, T. F., & Lopez-Ribot, J. L. (2018). Screening a repurposing library for inhibitors of multidrug-resistant *Candida auris* identifies ebselen as a repositionable candidate for antifungal drug development. *Antimicrobial agents and chemotherapy*, *62*(10), e01084–18.

[87] Goncalves, S. S., Souza, A. C. R., Chowdhary, A., Meis, J. F., & Colombo, A. L. (2016). Epidemiology and molecular mechanisms of antifungal resistance in candida and aspergillus. *Mycoses*, *59*(4), 198–219.

[88] Lockhart, S. R. (2019). *Candida auris* and multidrug resistance: Defining the new normal. *Fungal Genetics and Biology*, *131*, 103243.

[89] Cowen, L. E., Sanglard, D., Howard, S. J., Rogers, P. D., & Perlin, D. S. (2015). Mechanisms of antifungal drug resistance. *Cold Spring Harbor perspectives in medicine*, *5*(7), a019752.

[90] Berkow, E. L., & Lockhart, S. R. (2017). Fluconazole resistance in candida species: A current perspective. *Infection and drug resistance*, *10*, 237.

[91] Rybak, J. M., Muñoz, J. F., Barker, K. S., Parker, J. E., Esquivel, B. D., Berkow, E. L., Lockhart, S. R., Gade, L., Palmer, G. E., White, T. C., et al. (2020). Mutations in *TAC1b*: A novel genetic determinant of clinical fluconazole resistance in *Candida auris*. *MBio*, *11*(3), e00365–20.

[92] Li, J., Coste, A. T., Liechti, M., Bachmann, D., Sanglard, D., & Lamoth, F. (2021). Novel *ERG11* and *TAC1b* mutations associated with azole resistance in *Candida auris*. *Antimicrobial agents and chemotherapy*, *65*(5), e02663–20.

[93] Rybak, J. M., Doorley, L. A., Nishimoto, A. T., Barker, K. S., Palmer, G. E., & Rogers, P. D. (2019). Abrogation of triazole resistance upon deletion of *CDR1*1 in a clinical isolate of *Candida auris*. *Antimicrobial agents and chemotherapy*, *63*(4), e00057–19.

[94] Wasi, M., Khandelwal, N. K., Moorhouse, A. J., Nair, R., Vishwakarma, P., Bravo Ruiz, G., Ross, Z. K., Lorenz, A., Rudramurthy, S. M., Chakrabarti, A., et al. (2019). Abc transporter genes show upregulated expression in drug-resistant clinical isolates of *Candida auris*: A genome-wide characterization of atp-binding cassette (abc) transporter genes. *Frontiers in microbiology*, 1445.

[95] Healey, K. R., Kordalewska, M., Jiménez Ortigosa, C., Singh, A., Berrío, I., Chowdhary, A., & Perlin, D. S. (2018). Limited *ERG11* mutations identified in isolates of *Candida auris* directly contribute to reduced azole susceptibility. *Antimicrobial agents and chemotherapy*, *62*(10), e01427–18.

[96] Morio, F., Pagniez, F., Lacroix, C., Miegeville, M., & Le Pape, P. (2012). Amino acid substitutions in the *Candida albicans* sterol Δ5, 6-desaturase (erg3p) confer azole resistance: Characterization of two novel mutants with impaired virulence. *Journal of antimicrobial chemotherapy*, *67*(9), 2131–2138.

[97] Flowers, S. A., Barker, K. S., Berkow, E. L., Toner, G., Chadwick, S. G., Gygax, S. E., Morschhäuser, J., & Rogers, P. D. (2012). Gain-of-function mutations in *UPC2* are a frequent cause of *ERG11* upregulation in azole-resistant clinical isolates of *Candida albicans*. *Eukaryotic cell*, *11*(10), 1289–1299.

[98] Bing, J., Hu, T., Zheng, Q., Muñoz, J. F., Cuomo, C. A., & Huang, G. (2020). Experimental evolution identifies adaptive aneuploidy as a mechanism of fluconazole resistance in *Candida auris*. *Antimicrobial agents and chemotherapy*, *65*(1), e01466–20.

[99] Carolus, H., Pierson, S., Muñoz, J. F., Subotić, A., Cruz, R. B., Cuomo, C. A., & Van Dijck, P. (2020). Genome-wide analysis of experimentally evolved *Candida auris* reveals multiple novel mechanisms of multidrug-resistance. *bioRxiv*.

[100] Chowdhary, A., Anil Kumar, V., Sharma, C., Prakash, A., Agarwal, K., Babu, R., Dinesh, K., Karim, S., Singh, S., Hagen, F., et al. (2014). Multidrug-resistant endemic clonal strain of *Candida auris* in india. *European journal of clinical microbiology & infectious diseases*, *33*(6), 919–926.

[101] Larsen, R. A. (2011). Flucytosine. In *Essentials of clinical mycology* (pp. 57–60). Springer.

[102] Garcia-Effron, G., Park, S., & Perlin, D. S. (2009). Correlating echinocandin mic and kinetic inhibition of fks1 mutant glucan synthases for *Candida albicans*: Implications for interpretive breakpoints. *Antimicrobial agents and chemotherapy*, *53*(1), 112–122.

[103] Perlin, D. S. (2015). Echinocandin resistance in *Candida*. *Clinical Infectious Diseases*, *61*(suppl_6), S612–S617.

[104] Cortegiani, A., Misseri, G., Fasciana, T., Giammanco, A., Giarratano, A., & Chowdhary, A. (2018). Epidemiology, clinical characteristics, resistance, and treatment of infections by *Candida auris*. *Journal of intensive care*, *6*(1), 1–13.

[105] Garcia-Effron, G., Lee, S., Park, S., Cleary, J. D., & Perlin, D. S. (2009). Effect of *Candida glabrata FKS1* and *FKS2* mutations on echinocandin sensitivity and kinetics of 1, 3-β-d-glucan synthase: Implication for the existing susceptibility breakpoint. *Antimicrobial agents and chemotherapy*, *53*(9), 3690–3699.

[106] Desnos-Ollivier, M., Bretagne, S., Raoux, D., Hoinard, D., Dromer, F., & Dannaoui, E. (2008). Mutations in the *FKS1* gene in *Candida albicans*, c. tropicalis, and c. krusei correlate with elevated caspofungin mics uncovered in am3 medium using the method of the european committee on antibiotic susceptibility testing. *Antimicrobial agents and chemotherapy*, *52*(9), 3092–3098.

[107] Walker, L. A., Munro, C. A., De Bruijn, I., Lenardon, M. D., McKinnon, A., & Gow, N. A. (2008). Stimulation of chitin synthesis rescues *Candida albicans* from echinocandins. *PLoS pathogens*, *4*(4), e1000040.

[108] Sharma, D., Paul, R. A., Rudramurthy, S. M., Kashyap, N., Bhattacharya, S., Soman, R., Shankarnarayan, S. A., Chavan, D., Singh, S., Das, P., et al. (2021). Impact of *FKS1* genotype on echinocandin in vitro susceptibility in *Candida auris* and in vivo response in a murine model of infection. *Antimicrobial Agents and Chemotherapy*, *66*(1), e01652–21.

[109] Ben-Ami, R., Garcia-Effron, G., Lewis, R. E., Gamarra, S., Leventakos, K., Perlin, D. S., & Kontoyiannis, D. P. (2011). Fitness and virulence costs of *Candida albicans FKS1* hot spot mutations associated with echinocandin resistance. *Journal of Infectious Diseases*, *204*(4), 626–635.

[110] Munro, C. A., Selvaggini, S., De Bruijn, I., Walker, L., Lenardon, M. D., Gerssen, B., Milne, S., Brown, A. J., & Gow, N. A. (2007). The pkc, hog and ca2+ signalling pathways co-ordinately regulate chitin synthesis in *Candida albicans*. *Molecular microbiology*, *63*(5), 1399–1413.

[111] Lima, S. L., Colombo, A. L., & de Almeida Junior, J. N. (2019). Fungal cell wall: Emerging antifungals and drug resistance. *Frontiers in microbiology*, 2573.

[112] Stover, K. R., & Cleary, J. D. (2015). The eagle-like effect of the echinocandins: Is it relevant for clinical decisions? *Current Fungal Infection Reports*, *9*(2), 88–93.

[113] Vincent, B. M., Lancaster, A. K., Scherz-Shouval, R., Whitesell, L., & Lindquist, S. (2013). Fitness trade-offs restrict the evolution of resistance to amphotericin b. *PLoS biology*, *11*(10), e1001692.

[114] Geber, A., Hitchcock, C. A., Swartz, J. E., Pullen, F. S., Marsden, K. E., Kwon-Chung, K. J., & Bennett, J. E. (1995). Deletion of the *Candida glabrata ERG3* and *ERG11* genes: Effect on cell viability, cell growth, sterol composition, and antifungal susceptibility. *Antimicrobial Agents and Chemotherapy*, *39*(12), 2708–2717.

[115] Sanglard, D., Ischer, F., Parkinson, T., Falconer, D., & Bille, J. (2003). *Candida albicans* mutations in the ergosterol biosynthetic pathway and resistance to several antifungal agents. *Antimicrobial agents and chemotherapy*, *47*(8), 2404–2412.

[116] Young, L. Y., Hull, C. M., & Heitman, J. (2003). Disruption of ergosterol biosynthesis confers resistance to amphotericin b in *Candida lusitaniae*. *Antimicrobial agents and chemotherapy*, *47*(9), 2717–2724.

[117] Phillips, A. J., Sudbery, I., & Ramsdale, M. (2003). Apoptosis induced by environmental stresses and amphotericin b in *Candida albicans*. *Proceedings of the National Academy of Sciences*, *100*(24), 14327–14332.

[118] LAMP-FREUND, M. T., FERREIRA, V. F., & SCHREIER, S. (1985). Mechanism of inactivation of the polyene antibiotic amphotericin b evidence for radical formation in the process of autooxidation. *The Journal of antibiotics*, *38*(6), 753–757.

[119] Sangalli-Leite, F., Scorzoni, L., Mesa-Arango, A. C., Casas, C., Herrero, E., Gianinni, M. J. S. M., Rodríguez-Tudela, J. L., Cuenca-Estrella, M., & Zaragoza, O. (2011). Amphotericin b mediates killing in *Cryptococcus neoformans* through the induction of a strong oxidative burst. *Microbes and infection*, *13*(5), 457–467.

[120] Perlin, D. S., Rautemaa-Richardson, R., & Alastruey-Izquierdo, A. (2017). The global problem of antifungal resistance: Prevalence, mechanisms, and management. *The Lancet infectious diseases*, *17*(12), e383–e392.

[121] Blum, G., Perkhofer, S., Haas, H., Schrettl, M., Würzner, R., Dierich, M. P., & Lass-Flörl, C. (2008). Potential basis for amphotericin b resistance in aspergillus terreus. *Antimicrobial agents and chemotherapy*, *52*(4), 1553–1555.

[122] Posch, W., Blatzer, M., Wilflingseder, D., & Lass-Flörl, C. (2018). Aspergillus terreus: Novel lessons learned on amphotericin b resistance. *Medical Mycology*, *56*(suppl_1), S73–S82.

[123] Kaloriti, D., Jacobsen, M., Yin, Z., Patterson, M., Tillmann, A., Smith, D. A., Cook, E., You, T., Grimm, M. J., Bohovych, I., et al. (2014). Mechanisms underlying the exquisite sensitivity of *Candida albicans* to combinatorial cationic and oxidative stress that enhances the potent fungicidal activity of phagocytes. *MBio*, *5*(4), e01334–14.

[124] Zhang, X., De Micheli, M., Coleman, S. T., Sanglard, D., & Moye-Rowley, W. S. (2000). Analysis of the oxidative stress regulation of the *Candida albicans* transcription factor, cap1p. *Molecular microbiology*, *36*(3), 618–629.

[125] Brown, A. J., Budge, S., Kaloriti, D., Tillmann, A., Jacobsen, M. D., Yin, Z., Ene, I. V., Bohovych, I., Sandai, D., Kastora, S., et al. (2014). Stress adaptation in a pathogenic fungus. *Journal of Experimental Biology*, *217*(1), 144–155.

[126] Pál, C., Papp, B., & Lázár, V. (2015). Collateral sensitivity of antibiotic-resistant microbes. *Trends in microbiology*, *23*(7), 401–407.

[127] Efferth, T., Saeed, M. E., Kadioglu, O., Seo, E.-J., Shirooie, S., Mbaveng, A. T., Nabavi, S. M., & Kuete, V. (2020). Collateral sensitivity of natural products in drug-resistant cancer cells. *Biotechnology advances*, *38*, 107342.

[128] Imamovic, L., & Sommer, M. O. (2013). Use of collateral sensitivity networks to design drug cycling protocols that avoid resistance development. *Science translational medicine*, *5*(204), 204ra132–204ra132.

[129] Szybalski, W., & Bryson, V. (1952). Genetic studies on microbial cross resistance to toxic agents i., cross resistance of *Escherichia coli* to fifteen antibiotics. *Journal of bacteriology*, *64*(4), 489–499.

[130] Roemhild, R., & Andersson, D. I. (2021). Mechanisms and therapeutic potential of collateral sensitivity to antibiotics. *PLoS Pathogens*, *17*(1), e1009172.

[131] Pluchino, K. M., Hall, M. D., Goldsborough, A. S., Callaghan, R., & Gottesman, M. M. (2012). Collateral sensitivity as a strategy against cancer multidrug resistance. *Drug Resistance Updates*, *15*(1-2), 98–105.

[132] Lázár, V., Pal Singh, G., Spohn, R., Nagy, I., Horváth, B., Hrtyan, M., Busa-Fekete, R., Bogos, B., Méhi, O., Csörgő, B., et al. (2013). Bacterial evolution of antibiotic hypersensitivity. *Molecular systems biology*, *9*(1), 700.

[133] Griffith, J. K., Kogoma, T., Corvo, D. L., Anderson, W. L., & Kazim, A. (1988). An n-terminal domain of the tetracycline resistance protein increases susceptibility to aminoglycosides and complements potassium uptake defects in *Escherichia coli*. *Journal of bacteriology*, *170*(2), 598–604.

[134] Merlin, T., Davis, G., Anderson, W., Moyzis, R., & Griffith, J. (1989). Aminoglycoside uptake increased by tet gene expression. *Antimicrobial agents and chemotherapy*, *33*(9), 1549–1552.

[135] Podnecky, N. L., Fredheim, E. G., Kloos, J., Sørum, V., Primicerio, R., Roberts, A. P., Rozen, D. E., Samuelsen, Ø., & Johnsen, P. J. (2018). Conserved collateral antibiotic susceptibility networks in diverse clinical strains of *Escherichia coli*. *Nature Communications*, *9*(1), 1–11.

[136] Apjok, G., Boross, G., Nyerges, Á., Fekete, G., Lázár, V., Papp, B., Pál, C., & Csörgő, B. (2019). Limited evolutionary conservation of the phenotypic effects of antibiotic resistance mutations. *Molecular biology and evolution*, *36*(8), 1601–1611.

[137] Barbosa, C., Römhild, R., Rosenstiel, P., & Schulenburg, H. (2019). Evolutionary stability of collateral sensitivity to antibiotics in the model pathogen pseudomonas aeruginosa. *Elife*, *8*, e51481.

[138] Gottesman, M. M., Fojo, T., & Bates, S. E. (2002). Multidrug resistance in cancer: Role of atp–dependent transporters. *Nature reviews cancer*, *2*(1), 48–58.

[139] Leonard, G. D., Fojo, T., & Bates, S. E. (2003). The role of abc transporters in clinical practice. *The oncologist*, *8*(5), 411–424.

[140] Fox, E., & Bates, S. E. (2007). Tariquidar (xr9576): A p-glycoprotein drug efflux pump inhibitor. *Expert review of anticancer therapy*, *7*(4), 447–459.

[141] Broxterman, H. J., Pinedo, H. M., Kuiper, C. M., Kaptein, L. C., Schuurhuis, G. J., & Lankelma, J. (1988). Induction by verapamil of a rapid increase in atp consumption in multidrug-resistant tumor cells. *The FASEB Journal*, *2*(7), 2278–2282.

[142] Karwatsky, J., Lincoln, M. C., & Georges, E. (2003). A mechanism for p-glycoprotein-mediated apoptosis as revealed by verapamil hypersensitivity. *Biochemistry*, *42*(42), 12163–12173.

[143] Laberge, R.-M., Ambadipudi, R., & Georges, E. (2009). P-glycoprotein (abcb1) modulates collateral sensitivity of a multidrug resistant cell line to verapamil. *Archives of biochemistry and biophysics*, *491*(1-2), 53–60.

[144] Shutt, D., O'Dorisio, M. S., Aykin-Burns, N., & Spitz, D. (2010). 2-deoxy-d-glucose induces oxidative stress and cell killing in human neuroblastoma cells. *Cancer biology & therapy*, *9*(11), 853–861.

[145] Fath, M. A., Diers, A. R., Aykin-Burns, N., Simons, A. L., Hua, L., & Spitz, D. R. (2009). Mitochondrial electron transport chain blockers enhance 2-deoxy-d-glucose induced oxidative stress and cell killing in human colon carcinoma cells. *Cancer biology & therapy*, *8*(13), 1228–1236.

[146] Callaghan, R., & Riordan, J. R. (1995). Collateral sensitivity of multidrug resistant cells to narcotic analgesics is due to effects on the plasma membrane. *Biochimica et Biophysica Acta (BBA)-Biomembranes*, *1236*(1), 155–162.

[147] Bal, A., Kumar, A., & Gould, I. (2010). Antibiotic heterogeneity: From concept to practice. *Annals of the New York Academy of Sciences*, *1213*(1), 81–91.

[148] Niederman, M. S. (2003). Appropriate use of antimicrobial agents: Challenges and strategies for improvement. *Critical care medicine*, *31*(2), 608–616.

[149] Aulin, L., Liakopoulos, A., van der Graaf, P. H., Rozen, D. E., & van Hasselt, J. (2021). Design principles of collateral sensitivity-based dosing strategies. *Nature communications*, *12*(1), 1–14.

[150] Nowell, P. C. (1976). The clonal evolution of tumor cell populations: Acquired genetic lability permits stepwise selection of variant sublines and underlies tumor progression. *Science*, *194*(4260), 23–28.

[151] Negrini, S., Gorgoulis, V. G., & Halazonetis, T. D. (2010). Genomic instability—an evolving hallmark of cancer. *Nature reviews Molecular cell biology*, *11*(3), 220–228.

[152] Fisher, R., Pusztai, L., & Swanton, C. (2013). Cancer heterogeneity: Implications for targeted therapeutics. *British journal of cancer*, *108*(3), 479–485.

[153] Zhao, B., Sedlak, J. C., Srinivas, R., Creixell, P., Pritchard, J. R., Tidor, B., Lauffenburger, D. A., & Hemann, M. T. (2016). Exploiting temporal collateral sensitivity in tumor clonal evolution. *Cell*, *165*(1), 234–246.

[154] Andersson, D. I., & Hughes, D. (2010). Antibiotic resistance and its cost: Is it possible to reverse resistance? *Nature Reviews Microbiology*, *8*(4), 260–271.

[155] Ottmann, O. G., & Pfeifer, H. (2009). Management of philadelphia chromosome–positive acute lymphoblastic leukemia (ph+ all). *ASH Education Program Book*, *2009*(1), 371–381.

[156] Rex, J. H., Alexander, B. D., Andes, D., Arthington-Skaggs, B., Brown, S. D., Chaturvedi, V., Ghannoum, M. A., Espinel-Ingroff, A., Knapp, C. C., Ostrosky-Zeichner, L., Pfaller, M. A., Sheehan, D. J., & Walsh, T. J. (2008). Reference method for broth dilution antifungal susceptibility testing of yeasts: Approved standard - third edition. *Clinical and Laboratory Standards Institute (CLSI)*.

[157] inc., N. E. B. (n.d.). *Tm calculator*. https://tmcalculator.neb.com/#!/main

[158] Eurofins. (n.d.). *The tubeseq service is sanger sequencing with the extra bit*. https://eurofinsgenomics.eu/en/custom-dna-sequencing/eurofins-services/tubeseq-service/

[159] Open, R. L. (n.d.). *Snap2*. https://rostlab.org/owiki/index.php/Snap2 (accessed: 20.07.2022)

[160] Kathuria, S., Singh, P. K., Sharma, C., Prakash, A., Masih, A., Kumar, A., Meis, J. F., & Chowdhary, A. (2015). Multidrug-resistant *Candida auris* misidentified as *Candida haemulonii*: Characterization by matrix-assisted laser desorption ionization–time of flight mass spectrometry and dna sequencing and its antifungal susceptibility profile variability by vitek 2, clsi broth microdilution, and etest method. *Journal of clinical microbiology*, *53*(6), 1823–1830.

[161] Veitch, Z. W., Guo, B., Hembruff, S. L., Bewick, A. J., Heibein, A. D., Eng, J., Cull, S., Maclean, D. A., & Parissenti, A. M. (2009). Induction of 1c aldoketoreductases and other drug dose-dependent genes upon acquisition of anthracycline resistance. *Pharmacogenetics and genomics*, *19*(6), 477–488.

[162] Björkman, J., Hughes, D., & Andersson, D. I. (1998). Virulence of antibiotic-resistant salmonella typhimurium. *Proceedings of the National Academy of Sciences*, *95*(7), 3949–3953.

[163] Maisnier-Patin, S., Berg, O. G., Liljas, L., & Andersson, D. I. (2002). Compensatory adaptation to the deleterious effect of antibiotic resistance in salmonella typhimurium. *Molecular microbiology*, *46*(2), 355–366.

[164] Gullberg, E., Cao, S., Berg, O. G., Ilbäck, C., Sandegren, L., Hughes, D., & Andersson, D. I. (2011). Selection of resistant bacteria at very low antibiotic concentrations. *PLoS pathogens*, *7*(7), e1002158.

[165] Bosch, F. v. d., Oliver, R., Berg, F. v. d., & Paveley, N. (2014). Governing principles can guide fungicide-resistance management tactics. *Annual Review of Phytopathology*, *52*, 175–195.

[166] Van Den Bosch, F., Paveley, N., Shaw, M., Hobbelen, P., & Oliver, R. (2011). The dose rate debate: Does the risk of fungicide resistance increase or decrease with dose? *Plant Pathology*, *60*(4), 597–606.

[167] van den Bosch, F., & Gilligan, C. A. (2008). Models of fungicide resistance dynamics. *Annu. Rev. Phytopathol.*, *46*, 123–147.

[168] Zur Wiesch, P. A., Kouyos, R., Engelstädter, J., Regoes, R. R., & Bonhoeffer, S. (2011). Population biological principles of drug-resistance evolution in infectious diseases. *The Lancet infectious diseases*, *11*(3), 236–247.

[169] Kilburn, S., Innes, G., Quinn, M., Southwick, K., Ostrowsky, B., Greenko, J. A., Lutterloh, E., Greeley, R., Magleby, R., Chaturvedi, V., et al. (2022). Antifungal resistance trends of *Candida auris* clinical isolates in new york and new jersey from 2016 to 2020. *Antimicrobial Agents and Chemotherapy*, *66*(3), e02242–21.

[170] for Disease Control, C., & Prevention. (n.d.). *Antifungal susceptibility testing and interpretation*. https://www.cdc.gov/fungal/candida-auris/c-auris-antifungal.html (accessed: 29.07.2022)

[171] Escandón, P., Chow, N. A., Caceres, D. H., Gade, L., Berkow, E. L., Armstrong, P., Rivera, S., Misas, E., Duarte, C., Moulton-Meissner, H., et al. (2019). Molecular epidemiology of *Candida auris* in colombia reveals a highly related, countrywide colonization with regional patterns in amphotericin b resistance. *Clinical Infectious Diseases*, *68*(1), 15–21.

[172] Rybak, J. M., Barker, K. S., Muñoz, J. F., Parker, J. E., Ahmad, S., Mokaddas, E., Abdullah, A., Elhagracy, R. S., Kelly, S. L., Cuomo, C. A., et al. (2022). In vivo emergence of high-level resistance during treatment reveals the first identified mechanism of amphotericin b resistance in *Candida auris*. *Clinical Microbiology and Infection*, *28*(6), 838–843.

[173] Fuchs, F., Hof, H., Hofmann, S., Kurzai, O., Meis, J. F., & Hamprecht, A. (2021). Antifungal activity of nitroxoline against *Candida auris* isolates. *Clinical Microbiology and Infection*, *27*(11), 1697–e7.

[174] Hao, W., Wang, Y., Xi, Y., Yang, Z., Zhang, H., & Ge, X. (2022). Activity of chlorhexidine acetate in combination with fluconazole against suspensions and biofilms of *Candida auris*. *Journal of Infection and Chemotherapy*, *28*(1), 29–34.

[175] Betts, M. J., & Russell, R. B. (2003). Amino acid properties and consequences of substitutions. *Bioinformatics for geneticists*, *317*, 289.

[176] Berkow, E. L., & Lockhart, S. R. (2018). Activity of cd101, a long-acting echinocandin, against clinical isolates of *Candida auris*. *Diagnostic microbiology and infectious disease*, *90*(3), 196–197.

[177] Roberts, S. M., & Gibb, A. J. (2013). Introduction to enzymes, receptors and the action of small molecule drugs. In *Introduction to biological and small molecule drug research and development* (pp. 1–55). Elsevier.

[178] (SGD), S. G. D. (n.d.[a]). *ERG3 / ylr056w overview*. https://www.yeastgenome.org/locus/S000004046 (accessed: 20.05.2022

[179] (SGD), S. G. D. (n.d.[b]). *ERG11 / yhr007c overview*. https://www.yeastgenome.org/locus/S000001049 (accessed: 20.05.2022

[180] Charlier, C., El Sissy, C., Bachelier-Bassi, S., Scemla, A., Quesne, G., Sitterlé, E., Legendre, C., Lortholary, O., & Bougnoux, M.-E. (2016). Acquired flucytosine resistance during combination therapy with caspofungin and flucytosine for *Candida glabrata* cystitis. *Antimicrobial Agents and Chemotherapy*, *60*(1), 662–665.

[181] ElBaradei, A. (2020). A decade after the emergence of *Candida auris*: What do we know? *European Journal of Clinical Microbiology & Infectious Diseases*, *39*(9), 1617–1627.

[182] Costa, C., Ponte, A., Pais, P., Santos, R., Cavalheiro, M., Yaguchi, T., Chibana, H., & Teixeira, M. C. (2015). New mechanisms of flucytosine resistance in c. glabrata unveiled by a chemogenomics analysis in s. cerevisiae. *PloS one*, *10*(8), e0135110.

[183] (SGD), S. G. D. (n.d.[c]). *Fcy1 / ypr062w overview*. https://www.yeastgenome.org/locus/S000006266 (accessed: 20.05.2022

[184] (SGD), S. G. D. (n.d.[d]). *Fcy2 / yer056c overview*. https://www.yeastgenome.org/locus/S000000858 (accessed: 20.05.2022

[185] Rhodes, J., Abdolrasouli, A., Farrer, R. A., Cuomo, C. A., Aanensen, D. M., Armstrong-James, D., Fisher, M. C., & Schelenz, S. (2018). Genomic epidemiology of the uk outbreak of the emerging human fungal pathogen *Candida auris*. *Emerging microbes & infections*, *7*(1), 1–12.

[186] Jacobs, S. E., Jacobs, J. L., Dennis, E. K., Taimur, S., Rana, M., Patel, D., Gitman, M., Patel, G., Schaefer, S., Iyer, K., et al. (2022). *Candida auris* pan-drug-resistant to four classes of antifungal agents. *Antimicrobial Agents and Chemotherapy*, e00053–22.

[187] Berman, J., & Krysan, D. J. (2020). Drug resistance and tolerance in fungi. *Nature Reviews Microbiology*, *18*(6), 319–331.

[188] Delarze, E., & Sanglard, D. (2015). Defining the frontiers between antifungal resistance, tolerance and the concept of persistence. *Drug Resistance Updates*, *23*, 12–19.

[189] O'Kane, C. J., & Hyland, E. M. (2019). Yeast epigenetics: The inheritance of histone modification states. *Bioscience Reports*, *39*(5).

[190] Pristov, K., & Ghannoum, M. (2019). Resistance of *Candida* to azoles and echinocandins worldwide. *Clinical Microbiology and Infection*, *25*(7), 792–798.

[191] Panackal, A. A., Gribskov, J. L., Staab, J. F., Kirby, K. A., Rinaldi, M., & Marr, K. A. (2006). Clinical significance of azole antifungal drug cross-resistance in *Candida glabrata*. *Journal of Clinical Microbiology*, *44*(5), 1740–1743.

[192] Sanguinetti, M., Posteraro, B., Fiori, B., Ranno, S., Torelli, R., & Fadda, G. (2005). Mechanisms of azole resistance in clinical isolates of *Candida glabrata* collected during a hospital survey of antifungal resistance. *Antimicrobial agents and chemotherapy*, *49*(2), 668–679.

[193] Schuetzer-Muehlbauer, M., Willinger, B., Krapf, G., Enzinger, S., Presterl, E., & Kuchler, K. (2003). The *Candida albicans* cdr2p atp-binding cassette (abc) transporter confers resistance to caspofungin. *Molecular microbiology*, *48*(1), 225–235.

[194] Pham, C. D., Iqbal, N., Bolden, C. B., Kuykendall, R. J., Harrison, L. H., Farley, M. M., Schaffner, W., Beldavs, Z. G., Chiller, T. M., Park, B. J., et al. (2014). Role of fks mutations in *Candida glabrata*: Mic values, echinocandin resistance, and multidrug resistance. *Antimicrobial agents and chemotherapy*, *58*(8), 4690–4696.

[195] Kelly, S. L., Lamb, D. C., Corran, A. J., Baldwin, B. C., & Kelly, D. E. (1995). Mode of action and resistance to azole antifungals associated with the formation of 14α-methylergosta-8, 24 (28)-dien-3β, 6α-diol. *Biochemical and biophysical research communications*, *207*(3), 910–915.

[196] Hull, C. M., Parker, J. E., Bader, O., Weig, M., Gross, U., Warrilow, A. G., Kelly, D. E., & Kelly, S. L. (2012). Facultative sterol uptake in an ergosterol-deficient clinical isolate of *Candida glabrata* harboring a missense mutation in *ERG11* and exhibiting cross-resistance to azoles and amphotericin b. *Antimicrobial agents and chemotherapy*, *56*(8), 4223–4232.

[197] Douglas, C., D'ippolito, J., Shei, G., Meinz, M., Onishi, J., Marrinan, J., Li, W., Abruzzo, G., Flattery, A., Bartizal, K., et al. (1997). Identification of the *FKS1* gene of *Candida albicans* as the essential target of 1, 3-beta-d-glucan synthase inhibitors. *Antimicrobial agents and chemotherapy*, *41*(11), 2471–2479.

[198] Picard, D. (2002). Heat-shock protein 90, a chaperone for folding and regulation. *Cellular and Molecular Life Sciences CMLS*, *59*(10), 1640–1648.

[199] Cowen, L. E. (2009). Hsp90 orchestrates stress response signaling governing fungal drug resistance. *PLoS pathogens*, *5*(8), e1000471.

[200] Singh, S. D., Robbins, N., Zaas, A. K., Schell, W. A., Perfect, J. R., & Cowen, L. E. (2009). Hsp90 governs echinocandin resistance in the pathogenic yeast *Candida albicans* via calcineurin. *PLoS pathogens*, *5*(7), e1000532.

[201] LaFayette, S. L., Collins, C., Zaas, A. K., Schell, W. A., Betancourt-Quiroz, M., Gunatilaka, A. L., Perfect, J. R., & Cowen, L. E. (2010). Pkc signaling regulates drug resistance of the fungal pathogen *Candida albicans* via circuitry comprised of mkc1, calcineurin, and hsp90. *PLoS pathogens*, *6*(8), e1001069.

[202] Sreedhar, A. S., Mihály, K., Pató, B., Schnaider, T., Steták, A., Kis-Petik, K., Fidy, J., Simonics, T., Maráz, A., & Csermely, P. (2003). Hsp90 inhibition accelerates cell lysis: Anti-hsp90 ribozyme reveals a complex mechanism of hsp90 inhibitors involving both superoxide-and hsp90-dependent events. *Journal of Biological Chemistry*, *278*(37), 35231–35240.

[203] Lin, J., Zangi, M., Kumar, T. V. N. H., Shakar Reddy, M., Reddy, L. V. R., Sadhukhan, S. K., Bradley, D. P., Moreira-Walsh, B., Edwards, T. C., O'Dea, A. T., et al. (2021). Synthetic derivatives of ciclopirox are effective inhibitors of *Cryptococcus neoformans*. *ACS omega*, *6*(12), 8477–8487.

[204] Guembe, M., Guinea, J., Peláez, T., Torres-Narbona, M., & Bouza, E. (2007). Synergistic effect of posaconazole and caspofungin against clinical zygomycetes. *Antimicrobial agents and chemotherapy*, *51*(9), 3457–3458.

[205] Medić-Šarić, M., Maysinger, D., Movrin, M., & Dvoržak, I. (1980). Antibacterial and antifungal activities of nitroxoline mannich bases. *Chemotherapy*, *26*(4), 263–267.

[206] Pelletier, C., Prognon, P., & Bourlioux, P. (1995). Roles of divalent cations and ph in mechanism of action of nitroxoline against *Escherichia coli* strains. *Antimicrobial agents and chemotherapy*, *39*(3), 707–713.

[207] Waugh, C. D. (2007). Agents acting on fungal cell membranes.

[208] Prachayasittikul, V., Prachayasittikul, S., Ruchirawat, S., & Prachayasittikul, V. (2013). 8-hydroxyquinolines: A review of their metal chelating properties and medicinal applications. *Drug design, development and therapy*, *7*, 1157.

[209] Kresken, M., & Körber-Irrgang, B. (2014). In vitro activity of nitroxoline against *Escherichia coli* urine isolates from outpatient departments in germany. *Antimicrobial Agents and Chemotherapy*, *58*(11), 7019–7020.

[210] Mamouei, Z., Alqarihi, A., Singh, S., Xu, S., Mansour, M. K., Ibrahim, A. S., & Uppuluri, P. (2018). Alexidine dihydrochloride has broad-spectrum activities against diverse fungal pathogens. *Msphere*, *3*(5), e00539–18.

[211] Wu, Y., Wu, M., Gao, J., & Ying, C. (2020). Antifungal activity and mode of action of miltefosine against clinical isolates of *Candida krusei*. *Frontiers in Microbiology*, *11*, 854.

[212] Wu, Y., Totten, M., Memon, W., Ying, C., & Zhang, S. X. (2020). In vitro antifungal susceptibility of the emerging multidrug-resistant pathogen *Candida auris* to miltefosine alone and in combination with amphotericin b. *Antimicrobial agents and chemotherapy*, *64*(2), e02063–19.

[213] Baddley, J. W., & Poppas, P. G. (2005). Antifungal combination therapy. *Drugs*, *65*(11), 1461–1480.

[214] Campitelli, M., Zeineddine, N., Samaha, G., & Maslak, S. (2017). Combination antifungal therapy: A review of current data. *Journal of clinical medicine research*, *9*(6), 451.

[215] Olson, J. A., Adler-Moore, J. P., Smith, P., & Proffitt, R. T. (2005). Treatment of *Candida glabrata* infection in immunosuppressed mice by using a combination of liposomal amphotericin b with caspofungin or micafungin. *Antimicrobial agents and chemotherapy*, *49*(12), 4895–4902.

[216] Barchiesi, F., Spreghini, E., Tomassetti, S., Giannini, D., & Scalise, G. (2007). Caspofungin in combination with amphotericin b against *Candida parapsilosis*. *Antimicrobial agents and chemotherapy*, *51*(3), 941–945.

[217] for Clinical Laboratory Standards, N. C., & Barry, A. L. (1999). *Methods for determining bactericidal activity of antimicrobial agents: Approved guideline* (Vol. 19). National Committee for Clinical Laboratory Standards Wayne, PA.

[218] Zarember, K. A., Cruz, A. R., Huang, C.-Y., & Gallin, J. I. (2009). Antifungal activities of natural and synthetic iron chelators alone and in combination with azole and polyene antibiotics against aspergillus fumigatus. *Antimicrobial agents and chemotherapy*, *53*(6), 2654–2656.

[219] Marr, K. A., Boeckh, M., Carter, R. A., Kim, H. W., & Corey, L. (2004). Combination antifungal therapy for invasive aspergillosis. *Clinical infectious diseases*, *39*(6), 797–802.

[220] Nivoix, Y., Zamfir, A., Lutun, P., Kara, F., Remy, V., Lioure, B., Rigolot, J., Entz-Werle, N., Letscher-Bru, V., Waller, J., et al. (2006). Combination of caspofungin and an azole or an amphotericin b formulation in invasive fungal infections. *Journal of Infection*, *52*(1), 67–74.

[221] Shalit, I., Shadkchan, Y., Samra, Z., & Osherov, N. (2003). In vitro synergy of caspofungin and itraconazole against aspergillus spp.: Mic versus minimal effective concentration end points. *Antimicrobial agents and chemotherapy*, *47*(4), 1416–1418.

[222] Khalifa, H. O., Majima, H., Watanabe, A., & Kamei, K. (2021). In vitro characterization of twenty-one antifungal combinations against echinocandin-resistant and-susceptible *Candida glabrata*. *Journal of Fungi*, *7*(2), 108.

[223] Chen, Y.-L., Lehman, V. N., Averette, A. F., Perfect, J. R., & Heitman, J. (2013). Posaconazole exhibits in vitro and in vivo synergistic antifungal activity with caspofungin or fk506 against *Candida albicans*. *PLoS One*, *8*(3), e57672.

[224] Matthews, R. C., Rigg, G., Hodgetts, S., Carter, T., Chapman, C., Gregory, C., Illidge, C., & Burnie, J. (2003). Preclinical assessment of the efficacy of mycograb, a human recombinant antibody against fungal hsp90. *Antimicrobial agents and chemotherapy*, *47*(7), 2208–2216.

[225] Li, J., Coste, A. T., Bachmann, D., Sanglard, D., & Lamoth, F. (2022). Deciphering the mrr1/mdr1 pathway in azole resistance of *Candida auris*. *Antimicrobial Agents and Chemotherapy*, *66*(4), e00067–22.

[226] Vermitsky, J.-P., & Edlind, T. D. (2004). Azole resistance in *Candida glabrata*: Coordinate upregulation of multidrug transporters and evidence for a pdr1-like transcription factor. *Antimicrobial Agents and Chemotherapy*, *48*(10), 3773–3781.

[227] Whaley, S. G., Zhang, Q., Caudle, K. E., & Rogers, P. D. (2018). Relative contribution of the abc transporters cdr1, pdh1, and snq2 to azole resistance in *Candida glabrata*. *Antimicrobial Agents and Chemotherapy*, *62*(10), e01070–18.

[228] Vasicek, E. M., Berkow, E. L., Flowers, S. A., Barker, K. S., & Rogers, P. D. (2014). *UPC2* is universally essential for azole antifungal resistance in *Candida albicans*. *Eukaryotic cell*, *13*(7), 933–946.

[229] Branco, J., Ola, M., Silva, R., Fonseca, E., Gomes, N., Martins-Cruz, C., Silva, A., Silva-Dias, A., Pina-Vaz, C., Erraught, C., et al. (2017). Impact of *ERG3* mutations and expression of ergosterol genes controlled by *UPC2* and *NDT80* in *Candida parapsilosis* azole resistance. *Clinical Microbiology and Infection*, *23*(8), 575–e1.

[230] Beyda, N. D., Lewis, R. E., & Garey, K. W. (2012). Echinocandin resistance in *Candida* species: Mechanisms of reduced susceptibility and therapeutic approaches. *Annals of Pharmacotherapy*, *46*(7-8), 1086–1096.

[231] Dannaoui, E., Desnos-Ollivier, M., Garcia-Hermoso, D., Grenouillet, F., Cassaing, S., Baixench, M.-T., Bretagne, S., Dromer, F., Lortholary, O., Group, F. M. S., et al. (2012). *Candida spp.* with acquired echinocandin resistance, france, 2004–2010. *Emerging infectious diseases*, *18*(1), 86.

[232] Katiyar, S., Pfaller, M., & Edlind, T. (2006). *Candida albicans* and *Candida glabrata* clinical isolates exhibiting reduced echinocandin susceptibility. *Antimicrobial agents and chemotherapy*, *50*(8), 2892–2894.

[233] Silva, L. N., Oliveira, S. S., Magalhães, L. B., Andrade Neto, V. V., Torres-Santos, E. C., Carvalho, M. D., Pereira, M. D., Branquinha, M. H., & Santos, A. L. (2020). Unmasking the amphotericin b resistance mechanisms in *Candida haemulonii* species complex. *ACS Infectious Diseases*, *6*(5), 1273–1282.

[234] Sagatova, A. A. (2021). Strategies to bette target fungal squalene monooxygenase. *Journal of fungi (Basel), Vol.7 (1)*, p.1–13.

[235] Morio, F., Pagniez, F., Besse, M., Gay-andrieu, F., Miegeville, M., & Le Pape, P. (2013). Deciphering azole resistance mechanisms with a focus on transcription factor-encoding genes *TAC1, MRR1* and *UPC2* in a set of fluconazole-resistant clinical isolates of *Candida albicans*. *International journal of antimicrobial agents*, *42*(5), 410–415.

[236] Berkow, E. L., Manigaba, K., Parker, J. E., Barker, K. S., Kelly, S. L., & Rogers, P. D. (2015). Multidrug transporters and alterations in sterol biosynthesis contribute to azole antifungal resistance in *Candida parapsilosis*. *Antimicrobial agents and chemotherapy*, *59*(10), 5942–5950.

[237] Grossman, N. T., Pham, C. D., Cleveland, A. A., & Lockhart, S. R. (2015). Molecular mechanisms of fluconazole resistance in *Candida parapsilosis* isolates from a us surveillance system. *Antimicrobial agents and chemotherapy*, *59*(2), 1030–1037.

[238] Shivarathri, R., Jenull, S., Chauhan, M., Singh, A., Mazumdar, R., Chowdhary, A., Kuchler, K., & Chauhan, N. (2022). Comparative transcriptomics reveal possible mechanisms of amphotericin b resistance in *Candida auris*. *Antimicrobial Agents and Chemotherapy*, e02276–21.

[239] Udekwu, K. I., & Weiss, H. (2018). Pharmacodynamic considerations of collateral sensitivity in design of antibiotic treatment regimen. *Drug Design, Development and Therapy*, *12*, 2249.

[240] Van Hasselt, J. C., & Iyengar, R. (2019). Systems pharmacology: Defining the interactions of drug combinations. *Annual review of pharmacology and toxicology*, *59*, 21–40.

[241] Regoes, R. R., Wiuff, C., Zappala, R. M., Garner, K. N., Baquero, F., & Levin, B. R. (2004). Pharmacodynamic functions: A multiparameter approach to the design of antibiotic treatment regimens. *Antimicrobial agents and chemotherapy*, *48*(10), 3670–3676.

[242] Kochupurakkal, B. S., & Iglehart, J. D. (2013). Nourseothricin n-acetyl transferase: A positive selection marker for mammalian cells. *PloS one*, *8*(7), e68509.

[243] Cheung, H.-Y., Wong, M. M.-K., Cheung, S.-H., Liang, L. Y., Lam, Y.-W., & Chiu, S.-K. (2012). Differential actions of chlorhexidine on the cell wall of bacillus subtilis and *Escherichia coli*. *PLoS One*, *7*(5), e36659.

[244] Azad, G. K., & Tomar, R. S. (2014). Ebselen, a promising antioxidant drug: Mechanisms of action and targets of biological pathways. *Molecular biology reports*, *41*(8), 4865–4879.

[245] Amagata, T. (2010). Natural products structural diversity-ii secondary metabolites: Sources, structures and chemical biology. *Comprehensive Natural Products II*, *2*, 581–621.

[246] McCARTHY, P. J., TROKE, P. F., & GULL, K. (1985). Mechanism of action of nikkomycin and the peptide transport system of *Candida albicans*. *Microbiology*, *131*(4), 775–780.

[247] Sonzogni-Desautels, K., Renteria Flores, A., Vasquez Camargo, F., Di Lenardo, T. Z., Mikhail, A., Arrowood, M. J., Fortin, A., & Ndao, M. (2015). Oleylphosphocholine (olpc) arrests cryptosporidium parvum growth in vitro and prevents lethal infection in interferon gamma receptor knock-out mice. *Frontiers in microbiology*, *6*, 973.

[248] Li, B., Flaveny, C. A., Giambelli, C., Fei, D. L., Han, L., Hang, B. I., Bai, F., Pei, X.-H., Nose, V., Burlingame, O., et al. (2014). Repurposing the fda-approved pinworm drug pyrvinium as a novel chemotherapeutic agent for intestinal polyposis. *PloS one*, *9*(7), e101969.

[249] Ishii, I., Harada, Y., & Kasahara, T. (2012). Reprofiling a classical anthelmintic, pyrvinium pamoate, as an anti-cancer drug targeting mitochondrial respiration. *Frontiers in oncology*, *2*, 137.

[250] Bucchi, F., Cerletti, C., & de Gaetano, G. (1986). Inhibition of platelet thromboxane generation by suloctidil in man. *Pathophysiology of Haemostasis and Thrombosis*, *16*(5), 362–368.

[251] Gentilello, L. M., & Reed, R. L. (2008). Hypothermia and trauma. In *Current therapy of trauma and surgical critical care* (pp. 721–726). Elsevier Inc.

[252] Gaba, B., Fazil, M., Khan, S., Ali, A., Baboota, S., & Ali, J. (2015). Nanostructured lipid carrier system for topical delivery of terbinafine hydrochloride. *Bulletin of Faculty of Pharmacy, Cairo University*, *53*(2), 147–159.

Addendum

A. Risk assessment

C. auris is a fungal pathogen of biosafety level 2 (BSL2), as indicated by the CDC. This implies that *C. auris* mainly infects immunocompromised patients and that the pathogen is not airborne. Consequently, precautions have to be taken when handling *C. auris*. Working with this fungal pathogen requires experiments to be performed in a BSL2 lab, under a BSL2 flow hood and wearing the proper lab attire (gloves, lab coat) at all times. The lab coat is only worn in this room to prevent cross-contamination. Furthermore, gloves are always worn and frequently disinfected with 70% ethanol. After the experimental work, hands are washed with 1% chlorhexidine soap, the working surface of the flow hood and the personal bench are cleaned with Dettol and the UV-light in the flow hood is left on overnight for further sterilization.

Furthermore, PCI used for DNA extraction, should explicitly be used under a fume hood. Besides, SYBR™ Safe used to visualize DNA in agarose gels, is only used in a designated room with pippettes, tips and a waste bin solely for the purpose of gel electophoresis.

In the light of the COVID-19 pandemic, a mouth mask was worn in the laboratory.

B. Additional figures

B.1 Mechanisms of action of the selection antifungal and repurposed drugs

Table A1: Mode of action of selected antifungals and repurposed drugs.

Compound	Mode of action
5-FC	Inhibition of protein and DNA synthesis [64]
ALX	Targets PTPMT1 (mitochondrial tyrosine phosphatase) in mammals, resulting in mitochondrial apoptosis [210]
ANF	Inhibition of 1,3-β-D-glucan synthase [46]
AMB	Binding of ergosterol in the cell membrane of fungi, causing pore formation and ion leakage [53]
CAS	Inhibition of 1,3-β-D-glucan synthase[46]
CPX	iron chelator, inhibiting metal-dependent enzymes which play a role in the degradation of peroxides [207]
CHX	Binding of phosphate groups on cell surfaces causes impeded cell integrity and leakage of intracellular material. Drug molecules can then enter the cell and induce precipitation of cytoplasmic material [243]
DHQ	ion chelator of heavy metals [208]
EBS	Acts as a glutathione peroxidase, allowing it to protect cells against damage by ROS [244]
FLU	inhibits conversion to ergosterol by binding to cytochrome P-450 [40]
GEL	Blocks ATPase activity of Hsp90 by binding to the chaperone [245]
KTO	inhibits conversion to ergosterol by binding to cytochrome P-450 [40]
MCA	Inhibition of 1,3-β-D-glucan synthase[46]
NKZ	inhibits chitin synthase [246]
NIT	chelator of divalent cations, which are essential for the RNA polymerase in bacteria [209]
OPC	inhibits biosynthesis of phospholipids, causing apoptosis [247]
POS	inhibits conversion to ergosterol by binding to cytochrome P-450[40]
PAM	inhibition of Wnt signaling as antiparasitic[248] or inhibition of mitochondrial respiration complex 1, combined with suppression of UPR as an anticancer drug [249]
SLC	inhibition of thromboxane B2 (TxB2), involved in vasoconstriction and platelet aggregation [250, 251]
TRB	inhibition of squalene epoxidase in fungi [252]

B.2 PCR specifications of genes of interest

Table A2: PCR conditions and amplicon lengths of genes for which PCR reactions were conducted.

Gene	T_m	Amplicon length	Primer name
PCR			
ERG3	59°C	1381 bp	CauERG3_PCR/Seq1_F
			CauERG3_PCR/Seq2_R
ERG6	60°C	1392 bp	CauERG6_1F
			CauERG6_4R
ERG11	64°C	1847 bp	CauERG11_PCR/Seq1_F
			CauERG11_PCR/Seq2_R
FKS1 HS1-3	59°C	956 bp	CauFKS_B1120_Seq2.2.F
			CauFKS1_ASPCR_F
		617 bp	CauFKS_B1120_Seq2.2.F
			CauFKS1_B11220_Seq2_R
FKS1 HS2	64°C	519 bp	CauFKS1_B8441_HS2_F
			CauFKS1_B8441_HS2_RF
FUR1	63°C	770 bp	CauFUR1_F primer
			CauFUR1_R primer
FCY1	60°C	1732 bp	FCY1_US_F
			FCY1_DS_R
FCY2 (B9J08_002435)	60°C	2760	FCY2_2435_US_F
			FCY2_2435_DS_R
FCY2 (B9J08_002402)	60°C	2820	FCY2_2402_US_F
			FCY2_2402_DS_R
NCP1	60°C	3261 bp	NCP1_US_F
			NCP1_DS_R
TAC1b	67°C	2854 bp	CauTAC1b_B11220_Seq4_F
			CauTAC1b_B11220_PCR/Seq1_R

B.3 ETEST® amphotericin B

Figure A1: Result ETEST® to determine AMB MIC_{wt}. A YPD agar plate is depicted which contains an ETEST® strip for a range of amphotericin B concentrations from 0.002 to 32 μg/mL. Based on the halo, the strains exhibited an MIC of 0.25 µg/mL.

1x MIC_{50} AMB | 2x MIC_{50} AMB | 4x MIC_{50} AMB | 4x MIC_{50} AMB

Figure A2: Results ETEST® to determine MIC of AMB evolved strains. YPD agar plates are depicted which contain an ETEST® strip for a range of amphotericin B concentrations from 0.002 to 32 μg/mL. Based on the halo, all strains exhibit an MIC of 32μg/mL.

B.4 MIC_{50} and MFC_{99} resistance ratios of resistant strains

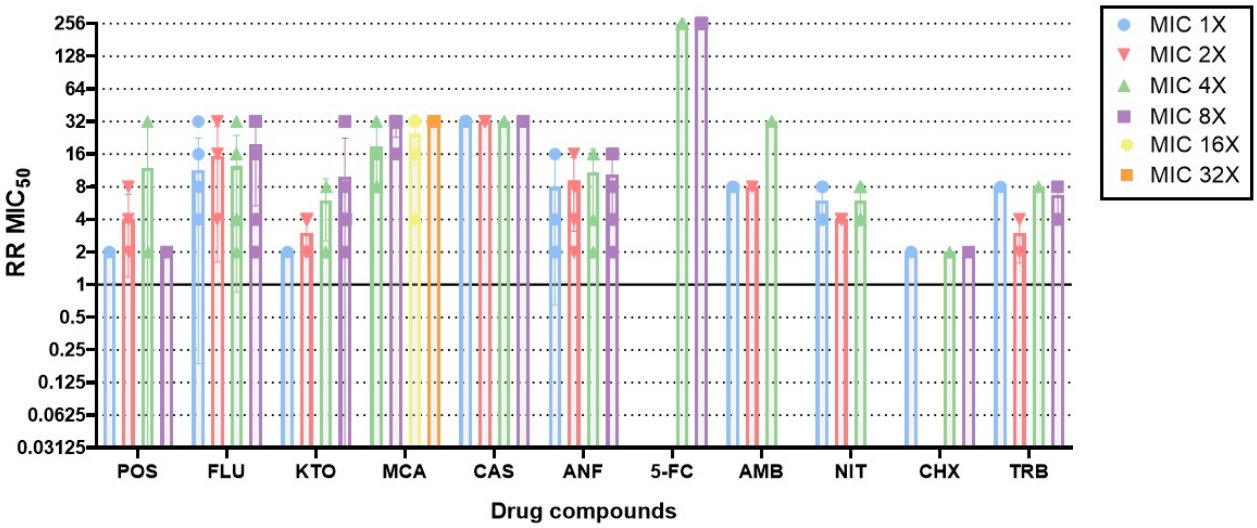

Figure A3: Distribution of mean RRs of drugs per drug condition of only resistant strains (RR > 1), based on MIC_{50}. Bar plots indicate the mean RRs MIC_{50} for each drug and drug condition (1x, 2x, 4x, and 8x MIC_{50}, except for MCA which was 4x, 8x, 16x, 32x MIC_{50}). Data points indicate the individual RR MIC_{50} in each condition, error bars depict standard deviations. A significant difference between drug conditions is indicated by an *.

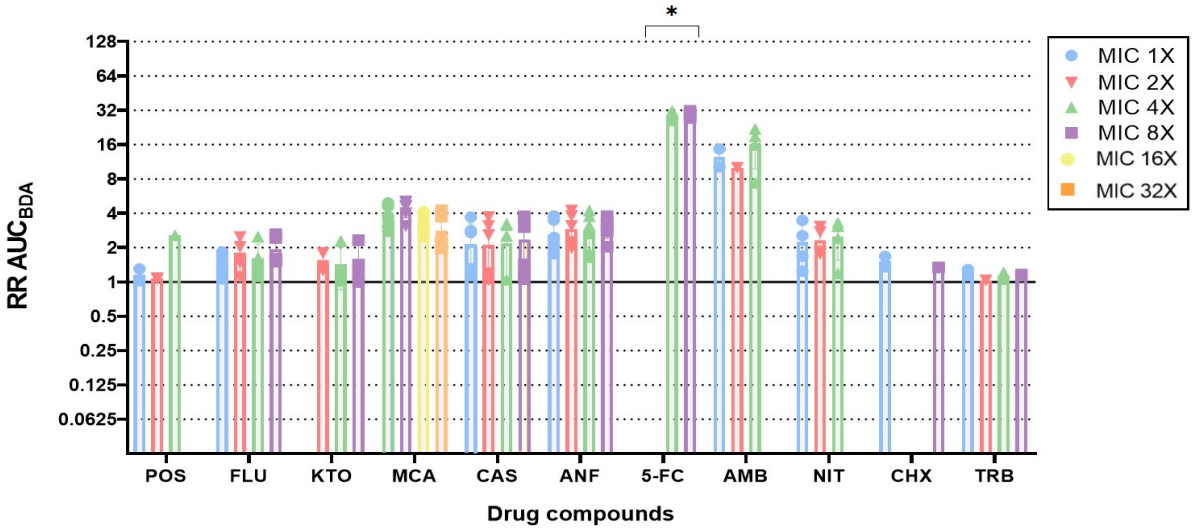

Figure A4: Distribution of mean RR per drug condition of only resistant strains (RR > 1), based on AUC_{BDA}. Bar plots indicate the mean RRs AUC for each drug and drug condition (1x, 2x, 4x, and 8x MIC_{50}, except for MCA which was 4x, 8x, 16x, 32x MIC_{50}). Data points indicate the individual RR AUC in each condition, error bars depict standard deviations. A significant difference between drug conditions is indicated by an *.

B.5 Summary of ratio of strains with and without mutations in the sequenced GOI

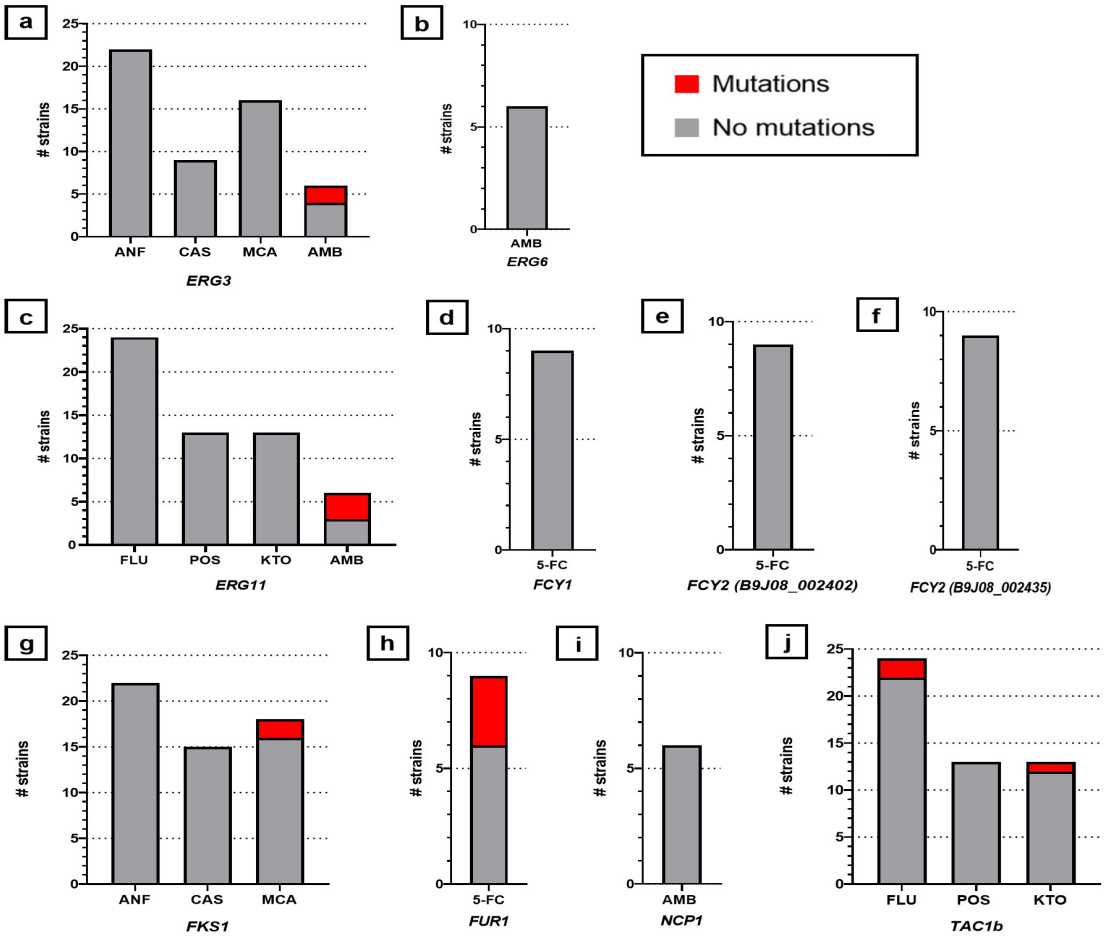

Figure A5: Sequenced resistant strains for their genes of interest, for which bar plots depict the total number of strains. In red, the number of strains that have acquired mutations is given, as well as the number of strains that have no mutations in grey. The following genes were sequenced: a) *ERG3* for ANF, CAS, MCA and AMB, b) *ERG6* for AMB, c) *ERG11* FLU, POS, KTO and AMB, d) *FCY1* for 5-FC, e and f) *FCY2* for 5-FC, g) *FKS1* for ANF, CAS and MCA, h) *FUR1* for 5-FC, i) *NCP1* for AMB and j) *FLU, POS and KTO* for TAC1b.

B.6 Collateral sensitivity ranges based on MIC_{50} and AUC_{BDA}

Table A3: Collateral sensitivity ranges between resistant strains and antifungal/repurposed drugs based on RR values of MIC_{50} and AUC_{BDA}, excluding intraclass XR.

Resistant strain	to which CS exhibited	RR MIC_{50}	RR AUC_{BDA}
AMB	ANF	0.25	0,20-0,26
	CAS	0.25-0.5	0,066-0,10
	MCA	0,125-0,5	0,077-0,11
	NIT	1	0,19-0,63
	GEL	1	0,133-0,93
	CPX	0,5-0,75	0,29-0,99
CAS	POS	0,002	0,09-0,125
	KTO	0,002-0,004	0,11-0,25
TRB	POS	0,75-1	0,45-0,6
	FLU	0,25-0,5	0,45-0,6
NIT	POS	0,25-0,375	0,17-1,29
	FLU	0,375-0,5	0,80-0,85
	KTO	0,5	0,051-0,58
	CAS	0,25-0,5	0,36-0,52
	ANF	0,25-0,75	0,05-0,92

B.7 SNAP2 analyses

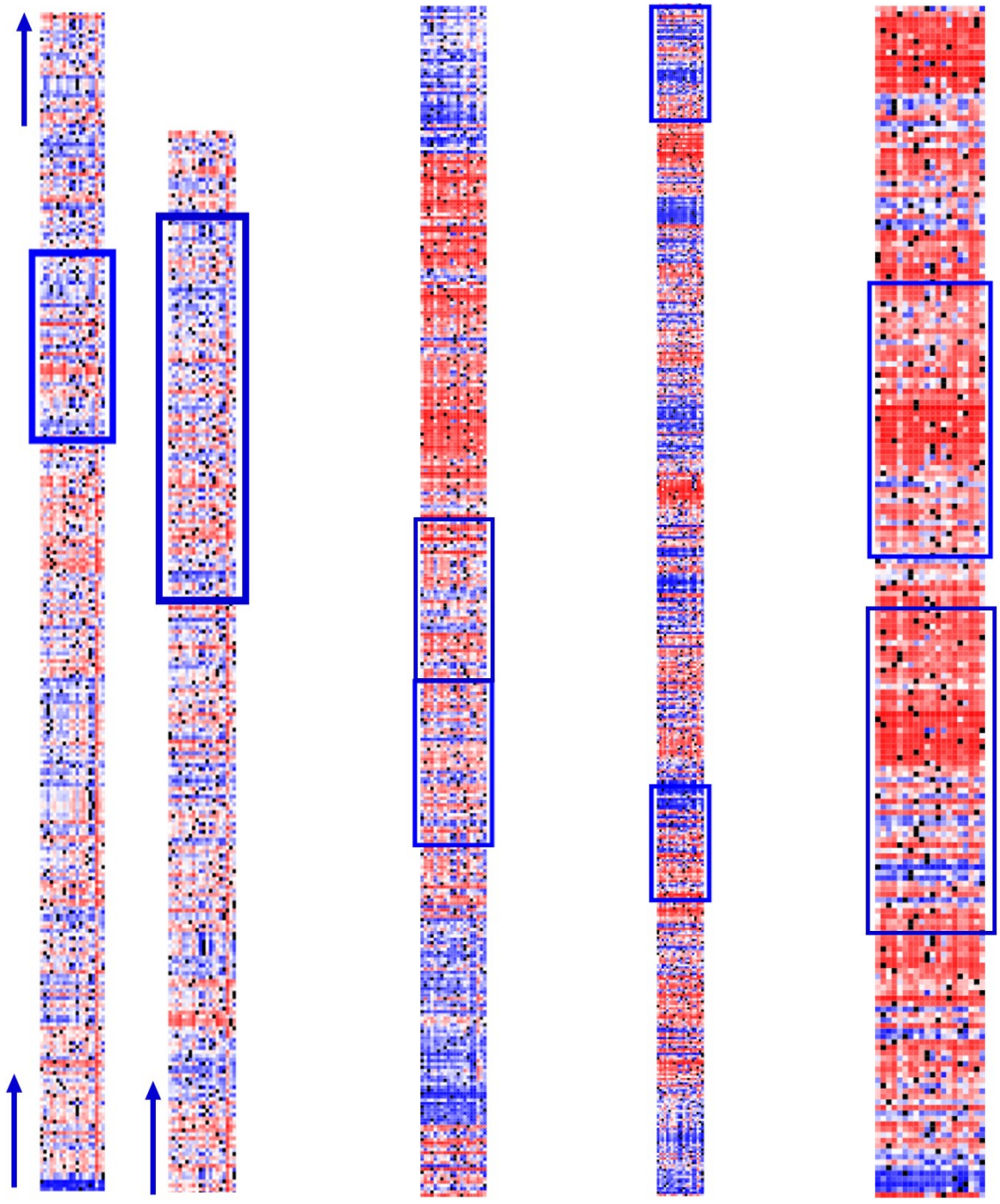

Figure A6: SNAP2 predicted functional effects heatmaps. (From left to right) *TAC1b, ERG3, ERG11* and *FUR1* SNAP2 heatmaps were presented, in which blue indicates neutral effect and red stands for effect. *FKS1* is not depicted due to its size (Boxes indicate the regions in which mutations were found.

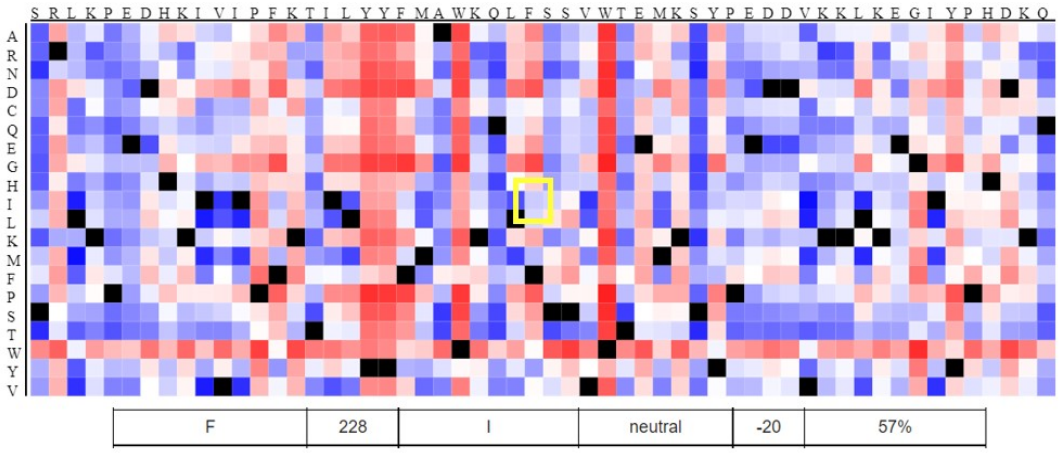

Figure A7: Heatmap of a region in the *TAC1b* sequence, in which the functional effects of aa substitutions were predicted. Indicated in yellow, the effect of an aa substitution at position 228 was displayed. In this case, Phenylalanine (F) was substituted for Isoleucine (I). The prediction effect and score, and expected accuracy are given in the table.

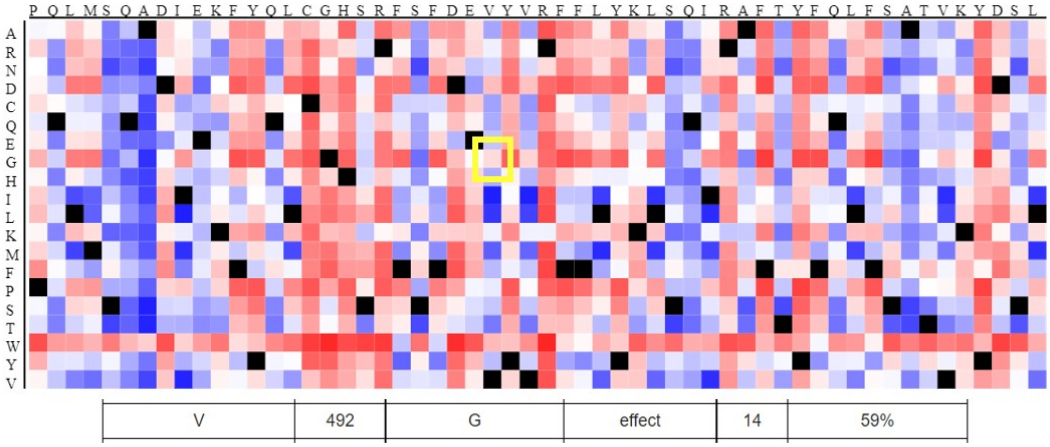

Figure A8: Heatmap of a region in the *TAC1b* sequence, in which the functional effects of aa substitutions were predicted. Indicated in yellow, the effect of an aa substitution at position 492 was displayed. In this case, Valine (V) was substituted for Glycine (G). The prediction effect and score, and expected accuracy are given in the table.

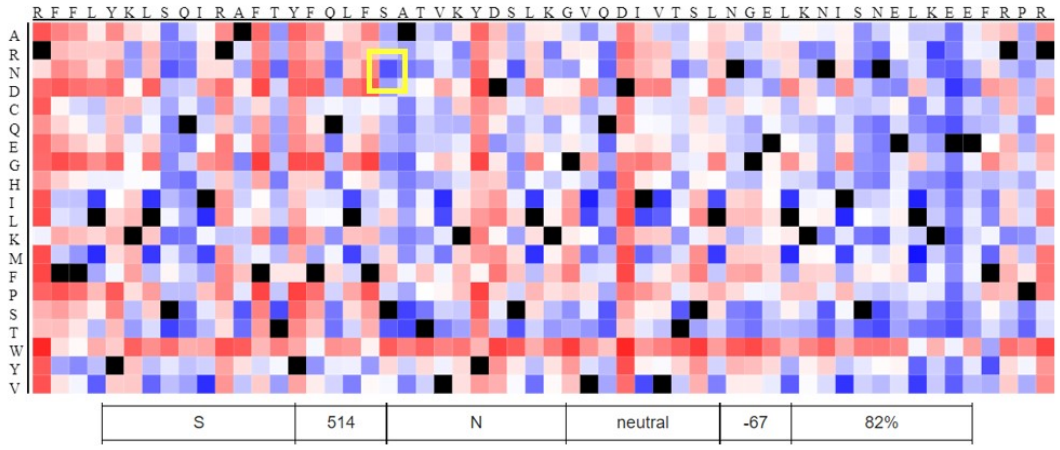

Figure A9: Heatmap of a region in the *TAC1b* sequence, in which the functional effects of aa substitutions were predicted. Indicated in yellow, the effect of an aa substitution at position 514 was displayed. In this case, Serine (S) was substituted for Asparagine (N). The prediction effect and score, and expected accuracy are given in the table

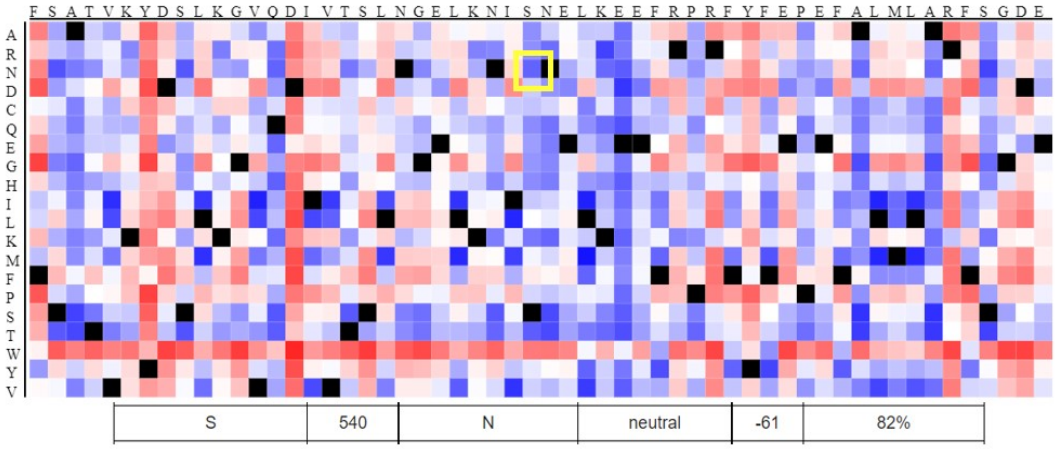

Figure A10: Heatmap of a region in the *TAC1b* sequence, in which the functional effects of aa substitutions were predicted. Indicated in yellow, the effect of an aa substitution at position 540 was displayed. In this case, Serine (S) was substituted for Asparagine (N). The prediction effect and score, and expected accuracy are given in the table.

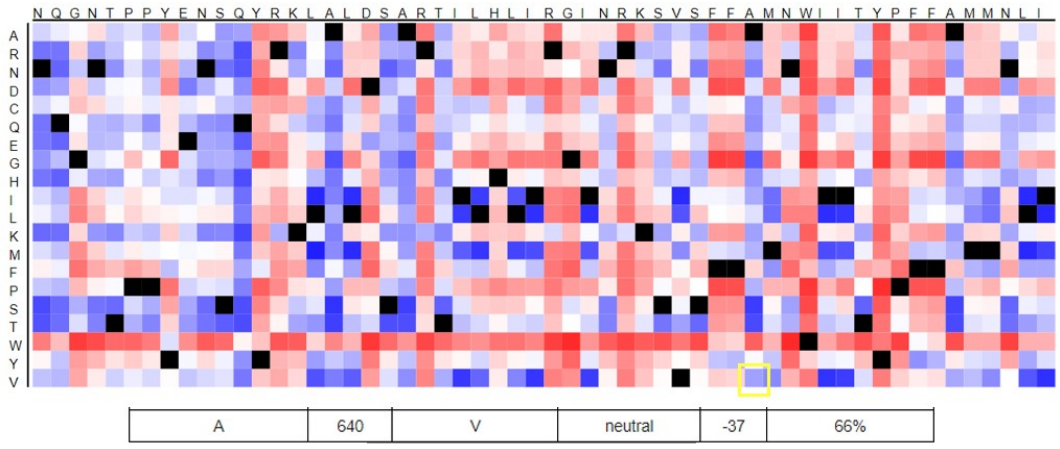

A	640	V	neutral	-37	66%

Figure A11: Heatmap of a region in the *TAC1b* sequence, in which the functional effect of the A640V mutation described by Rybak et al. (2020) is predicted. The position of the amino acid substitution indicated in yellow. In this case, Alanine (A) was substituted for Valine (V). The prediction effect and score, and expected accuracy are given in the table.

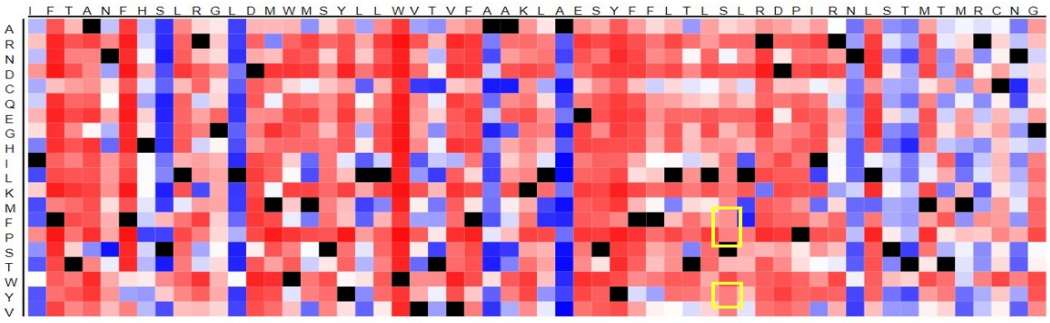

S	639	Y	effect	51	75%
S	639	F	effect	43	71%
S	639	P	effect	49	71%

Figure A12: Heatmap of a region in the *FKS1* sequence, in which the functional effects of aa substitutions were predicted. Indicated in yellow, the effect of an aa substitution at position 639 was displayed. In our data, Serine (S) was substituted for Tyrosine (Y) (S639Y) while in the literature, the mutation S639F was found. The prediction effect and score, and expected accuracy are given in the table.

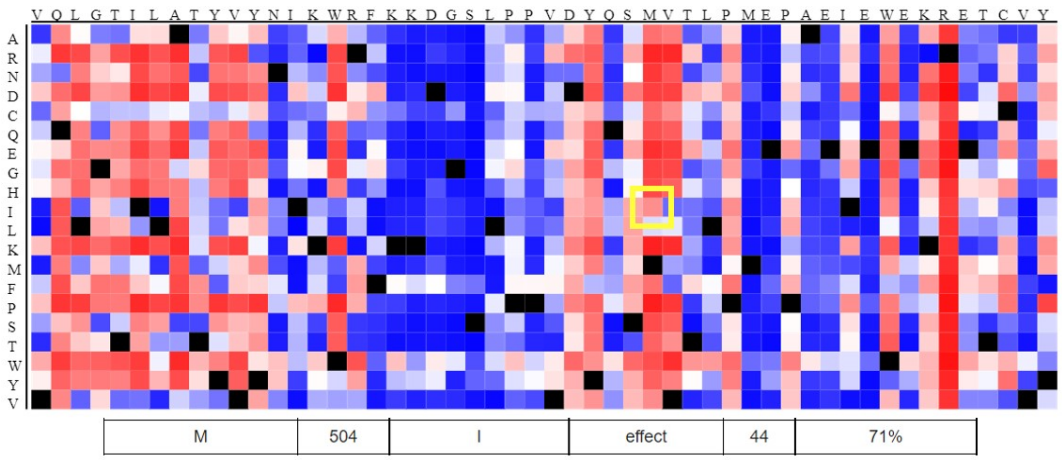

Figure A13: Heatmap of a region in *ERG11* was given, in which functional effects of aa substitutions were predicted. A non-synonymous mutation was found at aa position 504, indicated in yellow. Methionine (M) was substituted for Isoleucine (I), The prediction effect and score, and expected accuracy are given in the table.

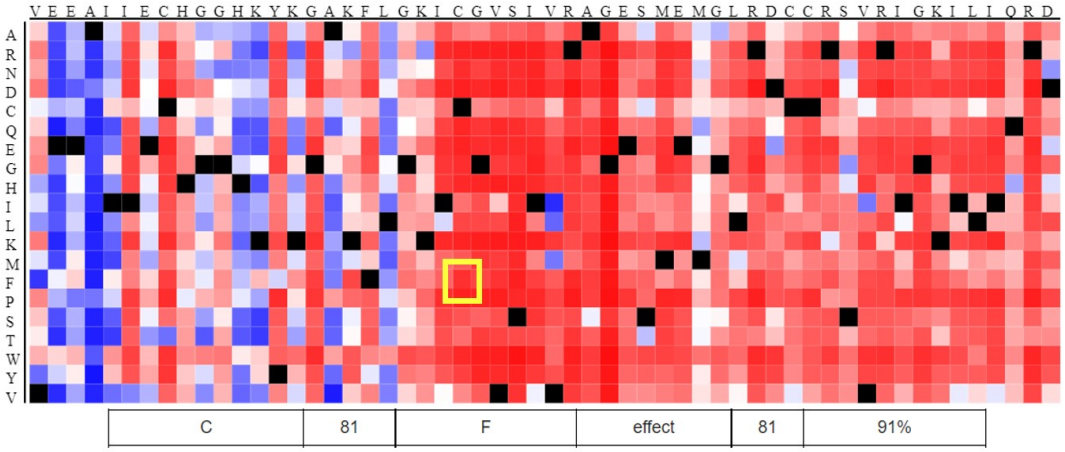

Figure A14: Heatmap of a region in *FUR1* was given, in which functional effects of aa substitutions were predicted. A non-synonymous mutation was found at aa position 81, indicated in yellow. Cytosine (C) was substituted for Phenylalanine (F). The prediction effect and score, and expected accuracy are given in the table.

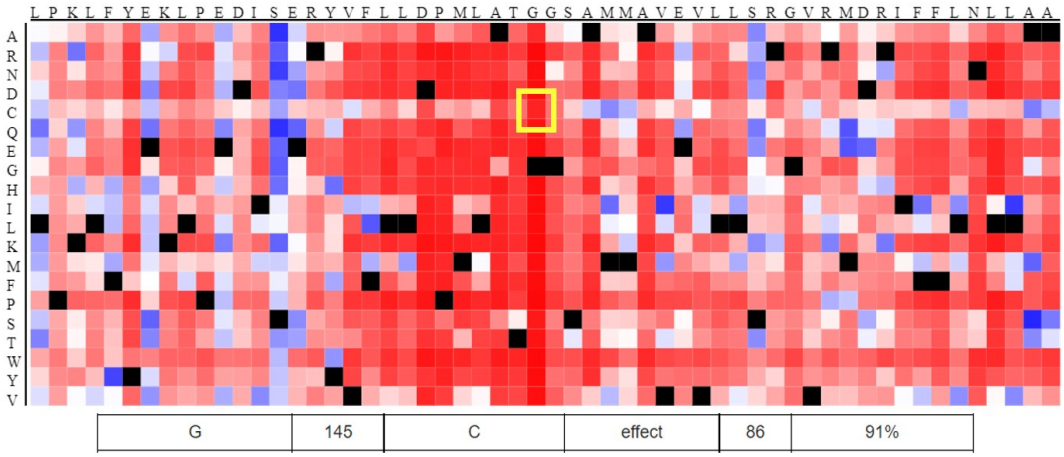

Figure A15: Heatmap of a region in *FUR1* was given, in which functional effects of aa substitutions were predicted. A non-synonymous mutation was found at aa position 145, indicated in yellow. Glycine (G) was substituted for Cysteine (C). The prediction effect and score, and expected accuracy are given in the table.

B.8 Growth dynamics of resistant cycling evolved strains

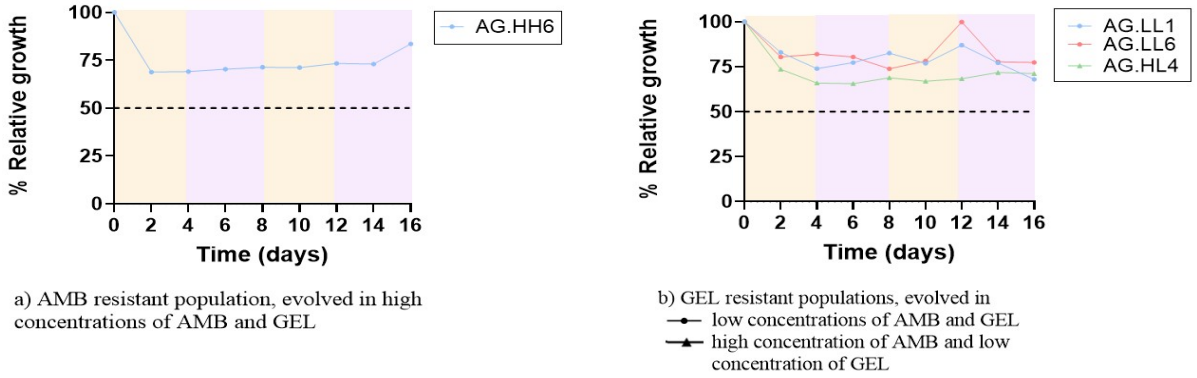

Figure A16: Relative growth of resistant populations of AMB-GEL cycling, based on AUC_{BDA}. Growth, relative to the mean value of 4 wt controls, is tracked for populations in which a) AMB-resistant strain in high concentrations (HH) of AMB and GEL b) GEL-resistant strains are found in either 1) low concentrations (LL) of AMB and GEL (1 μg/mL) or 2) high and low concentrations (HL) of AMB (2 μg/mL) and GEL respectively.

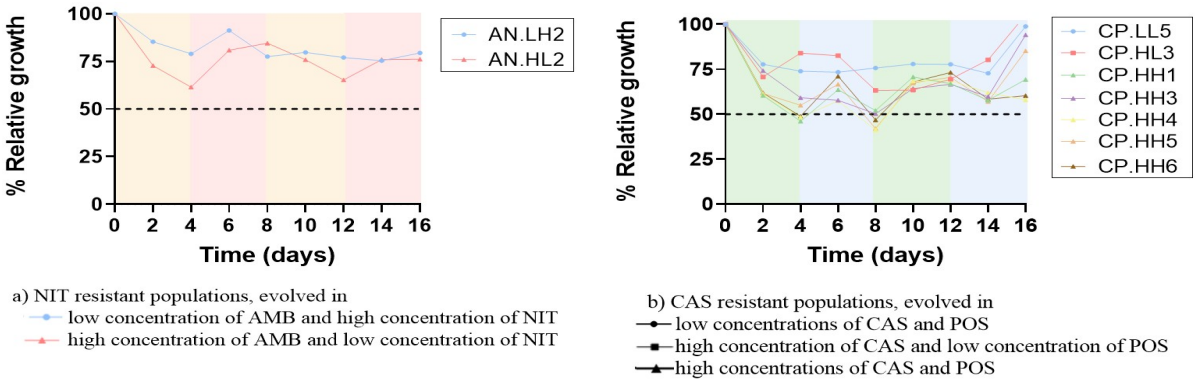

Figure A17: Relative growth of resistant populations of a) AMB-NIT and b) CAS-POS cycling, based on AUC_{BDA}. Growth, relative to the mean value of 4 wt controls, is tracked for populations in which a) NIT-resistant stains in low concentration of AMB (2 μg/mL) and high concentration of NIT (1 μg/mL), or b) CAS-resistant strains are found in either 1) low concentrations (LL) of CAS (0.5 μg/mL) and POS (0.25 μg/mL) or 2) high and low concentrations (HL) of CAS (1 μg/mL) and POS (0.25 μg/mL)respectively or 3) high concentrations (HH) of CAS (1 μg/mL) and POS (0.5 μg/mL).

B.9 Drug cycling survival spot assays

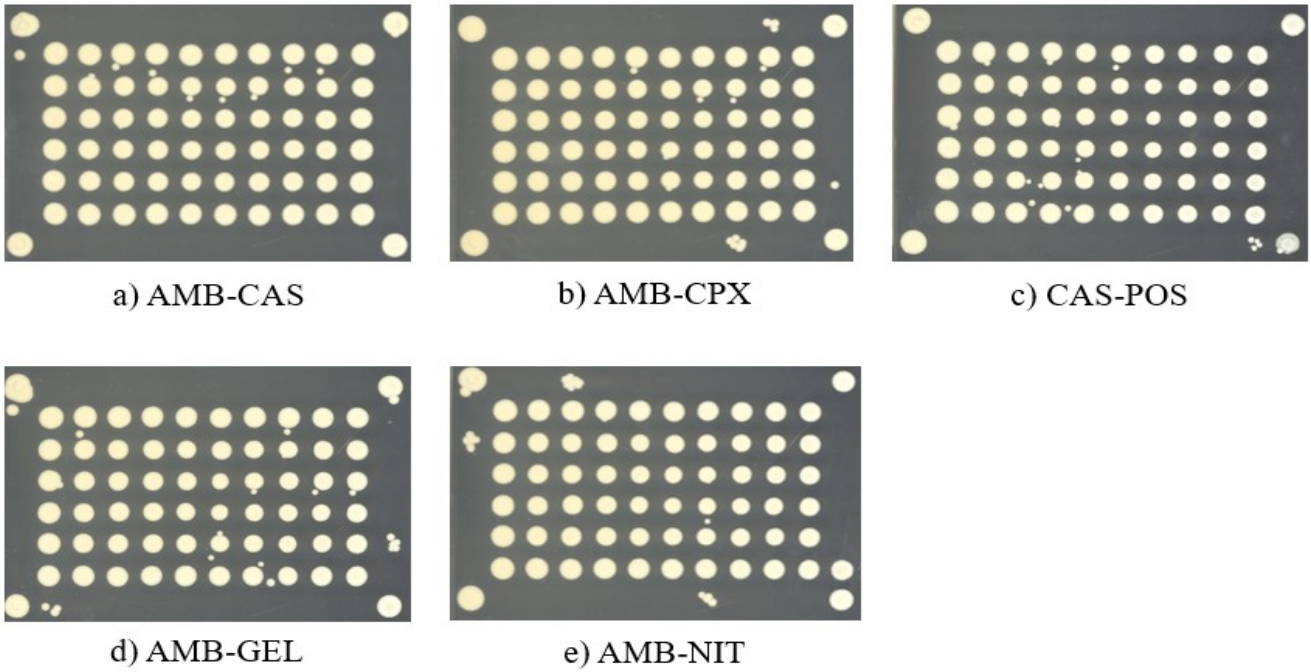

Figure A18: YPD spot assays of the cycling evolution experiments. Cycling evolution 96-well microtiter plates were spotted on YPD plates on day 16 of the experiment and incubated for 48 hours. The following plates represent the following drug combinations: a) AMB-CAS, b) AMB-CPX, c) CAS-POS, d) AMB-GEL, e) AMB-NIT.

B.10 Average relative growth during cycling evolution experiments.

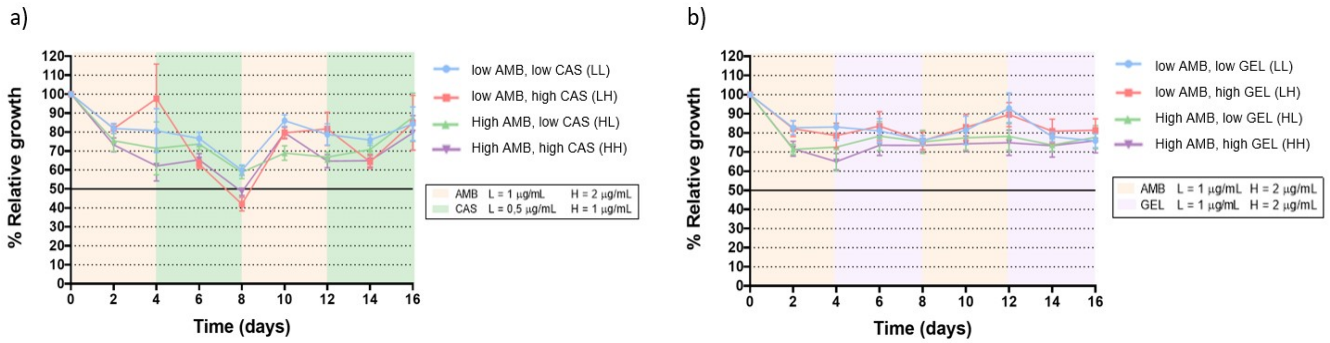

Figure A19: Average relative growth of wild type strains in the a) AMB-CAS and b) AMB-GEL cycling evolution experiment. The average relative percentage of growth based on 15 evolving populations per condition, relatively to the controls without drug, is measured at OD_{600} in function of time. The following colors represent relative growth in LL (blue), LH (red), HL (green) and HH (purple), for which L is [low] and H is [high]. Background colors indicate at which point in time the drugs are switched. Error bars indicate the variation of data points in each condition.

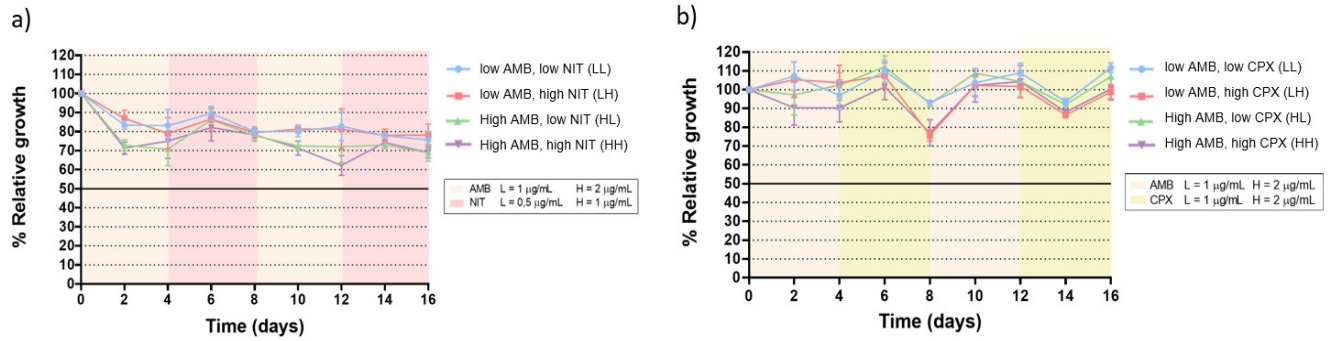

Figure A20: Average relative growth of wild type strains in the a) AMB-NIT and b) AMB-CPX cycling evolution experiment. The average relative percentage of growth based on 15 evolving populations per condition, relatively to the controls without drug, is measured at OD_{600} in function of time. The following colors represent relative growth in LL (blue), LH (red), HL (green) and HH (purple), for which L is [low] and H is [high]. Background colors indicate at which point in time the drugs are switched. Error bars indicate the variation of data points in each condition.

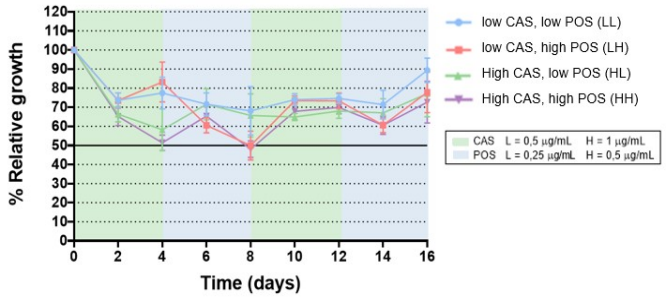

Figure A21: Average relative growth of wild type strains in the CAS-POS cycling evolution experiment. The average relative percentage of growth based on 15 evolving populations per condition, relatively to the controls without drug, is measured at OD_{600} in function of time. The following colors represent relative growth in LL (blue), LH (red), HL (green) and HH (purple), for which L is [low] and H is [high]. Background colors indicate at which point in time the drugs are switched. Error bars indicate the variation of data points in each condition.

B.11 Ergosterol biosynthesis pathway

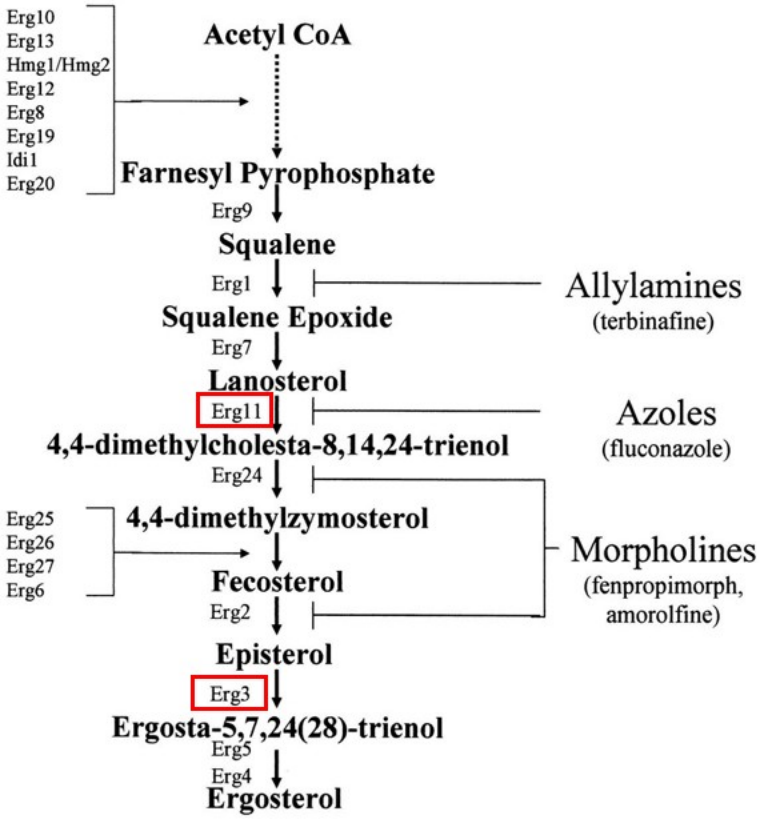

Figure A22: Ergosterol biosynthesis pathway with the genes *ERG3* and *ERG11* depicted in red.

Moleculaire Biotechnologie van Planten en Micro-organismen
Kasteelpark Arenberg 31 - bus 2438
3000 LEUVEN, BELGIË
tel. +32 16 32 15 00 fax +32 16 32 19 79
bio.kuleuven.be/mcb www.kuleuven.be